

ผลของการบดอะลูมินาต่อสมบัติของตัวเร่งปฏิกิริยาแพลเลเดียมบนอะลูมินา  
ในปฏิกิริยาไฮโดรจิเนชันแบบเลือกเกิดของอะเซทิลีน



นางสาวกมลวรรณ จันทร์มงคลทิพ

สถาบันวิทยบริการ  
วิทยานิพนธ์นี้เป็นส่วนหนึ่งของการศึกษาตามหลักสูตรปริญญาวิศวกรรมศาสตรมหาบัณฑิต  
สาขาวิชาวิศวกรรมเคมี ภาควิชาวิศวกรรมเคมี

คณะวิศวกรรมศาสตร์ จุฬาลงกรณ์มหาวิทยาลัย

ปีการศึกษา 2551

ลิขสิทธิ์ของจุฬาลงกรณ์มหาวิทยาลัย

EFFECT OF ALUMINA GRINDING ON THE PROPERTIES OF  
ALUMINA SUPPORTED PALLADIUM CATALYSTS IN SELECTIVE  
HYDROGENATION OF ACETYLENE



Miss Kamolwan Chanmongkolthip

A Thesis Submitted in Partial Fulfillment of the Requirements  
for the Degree of Master of Engineering Program in Chemical Engineering  
Department of Chemical Engineering  
Faculty of Engineering  
Chulalongkorn University  
Academic Year 2008  
Copyright of Chulalongkorn University

Thesis Title                    EFFECT OF ALUMINA GRINDING ON THE  
    PROPERTIES OF ALUMINA SUPPORTED  
    PALLADIUM CATALYSTS IN SELECTIVE  
    HYDROGENATION OF ACETYLENE

By                                    Miss Kamolwan Chanmongkolthip

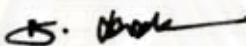
Field of Study                    Chemical Engineering

Advisor                            Assistant Professor Joongjai Panpranot, Ph.D.


Co-Advisor                        Assistant Professor Sirithan Jiemsirilers, Ph.D.


---

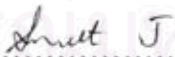
Accepted by the Faculty of Engineering, Chulalongkorn University in Partial  
Fulfillment of the Requirements for the Master's Degree


  
..... Dean of the Faculty of Engineering  
(Associate Professor Boonsom Lerdhirunwong, Dr.Ing.)

#### THESIS COMMITTEE

  
..... Chairman  
(Associate Professor Paisan Kittisupakorn, Ph.D.)

  
..... Advisor  
(Assistant Professor Joongjai Panpranot, Ph.D.)

  
..... Co-Advisor  
(Assistant Professor Sirithan Jiemsirilers, Ph.D.)

  
..... Examiner  
(Assistant Professor Varong Pavarajarn, Ph.D.)

  
..... External Examiner  
(Assistant Professor Okorn Mekasuwandumrong, D.Eng.)

กมลวรรณ จันทรมงคลทิพ: ผลของการบดอะลูมินาต่อสมบัติของตัวเร่งปฏิกิริยา แพลเลเดียมบนอะลูมินาในปฏิกิริยาไฮโดรจีเนชันแบบเลือกเกิดของอะเซทิลีน (EFFECT OF ALUMINA GRINDING ON THE PROPERTIES OF ALUMINA SUPPORTED PALLADIUM CATALYSTS IN SELECTIVE HYDROGENATION OF ACETYLENE) อ. ที่ปรึกษาวิทยานิพนธ์หลัก: ผศ.ดร. จุงใจ ปั้นประณต, อ.ที่ปรึกษาวิทยานิพนธ์ร่วม: ผศ. ดร. ศิริธันว์ เจียมศิริเลิศ, 95 หน้า.

งานวิจัยนี้ ศึกษาผลของการบดอะลูมินา และการบดออกไซด์ผสม (ซิงค์ออกไซด์-อะลูมินา และนิกเกิลออกไซด์-อะลูมินา) ที่อัตราส่วนโดยโมลของซิงค์ต่ออะลูมิเนียมและนิกเกิลต่ออะลูมิเนียมต่างๆ (0.1 และ 0.5) ในหม้อบดแบบแอททริชันต่อสมรรถนะของตัวเร่งปฏิกิริยา แพลเลเดียมบนอะลูมินาสำหรับปฏิกิริยาไฮโดรจีเนชันแบบเลือกเกิดของอะเซทิลีนเป็นเอทิลีน พบว่าสมรรถนะตัวเร่งปฏิกิริยาแพลเลเดียมบนตัวรองรับอะลูมินาที่ทำการบดที่ 12 ชั่วโมงให้ผลที่ดีกว่าตัวเร่งปฏิกิริยาแพลเลเดียมบนตัวรองรับอะลูมินาที่ไม่ได้ทำการบด อย่างไรก็ตาม ตัวเร่งปฏิกิริยาแพลเลเดียมบนตัวรองรับออกไซด์ผสมที่ทำการบดให้ค่าการเปลี่ยนของอะเซทิลีนและค่าเลือกเกิดของเอทิลีนลดลงเมื่อเปรียบเทียบกับตัวเร่งปฏิกิริยาแพลเลเดียมบนตัวรองรับอะลูมินาที่ทำการบดที่ 12 ชั่วโมง ผลวิเคราะห์จากการกระเจิงรังสีเอ็กซ์แสดงให้เห็นว่าเวลาที่ใช้ในการบดมีผลต่อขนาดผลึก พื้นที่ผิว และความเป็นกรดของอะลูมินา จากการวิเคราะห์โดยการดูดซับคาร์บอนมอนอกไซด์แสดงให้เห็นว่าการบดอะลูมินาส่งผลให้จำนวนของตำแหน่งที่ว่องไวของตัวเร่งปฏิกิริยาแพลเลเดียมบนตัวรองรับอะลูมินานี้มีมากขึ้น โดยที่อันตรกิริยาระหว่างตัวรองรับอะลูมินาและโลหะแพลเลเดียมไม่เปลี่ยนแปลง ส่งผลให้ตัวเร่งปฏิกิริยาแสดงค่าการเปลี่ยนของอะเซทิลีนและค่าเลือกเกิดเป็นเอทิลีนมากขึ้น นอกจากนี้ ความเป็นกรดที่เพิ่มขึ้นส่งผลต่อการเกิดได้กบนตัวเร่งปฏิกิริยาอีกด้วย

ภาควิชา.....วิศวกรรมเคมี..... ลายมือชื่อนิสิต..... กมลวรรณ จันทรมงคลทิพ.....  
 สาขาวิชา.....วิศวกรรมเคมี..... ลายมือชื่ออ.ที่ปรึกษาวิทยานิพนธ์หลัก..... ผศ.ดร. จุงใจ ปั้นประณต.....  
 ปีการศึกษา..... 2551..... ลายมือชื่ออ.ที่ปรึกษาวิทยานิพนธ์ร่วม..... ศิริธันว์ เจียมศิริเลิศ.....

# #5070532421: MAJOR CHEMICAL ENGINEERING

KEYWORDS: GRINDING/ ALUMINA/ SUPPORTED PALLADIUM CATALYSTS/  
SELECTIVE HYDROGENATION OF ACETYLENE

KAMOLWAN CHANMONGKOLTHIP: EFFECT OF ALUMINA GRINDING ON THE PROPERTIES OF ALUMINA SUPPORTED PALLADIUM CATALYSTS IN SELECTIVE HYDROGENATION OF ACETYLENE. ADVISOR: ASST. PROF. JOONGJAI PANPRANOT, Ph.D., CO-ADVISOR: ASST. PROF. SIRITHAN JIEMSIRILERS, Ph.D., 95 pp.

In this study, the effects of alumina grinding and mixed oxides ( $\text{ZnO-Al}_2\text{O}_3$  and  $\text{NiO-Al}_2\text{O}_3$ ) grinding with various Zn/Al and Ni/Al molar ratios (0.1 and 0.5) prepared by an attrition ball mill on catalytic performance of alumina supported Pd catalysts for selective hydrogenation of acetylene were investigated. It was found that catalytic performances of the Pd catalyst supported on  $\text{Al}_2\text{O}_3$  milled for 12 h were superior compared to those of Pd-supported on the unmilled  $\text{Al}_2\text{O}_3$ . However, all the catalysts prepared from milled mixed oxides presented lower acetylene conversion and ethylene selectivity than that of the catalyst prepared from alumina milled for 12 h. From X-ray diffraction, it was suggested that varying milling time directly affected the crystallite size, surface area and acidity of alumina supports. As revealed by CO chemisorption, milling of  $\text{Al}_2\text{O}_3$  supports could increase metal active sites of Pd/ $\text{Al}_2\text{O}_3$  catalysts without change in the interaction between Pd and the alumina support so that the catalysts exhibited higher acetylene activity and ethylene selectivity. Moreover, increasing of acidity affected coke formation on the catalysts.

สถาบันวิทยบริการ  
จุฬาลงกรณ์มหาวิทยาลัย

Department: ...Chemical Engineering..... Student's Signature: Kamolwan Chanmongkolthip  
Field of Study: ...Chemical Engineering..... Advisor's Signature: J. Panpranot  
Academic Year: .....2008..... Co-Advisor's Signature: Sirithan Jiemsirilers

## ACKNOWLEDGEMENTS

The author would like to express her sincere gratitude and appreciation to her advisor, Assistant Professor Joongjai Panpranot, for her invaluable suggestions, encouragement during her study, and useful discussion throughout this research. Without the continuous guidance and comments from her co-advisor, Assistant Professor Sirithan Jiemsirilers, this work would never have been achieved. In addition, the author would also be grateful to Associate Professor Paisarn Kittisupakorn, as the chairman, Assistant Professor Varong Pavarajarn and Assistant Professor Okorn Mekasuwandumrong as the members of the thesis committee. The financial supports of the Thailand Research Fund (TRF), TJTTP-JBIC and Graduate School of Chulalongkorn University are gratefully acknowledged.

Most of all, the author would like to express her highest gratitude to her parents who always pay attention to her all the times for their suggestions and have provided support and encouragements. The most success of graduation is devoted to her parents.

Finally, the author wishes to thank the members of the Center of Excellence on Catalysis and Catalytic Reaction Engineering, Department of Chemical Engineering, Faculty of Engineering, Chulalongkorn University for their friendship and assistance. To the many others, not specifically named, who have provided her with support and encouragement, please be assured that she thinks of you.

สถาบันวิทยบริการ  
จุฬาลงกรณ์มหาวิทยาลัย

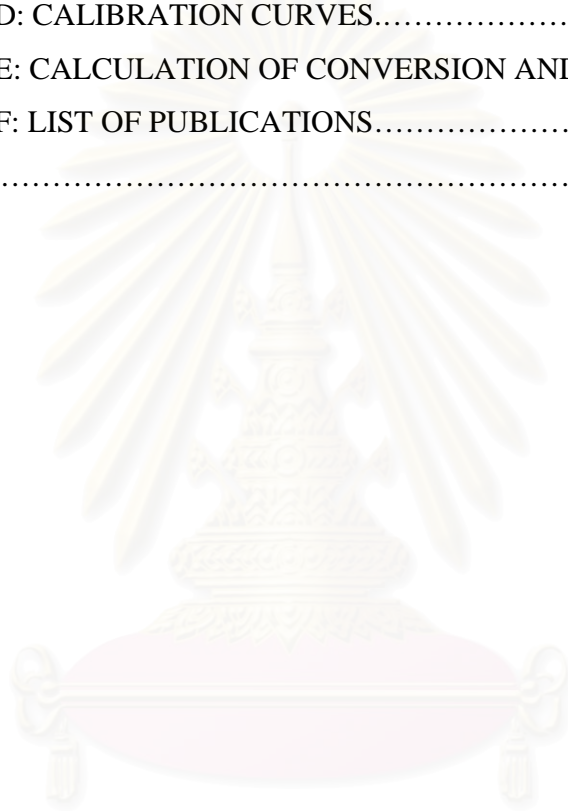
# CONTENTS

	<b>Page</b>
ABSTRACT (THAI).....	iv
ABSTRACT (ENGLISH).....	v
ACKNOWLEDGEMENTS.....	vi
CONTENTS.....	vii
LIST OF TABLES.....	x
LIST OF FIGURES.....	xi
CHAPTER	
I INTRODUCTION.....	1
1.1 Rationale.....	1
1.2 Research Objective.....	4
1.3 Research Scopes.....	4
1.4 Research Methodology.....	5
II THEORY .....	6
2.1 Palladium.....	6
2.2 Aluminium Oxide or Alumina (Al <sub>2</sub> O <sub>3</sub> ).....	8
2.3 Nickel Oxide (NiO).....	10
2.4 Zinc Oxide (ZnO).....	11
2.5 Acetylene Hydrogenation Reaction .....	12
2.6 Milling/Grinding.....	16
III LITERATURE REVIEWS.....	18
3.1 Supported Pd Catalyst in Selective Hydrogenation Reaction.....	18
3.2 Industrial Acetylene Hydrogenation System.....	22
3.3 Ni-modified Catalyst in Selective Hydrogenation Reaction.....	25
3.4 Zn-modified Catalyst.....	28
3.5 Mechanical activation.....	30
3.6 Comments on Previous Studies.....	32
IV EXPERIMENTS.....	33
4.1 Chemicals.....	33

CHAPTER	Page
4.2 Catalyst Preparation.....	33
4.2.1 Preparation of Al <sub>2</sub> O <sub>3</sub> by Grinding Method.....	33
4.2.2 Palladium loading .....	33
4.3 Catalyst Characterization.....	34
4.3.1 X-Ray Diffraction (XRD).....	34
4.3.2 N <sub>2</sub> Physisorption.....	34
4.3.3 CO-Pulse Chemisorption.....	34
4.3.4 NH <sub>3</sub> -Temperature Programmed Desorption (TPD).....	35
4.3.5 X-ray photoelectron spectroscopy (XPS).....	36
4.3.6 Transmission Electron Microscopy (TEM).....	36
4.3.7 Laser Diffraction Particle Size Analysis.....	36
4.3.8 Electron Spin Resonance (ESR).....	36
4.3.9 Thermal Gravimetric Analysis (TGA).....	36
4.4 Reaction Study in Selective Acetylene Hydrogenation.....	37
V RESULTS AND DISCUSSIONS.....	40
5.1 Milled Al <sub>2</sub> O <sub>3</sub> Supported Pd Catalyst.....	40
5.1.1 Characterization of the Catalysts.....	40
5.1.2 Catalytic Performance of the Catalysts.....	51
5.1.3 Characterization of the Spent Catalysts.....	55
5.2 Milled Mixed Oxides Supported Pd Catalyst.....	56
5.2.1 Characterization of the Catalysts.....	56
5.2.2 Catalytic Performance of the Catalysts.....	57
5.3 Effect of Alumina Grinding and Mixed Oxides (ZnO-Al <sub>2</sub> O <sub>3</sub> and NiO-Al <sub>2</sub> O <sub>3</sub> ) Grinding on the Properties of Pd/Al <sub>2</sub> O <sub>3</sub> Catalysts...	65
VI CONCLUSIONS AND RECOMMENDATIONS.....	71
6.1 Conclusions.....	71
6.2 Recommendations.....	72
REFERENCES.....	73
APPENDICES.....	80



	<b>Page</b>
CHAPTER	
APPENDIX A: CALCULATION FOR CATALYST PREPARATION.....	81
APPENDIX B: CALCULATION FOR THE CRYSTALLITE SIZE.....	86
APPENDIX C: CALCULATION FOR METAL ACTIVE SITES AND DISPERSION.....	89
APPENDIX D: CALIBRATION CURVES.....	90
APPENDIX E: CALCULATION OF CONVERSION AND SELECTIVITY...	92
APPENDIX F: LIST OF PUBLICATIONS.....	94
VITA.....	95



สถาบันวิทยบริการ  
จุฬาลงกรณ์มหาวิทยาลัย

## LIST OF TABLES

Table		Page
3.1	Typical acetylene concentration in the feed gas and conversion rate.....	23
3.2	Feed composition to acetylene hydrogenation reactors and the operating condition for front-end and tail-end processes.....	25
4.1	Operating condition of gas chromatograph.....	37
5.1	The average crystallite sizes of $\alpha$ -Al <sub>2</sub> O <sub>3</sub> supports milled at various time and Pd/ $\alpha$ -Al <sub>2</sub> O <sub>3</sub> catalysts.....	42
5.2	BET surface areas of $\alpha$ -Al <sub>2</sub> O <sub>3</sub> supports milled at various time and Pd/ $\alpha$ -Al <sub>2</sub> O <sub>3</sub> catalysts .....	44
5.3	Results from CO chemisorption of Pd supported $\alpha$ -Al <sub>2</sub> O <sub>3</sub> milled at various time.....	46
5.4	Atomic concentrations of catalysts from XPS.....	54
5.5	The average crystallite sizes of Al <sub>2</sub> O <sub>3</sub> , ZnO-Al <sub>2</sub> O <sub>3</sub> and NiO-Al <sub>2</sub> O <sub>3</sub> supports with various molar ratios of Zn to Al and Ni to Al milled at 12 h.....	59
5.6	BET surface areas of Al <sub>2</sub> O <sub>3</sub> , ZnO-Al <sub>2</sub> O <sub>3</sub> and NiO-Al <sub>2</sub> O <sub>3</sub> supports with various molar ratios of Zn to Al and Ni to Al milled at 12 h...	60
5.7	Results from CO chemisorption of Pd supported on Al <sub>2</sub> O <sub>3</sub> , ZnO-Al <sub>2</sub> O <sub>3</sub> and NiO-Al <sub>2</sub> O <sub>3</sub> supports with various molar ratios of Zn to Al and Ni to Al milled at 12 h .....	61

## LIST OF FIGURES

Figure		Page
2.1	Di- $\sigma$ bonded acetylene molecule to two neighboring Pd atoms (left) and a weakly $\pi$ -bonded acetylene molecule to isolated Pd atom (right).....	7
2.2	Illustration of Al and O atom packing in the basal plan.....	9
2.3	Desorption of water from alumina surface.....	10
2.4	Lewis acid and Lewis basic sites on alumina.....	10
2.5	Major reaction path of acetylene hydrogenation .....	14
2.6	Schematic drawing of laboratory stirred-ball mill .....	17
3.1	Reaction between a species ( $G^*$ ), formed on phase D, and then transferred to phase A by spill-over and surface diffusion, where it reacts with an adsorbed molecule R.....	19
3.2	Location of front-end acetylene hydrogenation reactors in a simplified scheme of downstream treatment of steam cracker effluents.....	24
3.3	Location of tail-end acetylene hydrogenation reactors in a simplified scheme of downstream treatment of steam cracker effluents.....	24
4.1	A schematic of acetylene hydrogenation system.....	39
5.1	The XRD patterns of (A) $\alpha$ - $Al_2O_3$ supports milled at various time and (B) Pd/ $\alpha$ - $Al_2O_3$ catalysts.....	41
5.2	TEM micrographs of $\alpha$ - $Al_2O_3$ supports milled at various time.....	44
5.3	$NH_3$ temperature programmed desorption of $\alpha$ - $Al_2O_3$ milled at various time.....	47
5.4	The particle size distribution of $Al_2O_3$ milled at various time.....	48
5.5	XPS results for the Pd 3d core level region of (A) unmilled $Al_2O_3$ (B) $Al_2O_3$ at 4 h (C) $Al_2O_3$ at 8 h and (D) $Al_2O_3$ at 12 h.....	49
5.6	ESR spectra of $Al_2O_3$ milled at various time.....	51

<b>Figure</b>	<b>Page</b>	
5.7	Temperature dependence of the catalytic performance (% conversion of C <sub>2</sub> H <sub>2</sub> ) of Pd/milled Al <sub>2</sub> O <sub>3</sub> catalysts with various time.....	53
5.8	Temperature dependence of the catalytic performance (% selectivity of C <sub>2</sub> H <sub>4</sub> ) of Pd/milled Al <sub>2</sub> O <sub>3</sub> catalysts with various time.....	54
5.9	Temperature dependence of the catalytic performance (% yield of C <sub>2</sub> H <sub>4</sub> ) of Pd/milled Al <sub>2</sub> O <sub>3</sub> catalysts with various time.....	54
5.10	TGA profiles of Pd/unmilled Al <sub>2</sub> O <sub>3</sub> and Pd/milled Al <sub>2</sub> O <sub>3</sub> catalysts after reaction.....	55
5.11	DTA profiles of Pd/unmilled Al <sub>2</sub> O <sub>3</sub> and Pd/milled Al <sub>2</sub> O <sub>3</sub> catalysts after reaction.....	56
5.12	The XRD patterns of milled mixed oxides supports (A) ZnO- Al <sub>2</sub> O <sub>3</sub> and (B) NiO-Al <sub>2</sub> O <sub>3</sub> milled at 12 h with various molar ratios of Zn to Al and Ni to Al .....	57
5.13	NH <sub>3</sub> temperature programmed desorption of (A) ZnO-Al <sub>2</sub> O <sub>3</sub> and (B) NiO-Al <sub>2</sub> O <sub>3</sub> supports with various molar ratios of Zn to Al and Ni to Al milled at 12 h.....	62
5.14	Temperature dependence of the catalytic performance (% conversion of C <sub>2</sub> H <sub>2</sub> ) of Pd/milled mixed oxide catalysts with various molar ratios of Zn to Al and Ni to Al .....	63
5.15	Temperature dependence of the catalytic performance (% selectivity of C <sub>2</sub> H <sub>4</sub> ) of Pd/milled mixed oxide catalysts with various molar ratios of Zn to Al and Ni to Al .....	64
5.16	Temperature dependence of the catalytic performance (% yield of C <sub>2</sub> H <sub>4</sub> ) of Pd/milled mixed oxide catalysts with various molar ratios of Zn to Al and Ni to Al .....	65
5.17	Conceptual model demonstrating four main types of surface on alumina-supported palladium catalyst.....	67

<b>Figure</b>		<b>Page</b>
5.18	A simplified representation of active sites created on a palladium surface by carbonaceous deposits ( $C_xH_y$ ).....	68
5.19	Three types of active sites created on the palladium surface by carbonaceous deposits ( $C_xH_y$ ) and schemes of the reactions occurring on the sites.....	69
B.1	The measured peak of the unmilled $\alpha$ - $Al_2O_3$ to calculate the crystallite size.....	88
B.2	The plot indicating the value of line broadening due to the equipment. The data were obtained by using $\alpha$ -alumina as standard.....	88
D.1	The calibration curve of hydrogen from TCD of GC-8A.....	91
D.2	The calibration curve of hydrogen from FID of GC-9A.....	91

# CHAPTER I

## INTRODUCTION

### 1.1 Rationale

Ethylene is the lightest olefin which does not occur in nature. It is an important raw material for a large variety of industrial process, particularly for the production of polyethylene which is formed by polymerization of n molecules of the monomer ethylene. Over 70 million metric tons per year of polyethylene is produced (The Global Chemical Market: CMAI, 2007) and used in large quantities of non-expensive synthetic material with modest physical properties like stiffness and excellent chemical resistance for nondurable applications which do not require properties like hardness or thermal resistance (Peacock *et al.*, 2000).

Ethylene can be prepared by dehydration of ethanol with sulfuric acid or by cracking and fractional distillation of natural gas and petroleum. Typically, ethylene stream from a naphtha cracker unit contains about 0.1-1 wt% of acetylene as an impurity. Acetylene must be removed to a level of low ppm-range because it poisons the catalyst used in subsequent ethylene polymerization process by adsorbing at the active sites for ethylene and blocking the polymerization. In addition, presence of acetylene in ethylene stream leads to selectivity degradation at high acetylene conversion and quality reduction of the produced polyethylene (Kim *et al.*, 2004). Moreover, acetylene can form metal acetylides, which are explosive contaminants (Huang *et al.*, 1994).

There have been two general methods to remove the trace amount of acetylene in ethylene stream. One is adsorption of acetylene from ethylene using zeolite, which is difficult and very costly method. Another is selective catalytic hydrogenation reaction of acetylene to ethylene which is more popular method for the industrial process (Kang *et al.*, 2000).

Mostly, hydrogenation reactions use noble metals catalysts or group VIII transition metals catalysts. The major advantages of these catalysts are their relatively high activity, mild process conditions, easy separation, and better handling properties. Noble metals such as Pd, Pt, Rh and Ru are particularly effective in hydrogenation reactions because they adsorb hydrogen molecules with dissociation which partly determines the catalyst activity and the bonding is not too strong. The hydrogenation activity typically decreases in the following sequence: Pd>Rh>Pt>Ru.

Alumina supported palladium catalyst has been proved to be the best catalyst so far for the selective hydrogenation reaction of acetylene to ethylene due to its good activity for the hydrogenation of acetylene in excess ethylene. Catalysis by noble metals is generally achieved via the high dispersion of low loading metals on an appropriate support.

Supports are usually the relatively inexpensive oxide such as alumina, silica, and titania. Generally, the catalyst support must present a good stability to high temperature and a sufficiently large specific surface area. Additionally, they can interact more or less with the active metal and can possess other functions, such as acidity or basicity (Guimon *et al.*, 2003). The most frequently studied support for palladium catalyst in selective hydrogenation of acetylene is alpha phase alumina.

In general, alpha phase alumina has a relatively low surface area of approximately 0.1-3 m<sup>2</sup>/g and Pd loading is around 0.001-1 wt%. Compared to Pd supported gamma phase alumina, lower ethane is formed on Pd supported alpha phase alumina catalyst due to the smaller amount of oligomers/deposits that can act as hydrogen reservoir for over hydrogenation of ethylene product (Sárkány *et al.*, 1986). Moreover, low dispersion catalysts have been suggested to give better selectivity towards ethylene (Hub *et al.*, 1988 and Boitiaux *et al.*, 1983) since certain fraction of sites that are not covered by acetylene provides ethylene hydrogenation.

Due to poor selectivity at high acetylene conversion and the demand for high purity ethylene, numerous attentions have been focused on the factors which improve activity and selectivity of acetylene hydrogenation catalysts. It was found that an alternative way for selectivity enhancement for palladium catalysts can be done by (i) modification of palladium surface by promoting with a second metal especially the metal of group IB such as Ag (Praserthdam *et al.*, 2002 and Ngamsom *et al.*, 2004), K (Park *et al.*, 1992), Si (Shin *et al.*, 1998), Au (Sárkány *et al.*, 2002), Cu (Guczi *et al.*, 1999) and Co (Sárkány *et al.*, 1995), (ii) pretreatment catalyst with O<sub>2</sub> and/or O<sub>2</sub>-containing compounds such as nickel oxide (Wongwaranon *et al.*, 2007) and zinc oxide (Zawadzki *et al.*, 2001), (iii) using different supports such as titania (Chu *et al.*, 2004) and silica (W. J. Kim *et al.*, 2003) and (iv) addition CO<sub>2</sub> to the reactant stream (D. L. Trimm *et al.*, 1980).

During the past few years, mechanical processing has received an increased interest in the preparation of heterogeneous catalysts. Milling of supports has been reported as an alternative way for activity and selectivity enhancement. The main goal of mechanical treatment is to obtain highly active and dispersed catalysts (Andonova *et al.*, 2006). A higher catalytic activity of the grinding-prepared catalyst has been observed in the hydrodesulfurization reaction, compared with the activity of an industrial catalyst (Kouzu *et al.*, 2004). A series of articles have been devoted to the study of influence of the mechanical treatment on the catalytic activity and selectivity of catalysts, on the morphology, degree of dispersion and on the acidic–basic properties of the superficial active sites of catalysts. However, a limited volume of data has been published so far about the effect of mechanical treatment of alumina support on the properties of Pd catalysts, designed for selective acetylene hydrogenation reaction.

Moreover, milling of mixed oxides such as Al<sub>2</sub>O<sub>3</sub> and CeO<sub>2</sub> has shown to result in improved properties for catalyst support in water gas shift reaction (D. Andreeva *et al.*, 2007). Thus, it is also interested to study the effect of milling on mixed oxides between alumina and other oxides such as NiO and ZnO on the properties of Pd/Al<sub>2</sub>O<sub>3</sub> in selective acetylene hydrogenation.



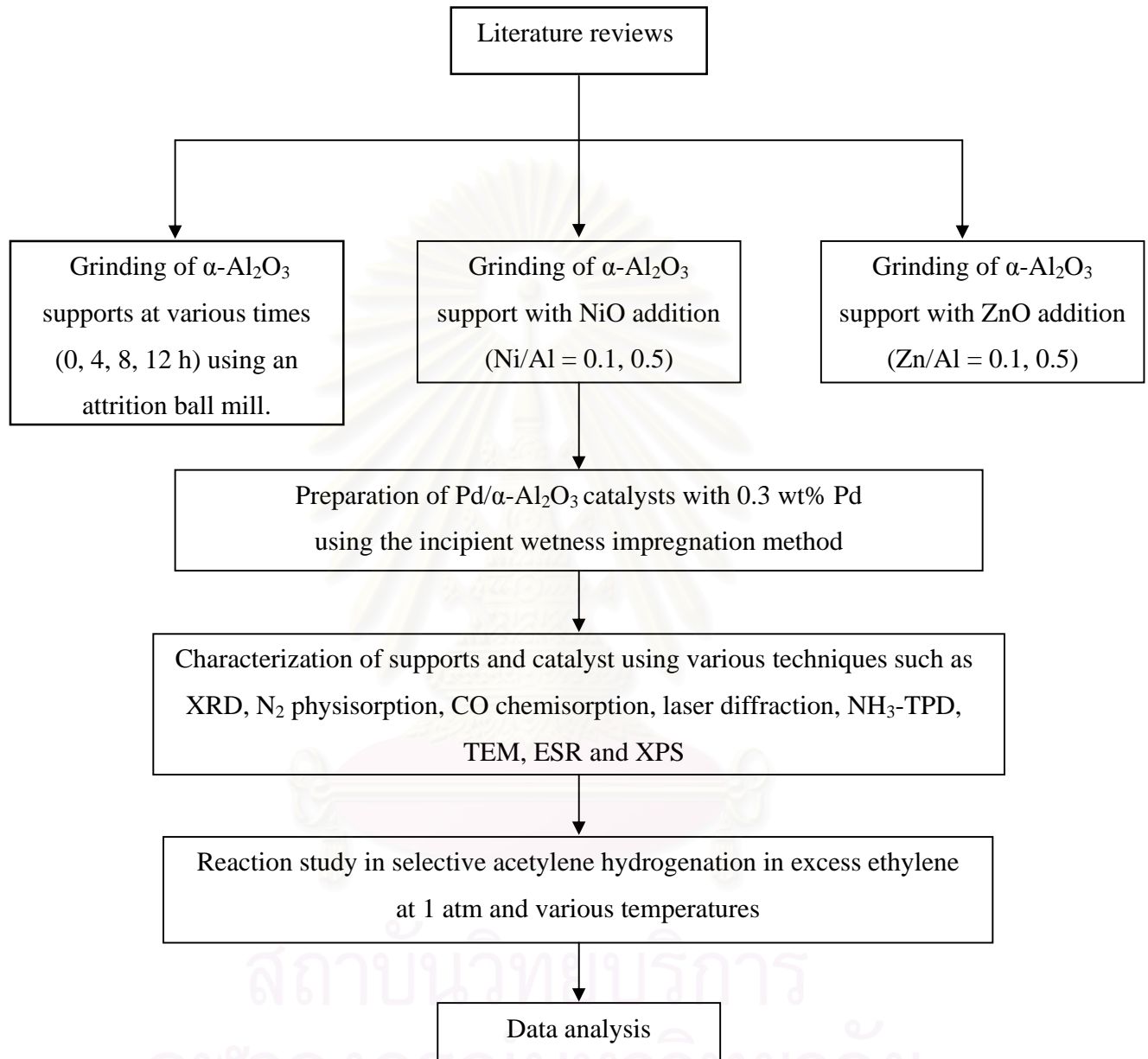
## 1.2 Objective

The objective of this research is to investigate the effect of mechanical milling on  $\text{Al}_2\text{O}_3$  on characteristics and catalytic properties of  $\text{Al}_2\text{O}_3$  supported Pd catalysts in selective acetylene hydrogenation.

## 1.3 Research Scopes

1. Grinding of  $\alpha\text{-Al}_2\text{O}_3$  support with various time (0-12 hr) using an attrition mill.
2. Grinding of  $\alpha\text{-Al}_2\text{O}_3$  support with NiO and ZnO addition (molar ratios of Ni/Al and Zn/Al = 0.1 - 0.5).
3. Preparation of Pd/ $\alpha\text{-Al}_2\text{O}_3$  catalysts with 0.3 wt% Pd using the incipient wetness impregnation method.
4. Characterization of the supports and the catalyst samples using X-ray diffraction (XRD),  $\text{N}_2$  physisorption, CO pulse chemisorption,  $\text{NH}_3$ -temperature program desorption ( $\text{NH}_3$ -TPD), transmission electron microscopy (TEM), laser diffraction, electron spin resonance (ESR) and X-ray photoelectron spectroscopy (XPS).
5. Study of catalyst performance in selective acetylene hydrogenation in excess ethylene at 1 atm and various temperatures.

## 1.4 Research Methodology



## CHAPTER II

### THEORY

This chapter focuses on the fundamental theory of the selective acetylene hydrogenation over supported palladium catalyst. The chapter consists of six main sections. Palladium used for acetylene hydrogenation is detailed in section 2.1. Details of catalyst supports (alumina) used for the selective hydrogenation of acetylene are in section 2.2. Nickel oxide is discussed in section 2.3. Zinc oxide is detailed in section 2.4. The acetylene hydrogenation and influencing parameters in the reaction are detailed in section 2.5. Finally, preparation method (grinding/milling) is discussed in section 2.6.

#### 2.1 Palladium

Palladium as a group VIII noble metal has unique catalytic properties in homogeneous and in heterogeneous reactions. In heterogeneous catalysis palladium is used for oxidation and hydrogenation reactions. One of the most remarkable properties of palladium is the ability to dissociate and dissolve hydrogen. Atomic hydrogen occupies the octahedral interstices between the Pd atoms of the cubic-closed packed metal. Palladium can absorb up to 935 times of its own volume of hydrogen. Depending on hydrogen partial pressure and temperature a so-called  $\alpha$ - and  $\beta$ -hydride is formed.

Some physical properties of palladium.

---

atomic number	46
atomic weight	106.42atomic
diameter	275.2 pm
melting point	1827 K
crystal structure	cubic closed packed
electron configuration	[Kr] 4d <sup>10</sup>
electron negativity (Allred & Rochow)	1.4

---

Like other group VIII metals, palladium can be used for hydrogenation of unsaturated hydrocarbons. Palladium shows the highest selectivity of these metals in heterogeneously catalyzed semi-hydrogenation of alkynes and dienes to the corresponding alkenes (Arnold *et al.*, 1997). Activity of palladium for hydrocarbon hydrogenation is based on the ability for the dissociative adsorption of hydrogen and chemisorption of unsaturated hydrocarbons. The chemisorption of alkenes and alkynes is based on the interaction of the d-band of the Pd metal with the  $\pi$ -bonding system of the unsaturated hydrocarbons (Pallassana *et al.*, 2000 and Mittendorfer *et al.*, 2003). Industrially used catalysts for acetylene hydrogenation contain relatively low Pd content ( $< 0.1$  wt%) and are supported on metal oxides like alumina. Palladium shows high activity but only limited selectivity and long-term stability for hydrogenation of acetylene. The limited selectivity is mainly due to enhanced ethane formation and the formation of by-products like C4 and higher hydrocarbons. Palladium shows a strong deactivation behavior because of hydrocarbon and carbon deposits. Catalyst deactivation by hydrocarbon and carbon deposits requires a frequent exchange or regeneration of the catalyst in the hydrogenation reactor. Moreover, fresh or regenerated catalysts show high activity and consequently lead to increased ethylene consumption and reduced selectivity. Furthermore, high activity of fresh or regenerated catalysts can lead to overheating (“thermal run away”) of the reactor because of the exothermic hydrogenation reaction.

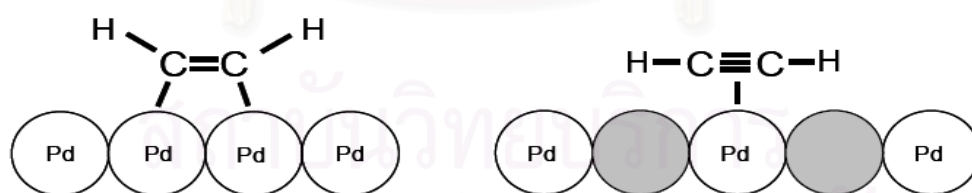


**Fig  
ure  
2.1  
Di-**

$\sigma$  bonded acetylene molecule to two neighbouring Pd atoms (left)  
and a weakly  $\pi$ -bonded acetylene molecule to an isolated Pd atom (right).  
Only the  $\pi$ -bonded acetylene is hydrogenated in high selectivity to ethylene.

The limited selectivity of Pd catalysts in acetylene hydrogenation can be attributed to the presence of ensembles of active sites on the catalyst surface (Derouane *et al.*, 1984, Coq *et al.*, 2001 and Guzzi *et al.*, 2003). Selectivity can be increased by active-site isolation (“geometric effect”), modification of the electronic structure by alloying or promoting of Pd catalysts ( “electronic effect”) or by suppressing hydride formation (“kinetic effect”).

## 2.2 Aluminium Oxides or Alumina ( $\text{Al}_2\text{O}_3$ )

Aluminum oxides, which are a term of alumina compounds, had transition phase and alpha phase alumina. Alumina can exist in many metastable phase before transforming to the stable  $\alpha$ -alumina (corundum form). There are six principle phase designated by The Greek letters Chi, kappa, eta, theta, delta and gamma. The nature of the product obtained by calcinations depends on the starting hydroxide (Gibbsite, boehmite and others) and on the calcinations conditions. Normally, transition alumina starts to lose their surface area even at temperature below  $800^\circ\text{C}$  due to the elimination of micro-pores. However, drastic loss occurs at temperature higher than  $1000^\circ\text{C}$  when the crystallization to the thermodynamically stable  $\alpha$ -alumina occurs (Dynys *et al.*, 1982).

Several studies have been carried out on the direct phase transformation of alumina. The mechanism of direct phase transformation and the direct phase transformation from  $\gamma$ -alumina to  $\alpha$ -alumina involve the conversion of the cubic close packing of oxygen ions into a stable hexagonal close packing (Simpson *et al.*, 1998; Levin *et al.*, 1998).

The structure of  $\alpha$ -alumina consists of close packed planes of the large oxygen ions stacking in A-B-A-B sequence, thus forming hexagonal close packed array of anions. The aluminium cations are located at octahedral sites of this basic array and from another type of close packed planes between the oxygen layers. To maintain neutral charge, however, only two third of the available octahedral sites are filled with cation.

Figure 2.2 illustrates the packing of Al and O atom in the basal plane. Since the vacant octahedral sites also form a regular hexagonal array, three different types of cation layer can be defined, namely a, b, and c layer, depending on the position of the vacant cation site within the layer. These layers are stacked in an a-b-c-a-b-c sequence in the structure of alumina.

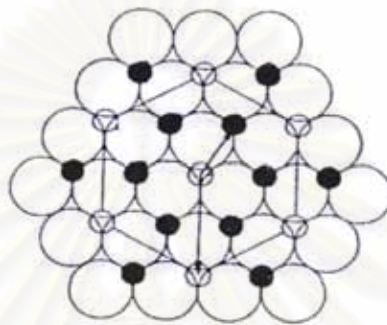


**Figure 2.2** Illustration of Al and O atom packing in the basal plan

$\alpha$ - $\text{Al}_2\text{O}_3$  (corundum) powders are applied in catalysis as supports, for example, of silver catalysts for ethylene oxidation to ethylene oxide, just because they have low Lewis acidity, low catalytic activity, and conversely, they are mechanically and thermally very strong.

Activated alumina can be used selectively to adsorb certain other chemical species from gaseous or liquid streams. Activated alumina has a surface with both Lewis and Brønsted acidic and basic sites. Acidity is derived from the  $\text{Al}^{3+}$  ions and  $\text{H}_2\text{O}$  molecules coordinated to cationic sites, while basicity is due to basic hydroxide groups and  $\text{O}^{2-}$  anion vacancies [Evans 1993]. If alumina contact to humidity, surface are adsorbed water molecules and when alumina were dried at  $100\text{ }^\circ\text{C}$  to  $150\text{ }^\circ\text{C}$ , water molecules are desorbed but remain hydroxyl group (-OH) cause acidity of alumina are weak Brønsted acid. (Figure 2.3) Calcination temperatures below  $300\text{ }^\circ\text{C}$ , the acid strength and concentration of alumina are low and at  $500\text{ }^\circ\text{C}$  reduce Brønsted acid sites. [Wittayakhun et al. 2004]

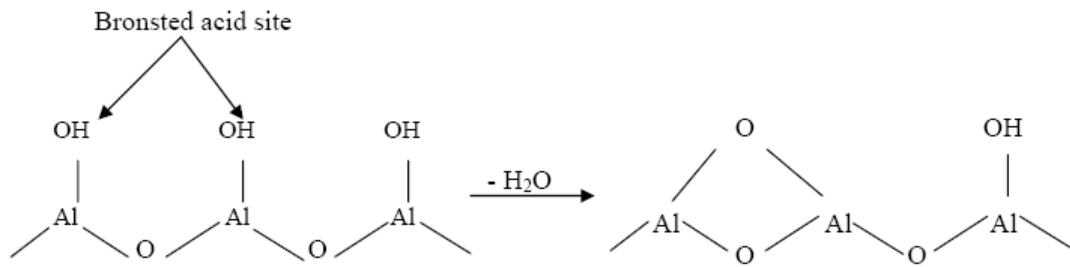


**Figure 2.3** Desorption of water from alumina surface [Wittayakhun et al. 2004].

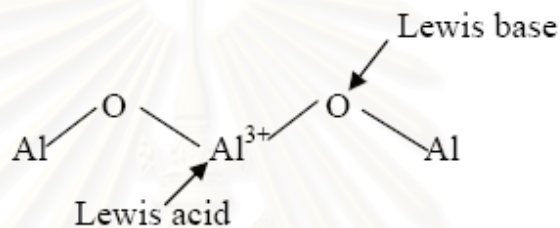


**Figure 2.4** Lewis acid and Lewis basic sites on alumina [Wittayakhun et al. 2004].

As shown in Figure 2.4, further increasing temperatures above 600 °C, adjacent –OH combine and more emit H<sub>2</sub>O and contribute to Al<sup>3+</sup> are Lewis acid sites and O<sup>2-</sup> are Lewis basic sites. Hardness of surface bring about no reaction between Lewis acid and Lewis base which both sites have high activity in various reaction such as Dehydration of alcohol and Isomerization of alkene. The decline in acidity for calcination temperatures above 800 °C can be attributed to the collapse in surface area as the alumina is converted to its alpha form [Wittayakhun et al. 2004].

### 2.3 Nickel Oxide (NiO)

Nickel oxide (NiO) is a green cubic crystal compound, mp 2090°C, density 7.45 g/cm<sup>3</sup>, the properties of which are related to its method of preparation. Green nickel oxide is prepared by firing a mixture of water and pure nickel powder in air at 1000°C or by firing a mixture of high purity nickel powder, nickel oxide and water in air. Whereas this temperature is required for full development of the crystal, the temperature is high enough that an equilibrium leading to dissociation back to the element is established.

Consequently, it is virtually impossible to obtain green nickel oxide made by high temperature firing that does not have traces of nickel metal.

Black nickel oxide, a microcrystalline form, results from calcination of the carbonate or nitrate at 600 °C. This incompletely annealed product typically has more oxygen than its formula indicates, i.e., 76-77 wt.% nickel compared to the green form, which has 78.5% nickel content. This results from chemisorption of oxygen on the surface of the crystal defects. Black nickel oxide compositions are chemically reactive and form simple nickel (II) salt when heated with mineral acid.

## **2.4 Zinc Oxide (ZnO)**

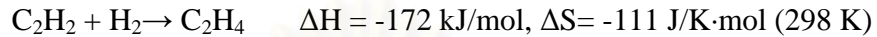
Zinc oxide is a chemical compound with the formula ZnO. It is nearly insoluble in water but soluble in acids and bases. It occurs as white hexagonal, wurtzite type crystals having 6mm of symmetry or a white powder commonly known as zinc white. Zinc oxide occurs in nature as the mineral zincite. Major applications of zinc oxide involve medical applications, chemical and biosensor applications, food additive, pigment, rubber manufacture and electronic materials.

Zinc oxide is produced by French process or American process. In French process, metallic zinc is melted and vaporized above 907°C. Zinc vapor instantaneously reacts with the oxygen in the air to give ZnO. Zinc oxide normally consists of agglomerated zinc oxide particles with an average size of 0.1 micrometres to a few micrometres. By weight, most of the world's zinc oxide is manufactured via French process. In direct process, zinc ores or roasted sulfide concentrates are mixed with coal. In a reduction furnace, ore is reduced to metallic zinc and the vaporized zinc is allowed to react with oxygen to form zinc oxide. In American process, ore of zinc (zinc ash) is dissolved (as ZnCl<sub>2</sub>) and precipitated with alkali. Zinc oxide made from this process is known as "Active Zinc Oxide". Dip in water after done.



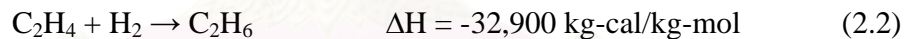
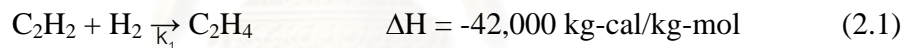
## 2.5 Acetylene Hydrogenation Reaction

Ethylene for the polymerization to polyethylene is produced by cracking of light alkanes in a steam cracker. The ethylene stream has to be purified and one step in the purification process is the selective hydrogenation of acetylene to ethylene.



Presence of acetylene in ethylene stream leads to poisoning of the polymerization catalyst because acetylene adsorbs at the active sites for ethylene and blocks the polymerization process. Therefore, the acetylene content in the ethylene feed has to be reduced to the low ppm-range. Hydrogenation of acetylene in the presence of ethylene requires high selectivity to ethylene to prevent hydrogenation of ethylene to ethane (Bos *et al.*, 1993, Arnold *et al.*, 1997).

Following reactions occur in an acetylene hydrogenation reactor.



The first reaction (2.1) is the most wanted reaction whereas the second reaction (2.2) is an undesired side reaction due to the consumption of ethylene product. There is also a third reaction occurring during normal operation, which adversely affects the catalyst performance, i.e., the polymerization reaction of  $\text{C}_2\text{H}_2$  with itself to form a longer chain molecule, commonly called “green oil”.

In relation to the above reactions relating acetylene hydrogenation, two influencing parameters on the desired reaction can be assigned. The first parameter is reaction temperature, which has a direct correlation with the kinetics of the system. However, it affects not only the reaction rate of the desired reaction ( $k_1$ ), but also the rate of ethylene hydrogenation ( $k_2$ ). The rate of polymerisation ( $k_3$ ) also increases with

temperature and the resulting green oil can affect catalyst activity by occupying active sites. When the catalyst is new or has just been regenerated, it has high activity. With time on stream, activity declines as the catalyst becomes fouled with green oil and other contaminants. By the end-of-run (EOR), the inlet temperature must be increased (25-40°C) over start-of-run (SOR) inlet temperature in order to maintain enough activity for complete acetylene removal. In order to selectively hydrogenate acetylene to ethylene, it is critical to maintain the differential between the activation energies of reaction (eq.2.1) and (eq.2.2). However, it is desirable that the ethylene remains intact during hydrogenation. Once energy is supplied to the system over a given catalyst by increasing the temperature, the differential between the activation energies disappears and complete removal of acetylene, which generally has the lower partial pressure, becomes virtually impossible. In other words, higher temperature reduces selectivity; more hydrogen is used to convert ethylene to ethane, thereby increasing ethylene loss. The inlet temperature should therefore be kept as low as possible while still removing acetylene to specification requirements. Low temperatures minimise the two undesirable side reactions and help optimise the converter operation.

An additional essential parameter affecting the selectivity of the system is the ratio between hydrogen and acetylene ( $H_2:C_2H_2$ ). Hypothetically, the  $H_2:C_2H_2$  ratio would be 1:1, which would mean that no hydrogen would remain for the side reaction (eq.2.2) after acetylene hydrogenation (eq.2.1). However, in practice, the catalyst is not 100% selective and the  $H_2:C_2H_2$  ratio is usually higher than 1:1 to get complete conversion of the acetylene. As hydrogen is one of the reactants, the overall acetylene conversion will increase with increasing hydrogen concentration. Increase of the  $H_2:C_2H_2$  ratio from SOR to EOR can help offset the decline in catalyst activity with time on stream. However, this increased acetylene conversion with a higher  $H_2:C_2H_2$  ratio can have a cost in selectivity which leads to ethylene loss. Typically, the  $H_2:C_2H_2$  ratio is between 1.1 and 2.5 (Derrien *et al.*, 1986 and Molnár *et al.*, 2001).

The mechanism of acetylene hydrogenation involves four major paths as shown in Fig. 2.3. Path I is the partial hydrogenation of acetylene to ethylene, which is either desorbed as a gaseous product or further hydrogenated to ethane via Path II. It previously

was proposed that Path I proceeds mostly on Pd sites, which are covered to a great extent with acetylene under typical industrial reaction conditions, and Path II occurs on support sites, particularly those covered with polymer species.

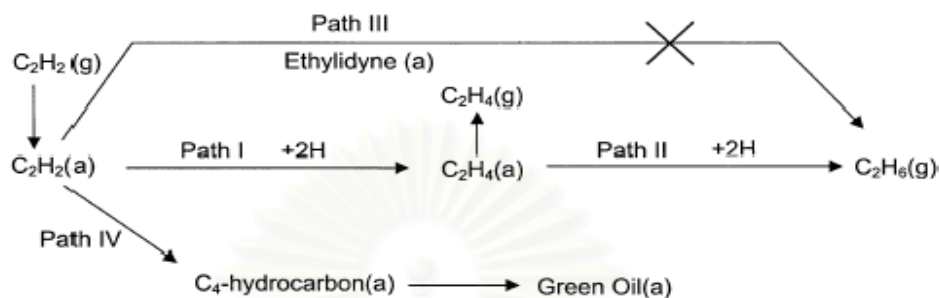


**Figure 2.5** Major reaction path of acetylene hydrogenation (Kang *et al.*, 2002)

Accordingly, selectivity may be improved by reducing both the strength of ethylene adsorption on Pd and the amount of polymer, which accumulates on the catalyst. One of the methods for improving selectivity is to maintain a low  $H_2$ /acetylene ratio in the reactant stream such that the low hydrogen concentration on Pd retards the full hydrogenation of the ethylenic species on the Pd surface. However, this method has the drawback of accelerating the polymer formation and therefore the  $H_2$ /acetylene ratio must be managed deliberately or sometimes controlled in two steps.

Path III, which allows for the direct full hydrogenation of acetylene, becomes negligible at high acetylene coverage and low hydrogen partial pressures. Ethyldyne was suggested as an intermediate in Path III but was later verified to be a simple spectator of surface reactions. Path IV, which allows for the dimerization of the  $C_2$  species, eventually leads to the production of green oil and the subsequent deactivation of the catalyst. Polymer formation lowers ethylene selectivity because it consumes acetylene without producing ethylene and, in addition, the polymer species, which is usually located on the support, acts as a hydrogen pool, thus promoting ethane formation (Kang *et al.*, 2002).

Considering the mechanism of acetylene hydrogenation described above, it was found that ethylene selectivity is improved when the C<sub>2</sub> species produced by Path I is readily desorbed from the catalyst surface and the other paths are simultaneously retarded.

In this study, the catalytic performance for selective hydrogenation of acetylene was evaluated in terms of activity for acetylene conversion and ethylene gain based on the following equation (2.1) and (2.2).

Activity of the catalyst for acetylene conversion is defined as moles of acetylene converted with respect to acetylene in the feed :

$$C_2H_2 \text{ conversion (\%)} = 100 \times \frac{\text{acetylene in feed} - \text{acetylene in product}}{\text{acetylene in feed}} \quad (i)$$

Ethylene gain is defined as the ratio of those parts of acetylene that are hydrogenated to ethylene to the amount of totally hydrogenated acetylene :

$$C_2H_4 \text{ gain (\%)} = 100 \times \frac{\text{acetylene hydrogenated to ethylene}}{\text{total hydrogenated acetylene}} \quad (ii)$$

Total hydrogenated acetylene is the difference between moles of acetylene in the product and in the feed ( $dC_2H_2$ ). In other works, acetylene hydrogenated to ethylene is the difference between the total hydrogenated acetylene ( $dC_2H_2$ ) and the ethylene loss by hydrogenation to ethane (eq.2.2). Regarding the difficulty in precise measurement of the ethylene change in the feed and product, the indirect calculation using the difference in the hydrogen amount (hydrogen consumed:  $dH_2$ ) was used.

The ethylene being hydrogenated to ethane is the difference between all the hydrogen consumed and all the acetylene totally hydrogenated.

$$C_2H_4 \text{ gain (\%)} = 100 \times \frac{[dC_2H_2 - (dH_2 - dC_2H_2)]}{dC_2H_2} \quad (iii)$$

As shown in equation (2.1) and (2.2), 2 moles of hydrogen were consumed for the acetylene lost to ethane, but only 1 mole of hydrogen for the acetylene gained as ethylene. The overall gain can also be written as:

$$\text{C}_2\text{H}_4 \text{ gain (\%)} = 100 \times \left[ 2 - \frac{d\text{H}_2}{d\text{C}_2\text{H}_2} \right] \quad (\text{iv})$$

Equation (iii) and (iv) are, of course the same, and ethylene gain discussed in this research is then calculated based on equation (iii). This value is the percentage of the theoretically possible ethylene gain which has been achieved in the operation. A positive value represents net production of ethylene while the negative value refers to ethylene loss. However, it should be noted that these calculations cannot provide a measure of acetylene polymerization reaction that forms green oil.

## 2.6 Milling/Grinding

Size reduction of particulate solids by milling is an essential unit operation in many industrial sectors such as chemical, metallurgy, pharmaceutical, nuclear and food. Recently, the increasing use of powders with particle sizes smaller than those achieved by conventional production methods emphasizes the importance of milling in powder. Compared with other methods, ball milling has the advantages of being a cheap method, simple process, presenting minimal environmental problems, convenient operation and absence of wastes. Energy absorbed by the material on impact may result in a modification of the particle surfaces by introducing dislocations, point defects, and other structural defects. This leads to materials with increased surface free energy, which makes them more reactive.

In many last years, mechanical processing is a novel technique for preparation of nanostructured materials. This includes vibratory ball mills, attrition mills, tumbler ball mills, and rod and hammer mills. A choice between these is determined by the end results required, and the chemical and physical properties of the powder.

Stirred-ball attrition mills are widely used for fine grinding of various materials in the industry as they are most efficient and effective in reducing particle size among

grinding media-based compression shear type mills. In addition, their superior advantages are the fast grinding, proficient temperature control and simple operation. The reduction of particle size by milling in liquids is a useful technique because fine grinding could be done effectively in wet atmosphere. It was found possible to reduce the grain size of particles to the nanometer range with the stirred-ball attrition mill. The feed material is comminuted among the moving media, the stirrer and the grinding chamber wall by friction, impact, and compression forces. The dominant breakage mechanism is based on the impact effect. Milling action is caused by a vertical rotating rod with horizontal arms or 'lifters' which stirs the balls causing them to lift up and fall back. There is thus a differential movement between the balls and the milled material, giving a high degree of surface contact. Milling, achieved by impact and shear forces, is very intensive because the force restoring the media downward is the weight of all media above it (PM technology focus, 1996).

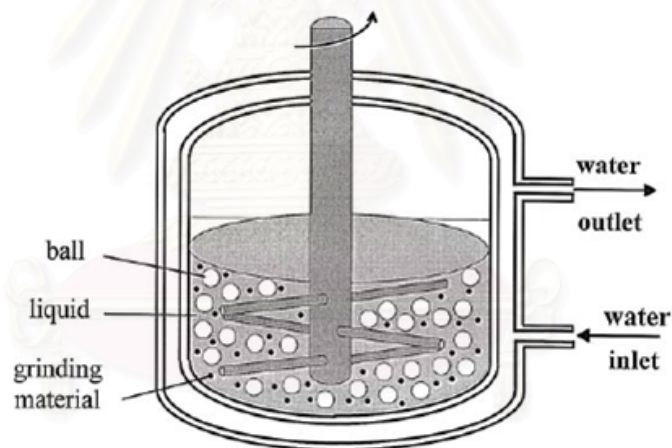


**Figure 2.6** Schematic drawing of laboratory stirred-ball mill (Shinohara *et al.*, 2002)

Currently, ball milling is used in a variety of applications, including dispersed alloy materials, metallic refinery, ore treatment, waste disposal, and synthesis of organic materials.

## CHAPTER III

### LITERATURE REVIEW

Selective hydrogenation of acetylene to ethylene is a well-known catalytic reaction used to purify ethylene feedstocks for the production of polyethylene. Typically, supported palladium catalyst is employed for this process due to its good activity and selectivity. Nevertheless, various factors have shown to affect the performance of Pd catalysts for the selective hydrogenation of acetylene such as preparation method, addition of a second metal. This chapter summarizes the recent reports on (3.1) supported Pd catalysts in selective hydrogenation reaction, (3.2) Ni-modified catalyst in selective hydrogenation reaction, (3.3) Zn-modified catalyst, and (3.4) mechanical activation. Comments on those previous studies which are given in section 3.5.

#### 3.1 Supported Pd catalyst in selective hydrogenation reaction

A. Sárkány *et al.* (1984) studied the hydrogenation of a mixture of 0.29 mole%  $C_2H_2$ , 0.44 mole%  $H_2$  and  $C_2H_4$  up to 100%, a so-call tail-end mixture, on palladium black and several Pd/ $Al_2O_3$  catalysts. Hydrogenation of  $C_2H_4$  increased with time on stream for all the  $Al_2O_3$ -supported catalysts; the opposite behaviour was noted with palladium black. Polymer formation was noted for all catalysts studied and also increased with time. It was recognized that a small number of  $C_2H_4$  hydrogenation sites were located on the metal but the majority were on the polymer-covered support. The authors proposed that  $C_2H_4$  adsorbed on the support and was hydrogenated there. Spillover hydrogen was tentatively identified as the source of hydrogen. Because of the parallelism between polymer formation and ethylene hydrogenation, it was proposed that the surface polymer served as a hydrogen pool or facilitated diffusion of hydrogen from Pd to the support.

B. K. Hodnett *et al.* (1986) studied that hydrogen spill-over is the deal of evidence used to suggest the surface-mobile species. It can play a role in catalytic reaction involving hydrogen. However, spill-over hydrogen is elusive, it has never been detected by physico-chemical means during catalysis. Therefore, it is difficult to determine the real role of this species in catalytic hydrogenation, hydrogenolysis and other hydrotreating reactions. The effects attributed to spill-over are usually chemical effect, e.g., hydrogenation by spill-over hydrogen of species adsorbed on a support, removal of carbonaceous deposits, occurrence or enhancement of a given reaction and, more generally, change in catalytic activity. These phenomena can be explained by invoking surface mobility and spill-over from one phase to another. The hydrogen spill-over phenomenon is described in Figure 3.1. Essentially, a hydrogen species is formed on one phase (usually a metal) and spilled over to react on the other phase.

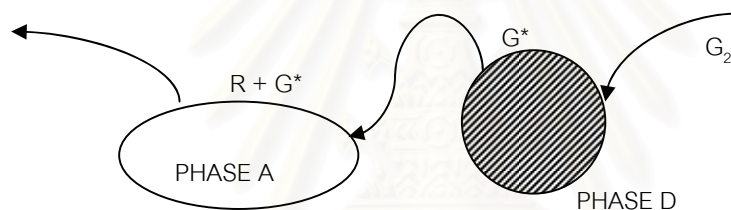


**Figure 3.1** Reaction between a species ( $G^*$ ), formed on phase D, and then transferred to phase A by spill-over and surface diffusion, where it reacts with an adsorbed molecule R. (re-drawn from B. K. Hodnett *et al.*, 1986)

S. Asplund (1996) studied the catalyst aging by coke formation for the selective hydrogenation of acetylene in excess ethylene on supported palladium catalyst. He found that the deposited coke have a substantial influence on the effective diffusivity, which decreased about one order of magnitude during 100 h of operation. He also observed the selectivity for the undesired ethane was higher on aged catalysts, while the activity was constant. However, these effects were strongly dependent on the catalyst particle size, although the behavior of fresh catalysts was unaffected by mass transfer limitations. When the catalyst was Pd/Al<sub>2</sub>O<sub>3</sub> the change in selectivity with aging could be explained as a consequence of the increased diffusion resistance. The mass transfer effects were important also on Pd/Al<sub>2</sub>O<sub>3</sub>, but on this catalyst there was an additional increase in ethane selectivity that could not be attributed to diffusion limitations. The coke was concentrated



towards the pellet periphery showing the influence of diffusion resistance also on the coke-forming reactions.

J. H. Kang *et al.* (2000) studied the effect of transition-metal oxides as promoters of the Pd catalyst for acetylene hydrogenation. Transition-metal oxides added to Pd/SiO<sub>2</sub> improve the activity and ethylene selectivity of the catalyst, which is caused by the interaction between oxides and the Pd surface similar to the case of the oxide-supported catalysts. They confirmed that metal oxide spread on and modify both geometrically and electronically the Pd surface after the catalyst is reduced at 500°C. They found that the oxide on the Pd surface retard the sintering of the dispersed Pd particles, suppresses adsorption of ethylene in multiply-bound mode, and facilitates desorption of ethylene produced in the reaction. Among the three metal oxides in this study, titanium oxide is found to have the most promotional effect.

E. W. Shin *et al.* (2002) studied the selectivity improvement over the supported Pd catalyst modified with Si, deposited on Pd by silane decomposition and oxidized in oxygen, by observing the adsorption and desorption behavior of acetylene, ethylene and hydrogen on the Pd surface. They reported that the adsorption strength of ethylene becomes weak and the amount of adsorbed hydrogen decreases when the Pd catalyst is modified. The Si modification also reduces the amounts of surface hydrocarbons deposited on the catalyst either during the temperature programmed desorption (TPD) of ethylene or during surface reactions. The hydrocarbon species deposited on the Si modified catalyst have shorter chain length than those produced on the Pd-only catalyst. These results are consistent with the improvement in ethylene selectivity on the Si-modified Pd catalyst.

W. J. Kim *et al.* (2003) studied the deactivation behavior of Si-modified Pd catalysts in acetylene hydrogenation. The TGA and IR analysis of green oil produced on the catalyst indicated that it was produced in smaller amounts and its average chain length was shorter on a Si-modified catalyst than on an unmodified one. These were due to deposition of Si on the Pd surface; such deposits effectively block multiply-coordinated adsorption sites on the catalyst and suppress the formation of green oil on the

catalyst surface, specifically on or in the vicinity of Pd. The Si species also retard the sintering of Pd crystallites during the regeneration step and slow down deactivation of the catalyst during the reaction, after regeneration. They suggested that the improvement in the deactivation behavior of the Si-modified catalyst was from the geometric modification of the Pd surface with small clusters of Si species.

A. Sárkány *et al.* (2003) synthesized Pd/SiO<sub>2</sub> (1.08 wt.%) catalyst via sol-derived route using poly (diallyldimethylammonium chloride) (PDDA) polycation as ionic stabiliser. The immobilized sol (monomer/Pd<sup>2+</sup> = 1.25) contains Pd particles of 3.1 nm. The immobilized sol showed good thermal stability but oxidation of PDDA to get “polymer free” sample causes sintering of Pd particles. They reported that the immobilized sample even in “as prepared state” possesses hydrogenation activity. Treatments at different temperatures in H<sub>2</sub> or Ar enhance the catalytic activity suggesting an increase in space around the metal particle. They suggested that the PDDA modified sample exhibits better competition selectivity than the “polymer free” sample pointing to surface structure variations caused by steric effects.

M. H. Chen *et al.* (2004) prepared the novel Pd/ $\alpha$ -Al<sub>2</sub>O<sub>3</sub> catalysts prepared by plasma method and investigated the influence of the preparation method, content of Pd active component, catalyst promoter and reaction temperature. They were found that the plasma processing exhibited the obvious advantages in catalytic performance at low temperature (<110°C). Compared to the samples prepared by conventional impregnation, the acetylene conversion of 100% with a selectivity of 71.3% for ethylene was obtained at 50°C over the plasma-prepared sample (0.15% Pd) on the palladium catalyst. This catalyst was stable during a test for more than 20 hours.

S. Aungkapipatanachai *et al.* (2005) studied the effect of regeneration of spent catalyst on the properties of Pd/Ag/Al<sub>2</sub>O<sub>3</sub> catalysts in selective hydrogenation of acetylene. The enhancement of the catalyst activity and ethylene selectivity by N<sub>2</sub>O pretreatment were found only for fresh catalysts. From characterization, the amounts of coke deposited on catalyst surface and oxygen concentration used in regeneration did not affect the metal active sites of recovered catalysts but change in morphology of surface

has been found. From the XRD results, palladium particle size was not changed after regeneration but particle size of silver was decreased since the Tamman temperature of silver was below regeneration temperature. In addition, CO-adsorption indicated that the increasing of metal active sites of Pd-Ag catalyst after N<sub>2</sub>O pretreatment was found in Pd-Ag catalyst prepared by sequential-impregnation. M, significant decrease of ethylene adsorbed on regenerated catalyst has been observed. They suggested that changes in the surface properties of Pd-Ag catalysts during regeneration made the catalysts not able to be activated by N<sub>2</sub>O pretreatment.

J. Wood *et al.* (2007) studied adsorption and hydrogenation of ethyne and ethene in ethyne hydrogenation reaction over: (1) a 0.02 wt.% Pd/ $\alpha$ -Al<sub>2</sub>O<sub>3</sub> catalyst and (2) a 2 wt.% Pd/ $\gamma$ -Al<sub>2</sub>O<sub>3</sub> catalyst using a flow switching experiment combined with diffuse reflectance infrared Fourier transform spectroscopy (DRIFTS) monitoring. During adsorption and hydrogenation of ethyne, a carbonaceous layer which has spectral features characteristic of octane, longer straight chain alkanes and green oil was formed on the catalyst surface but carbonaceous deposits were not observed during ethene adsorption under identical conditions. Hydrogen in the carbonaceous layer on the catalyst surface initially makes possible the hydrogenation of associatively adsorbed ethyne, which tends to form ethene rather than ethane. Upon heating the 2 wt.% catalyst to 200°C to remove hydrogen from the catalyst surface, then exposing it to ethyne, hydrogenation still occurred with more ethane production, suggesting that the carbonaceous layer was the more likely source of hydrogen. Less ethane was formed over the 0.02 wt.% Pd/ $\alpha$ -Al<sub>2</sub>O<sub>3</sub> catalyst compared with the 2 wt.% Pd/ $\gamma$ -Al<sub>2</sub>O<sub>3</sub>, as the former catalyst is designed to prevent hydrogenation to alkane through its low metal loading, optimal pore structure and Pd dispersion.

### 3.2 Industrial acetylene hydrogenation system

The acetylene hydrogenation reactor is typically a fixed bed catalytic reactor, normally operated adiabatically. There are also isothermal tubular reactors operated commercially. There are three major reactor configurations, i.e. the cracked gas train, the back-end and the front-end reactor. **Table 3.1** shows the typical feed compositions as the

function of reactor location (Kang *et al.*, 2002). Basically, acetylenes (inclusive of acetylene and methyl acetylene) in a naphtha cracker is higher than an ethane cracker.

**Table 3.1** Typical acetylene concentration in the feed gas and conversion rate (Walzl, 2002).

	Feedstock	Concentration (vol %)			Conversion Rate (%)		
		C <sub>2</sub> H <sub>2</sub>	C <sub>3</sub> H <sub>4</sub>	C <sub>4</sub> H <sub>6</sub>	C <sub>2</sub> H <sub>2</sub>	C <sub>3</sub> H <sub>4</sub>	C <sub>4</sub> H <sub>6</sub>
Back-end Hydrogenation	Naphtha	1.3	-	-	100	-	-
Front-end Hydrogenation (deethanizer)	Naphtha	0.61	-	-	100	-	-
Front-end Hydrogenation (depropanizer)	Naphtha	0.53	0.067	-	100	> 60	-
Raw Gas Hydrogenation	Ethane/ propane	0.3	0.13	0.85	100	> 60	> 90

- Raw gas catalytic hydrogenation reactors

In raw gas catalytic hydrogenation, the effluent of the cracked gas compressor, after minimal treatment, enters the acetylene converters for catalytic hydrogenation of the acetylene contained in the feed. Although the use of nickel catalysts has endured in this type of application, a progression to the use of the higher selective palladium technologies is occurring. In raw gas applications where the reactors precede the caustic tower, effective utilization of palladium catalyst is not possible without process modification. The feed in this case contains copious amounts of sulfur, which necessitate the use of supported, nickel-based catalysts. It has been suggested cobalt molybdate and Ni-Co-Cr catalysts to be used and steam to be added to improve the selectivity and inhibit the fouling of the catalyst (Miller, 1966).

- Commercial front-end and tail-end processes

There are two basic methods of selective hydrogenation of acetylene in ethylene-rich streams, the so-called front-end (**Figure 3.2**) and tail-end (**Figure 3.3**) processes (Derrien, 1986).

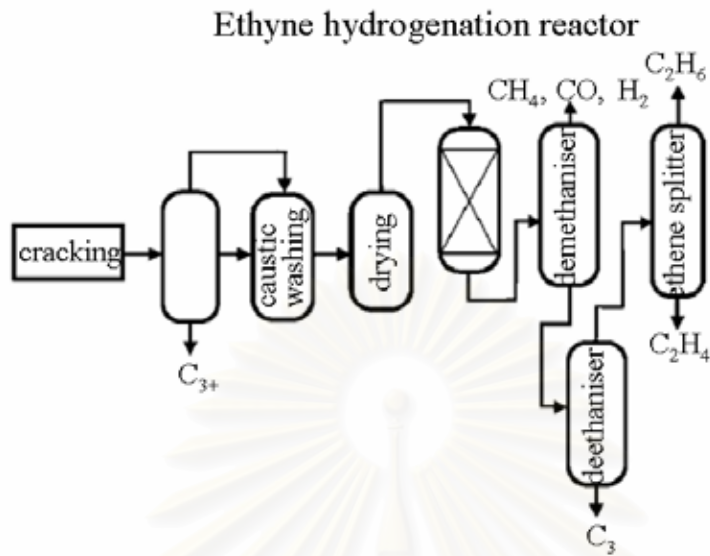


**Figure 3.2** Location of front-end acetylene hydrogenation reactors in a simplified scheme of downstream treatment of steam cracker effluents.

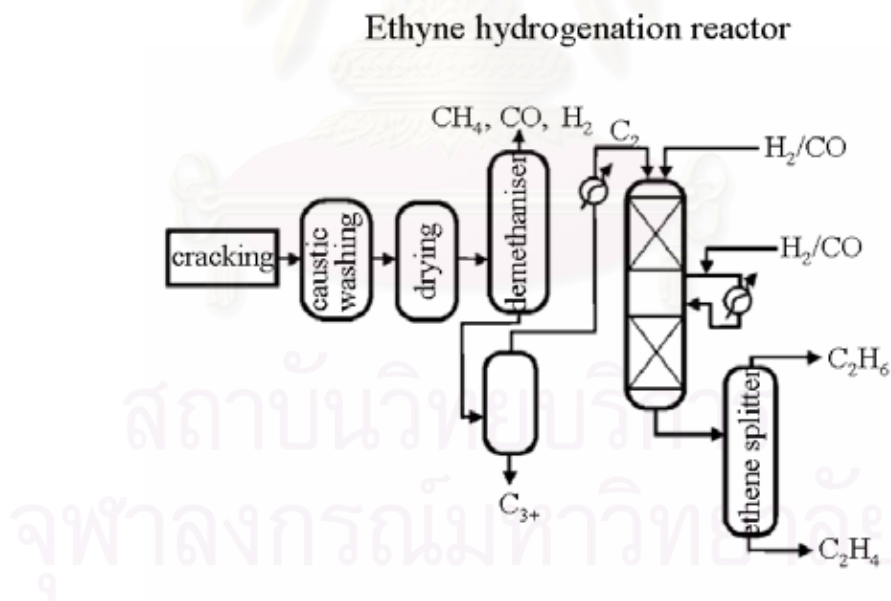


**Figure 3.3** Location of tail- and acetylene-hydrogenation reactors in a simplified scheme of downstream treatment of steam cracker effluents.

The methods differ in the location of the acetylene hydrogenation reactors (Chien *et al.*, 1982). In the tail-end method the reactors for acetylene hydrogenation are located after the demethanizer units, so the inlet hydrogenation stream mainly consists of C<sub>2</sub> hydrocarbons. Stoichiometric amounts of hydrogen with respect to acetylene are added to this C<sub>2</sub>-rich stream to ensure an optimal concentration of hydrogen in the reactor feed (1%-4% by volume). In some cases small amounts of carbon monoxide are also separately added to the inlet stream. In the front-end method the reactors for acetylene hydrogenation precede the demethanizer in the process. Consequently, the reactor feed contains typically 10-35 mol% of hydrogen, together with C<sub>2</sub> and lighter hydrocarbons. The comparison of the typical reactor feed compositions and the operating conditions for front-end and tail-end processes are shown in **Table 3.2**.

**Table 3.2** Typical feed composition to acetylene hydrogenation reactors and the operating conditions for front-end and tail-end processes.

	Front-end mole %	Tail-end mole %
Hydrogen (mole %)	22	2.4
Ethyne (mole %)	0.2	2
Ethene (mole %)	37	71
Methane (mole %)	12	—
Ethane (mole %)	28.4	25
Propene (mole %)	0.12	—
Carbon monoxide (ppm by vol.)	2800	40
H <sub>2</sub> /C <sub>2</sub> H <sub>2</sub> (inlet mol ratio)	110	1.5
Pressure (bar)	35	20
Temperature (K)	343	333
Space velocity (m <sup>3</sup> m <sub>cat.</sub> <sup>-3</sup> h <sup>-1</sup> )	2000	3000

### 3.3 Ni-modified catalyst in selective hydrogenation reaction

J. A. Pena (1995) studied Ni/NiAl<sub>2</sub>O<sub>4</sub> catalyst for the hydrogenation of acetylene to ethylene and ethane. They reported the evolution of activity and selectivity and coke behavior. These studies have been carried out on fresh catalyst and on catalyst samples subjected to an accelerated thermal aging process. The results show that the catalytic activity increases with time on stream (activation period), until a point is reached in

which catalyst deactivation predominates (deactivation period). They also found that a few coking/regeneration cycles are enough to cause significant changes in the kinetic behavior of the catalyst. These changes are selective in nature and decrease the coke formation rate, while increasing the total observed rates of hydrogenation to ethane and ethylene. The net rate of active site generation is higher for the aged catalyst, and a faster apparent activation rate is obtained. Also, because of the lower deactivation rate, a greater number of active sites are present when the activation and deactivation rate are balanced, and therefore higher maximum hydrogenation yields are obtained with the aged catalyst.

J. C. Rodriguez *et al.* (1997) studied the influence of zinc addition on the catalytic performance and physicochemical properties of nickel-based catalyst used in selective hydrogenation of acetylene were investigated. They found that the activity and selectivity to ethylene of the nickel-based catalysts were positively modified by incorporation of zinc into their solid structure. The zinc-modified catalysts produced smaller amounts of coke and methane than those not containing zinc. Coke deposition had a strong effect on the ethylene selectivity. However, this influence was much more significant for zinc-modified catalysts than for non modified nickel-based solids. They also found that the case of zinc-modified catalyst, the metal nickel phase was interacting strongly and highly interdispersed in a non stoichiometric zinc aluminate spinel matrix. The high interdispersion of the metal nickel phase diminished the number of three-nickel-atom arrangements necessary for the formation of surface intermediates that led to coke and methane production. The non modified nickel-based solids, however, were composed of large metal crystallites on which coke and methane precursors of large metal crystallites on which coke and methane precursors were very easily formed. The high interaction between metal nickel particles and the zinc aluminate matrix prevented whisker formation to some extent. The low concentration of acid sites on the solid surface considerably reduced amorphous-like coke deposition.

V. Rives *et al.* (1998) studied Ni-containing catalysts for selective acetylene hydrogenation to ethylene have been prepared by controlled calcination of hydrotalcite-like precursors. They also found that in addition to Ni and Al, Cr and Zn were added to improve the catalytic performance. Despite addition of Zn hinders coke formation, the

activity to gaseous products decreased as the Ni content is increased. An increase in coke concentration increases activity and selectivity to ethylene, especially in those samples with not too high Ni contents. The highest selectivity to ethylene is achieved for Zn/Ni = 4 (molar ratio).

C. Guimon *et al.* (2003) studied the effect of the support (silica and silica-alumina) and of the composition of Ni-based hydrogenation catalyst. They found that silica has very weak interactions with the metal. The pre-reduction induces a non-negligible sintering for the samples with high Ni content, and thus the formation of large size crystallites. The addition of alumina to silica leads to the existence of two types of Ni<sup>2+</sup> crystallites, one presenting strong interaction with the support, the other with very weak interaction (or none). The amount of the latter increases with the Ni content. This addition has a positive effect on the formation of coke. The TPO experiment showed the existence of at least three types of coke, ordering them according to their oxidability, filamentous carbon, amorphous coke, and strongly adsorbed hydrogenated carbon. The formation of the latter is facilitated by the acidity of silica-alumina, while filamentous carbon is generated by the sites with weak metal-support interactions and amorphous coke is formed by those with strong metal-support interactions. Although the production of coke is relatively high in the case of Ni/SiO<sub>2</sub>, it does not alter the desired selectivity to ethylene. On the contrary, for Ni/SiO<sub>2</sub>-Al<sub>2</sub>O<sub>3</sub> catalysts with high Ni contents, it improves the initial selectivity because the coke deactivates the hydrogenolytic sites which are active for the side reactions (production of saturated hydrocarbons), while the hydrogenating sites, active for the main reaction, should be covered by a monolayer of ethylidene that is a precursor of ethane.

N. Wongwaranon *et al.* (2008) studied the effect of nickel modified alumina supported Pd catalysts using sol-gel and solvothermal methods on catalytic performances for selective acetylene hydrogenation. They suggested that these catalysts were superior to Pd- supported on commercial  $\alpha$ -Al<sub>2</sub>O<sub>3</sub>. For the sol-gel-made samples, when Ni/Al ratio was 1, the highest ethylene selectivity was achieved whereas for the solvothermal-made samples, the ethylene selectivity was obtained when Ni/Al was 0.3. For the same Ni/Al (0.5), ethylene selectivity of the sol-gel-made samples was higher than



solvothermal-made. The XRD analysis indicated that varying Ni/Al ratio directly affected the crystalline phase of alumina and formation of nickel-alumina compounds. Moreover, incorporation of Ni atoms into  $\alpha$ -Al<sub>2</sub>O<sub>3</sub> resulted in a decrease of acid sites on the alumina hence reducing coke deposition on the catalyst surface. They suggested that the formation of NiAl<sub>2</sub>O<sub>4</sub> could modify the properties of Pd surface so that high ethylene selectivity was obtained.

Y. Shu *et al.* (2008) studied the effect of impregnation sequence on the formation of Pt/Ni bimetallic nanoparticles supported on  $\gamma$ -Al<sub>2</sub>O<sub>3</sub>, and hydrogenation activity and selectivity of these catalysts. These bimetallic catalysts were prepared with a fixed Pt loading (5 wt.%). The bimetallic Pt/Ni catalysts showed higher activity toward the disproportionation of cyclohexene and higher selectivity toward the acetylene hydrogenation than Pt/ $\gamma$ -Al<sub>2</sub>O<sub>3</sub> or Ni/ $\gamma$ -Al<sub>2</sub>O<sub>3</sub>. For catalysts with the Pt/Ni ratio of 3/1 (5 wt.% Pt, 0.5 wt.% Ni), the Pt-first catalyst, Ni-Pt/ $\gamma$ -Al<sub>2</sub>O<sub>3</sub>, showed higher activity than the Ni-first catalyst, Pt-Ni/ $\gamma$ -Al<sub>2</sub>O<sub>3</sub>. EXAFS measurements show the formation of Pt–Ni bimetallic bonds on the former but not on the latter catalyst. However, one possible explanation of this result is the diffusion of Ni into the cavities of the  $\gamma$ -Al<sub>2</sub>O<sub>3</sub> support when the Ni<sup>2+</sup> ion is deposited first. The effect of impregnation sequence to the catalytic activity for the disproportionation of cyclohexene was not as significant for catalysts with the Pt/Ni ratio of 1/1 (5 wt.% Pt, 1.5 wt.% Ni); though, EXAFS studies reveal the formation of Pt–Ni bonds in both catalysts.

### 3.4 Zn-modified catalyst

M.A. Valenzuela *et al.* (1997) studied the effect of preparation method (sol-gel, wet mixing or coprecipitation) on the surface structure of zinc aluminate and the addition of calcium or tin in order to modify the spinel surface. It was indicated that coprecipitated and sol-gel prepared ZnAl<sub>2</sub>O<sub>4</sub> were found to be present spinel structure. If calcium was added during synthesis, it was found to be deposited on top of the spinel surface. However, tin was added, the surface of ZnAl<sub>2</sub>O<sub>4</sub> was reconstructed. These aluminates were impregnated with platinum and tested in the isobutane dehydrogenation.

M.A. Valenzuela *et al.* (1997) also synthesized  $\text{ZnAl}_2\text{O}_4$  by hydrolyzing a mixture of aluminum alkoxide with zinc nitrate dissolved in hexylene glycol and calcining at  $800^\circ\text{C}$ . The results were compared with those obtained by wet mixing and coprecipitation. From the characteristic, it was suggested that the sol-gel synthesis provided a solid adequate to be used as a catalyst support because of its high surface area and monomodal pore size distribution. Furthermore, surface area and pore size distribution could be alter on purpose modifying the synthesis parameters.

M. Zawadzki *et al.* (2000) studied the hydrothermal synthesis of nanoporous zinc aluminate with high surface. Hydrothermal treatment at low temperatures was proposed for obtaining a nanocrystalline zinc aluminate spinel of interesting properties from catalytic point of view, including high specific surface area (up to  $340 \text{ m}^2/\text{g}$ ), nanoporosity, and narrow pore size distribution. The precursors for hydrothermal synthesis were basic aluminium nitrate having the empirical formula  $\text{Al}_2(\text{OH})_{6-x}(\text{NO}_3)_x$  wherein  $x$  was equal or closed to 1, and hydrated zinc acetate. The proposed synthesis, in contrast to other methods, did not require a high temperature calcination to obtain the spinel phase. The properties of hydrothermally obtained zinc aluminate spinel made them an advanced material suitable for use in catalytic or high-tech ceramic applications.

J. Wrzyszczyk *et al.* (2001) synthesized zinc aluminate from zinc acetate and different aluminium sources (basic aluminium nitrate or aluminium hydroxide) using hydrothermal method. They were indicated that the textural properties of the prepared  $\text{ZnAl}_2\text{O}_4$  samples were different from these one of the zinc aluminate prepared by conventional way. Surface area as well as mean pore radius of hydrothermal zinc aluminate can be controlled by the use of various aluminium compounds and zinc salt for the synthesis at relatively low temperature. From XRD and TEM analysis revealed that samples were single-phase material or mixture of  $\text{ZnAl}_2\text{O}_4$  with small amount of  $\gamma\text{-Al}_2\text{O}_3$ , with morphology of quasi-spherical shape. Applied method of synthesis, in contrast to other methods, did not require the high temperature calcination to obtain the spinel phase and provided an attractive alternative to method of zinc aluminate preparation.

A. Kanyanucharat *et al.* (2002) studied  $\text{CoAl}_2\text{O}_4$ ,  $\text{ZnAl}_2\text{O}_4$  and  $\text{NiAl}_2\text{O}_4$  by solvothermal method using toluene as a solvent at various reaction temperatures with the molar ratio 0.5. They found that the synthesis and calcination temperature affected the thermal stability of metal aluminate spinels. There was change in crystallite size and surface area. The varying of divalent ions in tetrahedral sites of metal aluminate spinels affected the thermal stability in the order of  $\text{NiAl}_2\text{O}_4 > \text{CoAl}_2\text{O}_4 > \text{ZnAl}_2\text{O}_4$ . That was the result of the difference in bond dissociation energy of metal oxides and cation distribution over sites with tetrahedral coordination in the spinel type structure.

X. Wei *et al.* (2006) studied nanosized  $\text{ZnAl}_2\text{O}_4$  spinel by sol-gel technique. Nanosized  $\text{ZnAl}_2\text{O}_4$  spinel has been obtained by the thermal decomposition of Zn–Al gel using oxalic acid as a chelating agent and calcination at different temperatures. From XRD, showed that the sample obtained by heating the precursor at  $700^\circ\text{C}$  for 5 hours was single-phase cubic material having the spinel-type structure, confirmed by IR. The particle size was 15–20 nm. And the specific surface area was  $58 \text{ m}^2 \text{ g}^{-1}$ .

### 3.5 Mechanical activation

T. Tsuchida and K. Horigome (1995) studied the effect of grinding on the thermal decomposition of alumina monohydrates. Two boehmites and a diasporite were ground in a planetary ball mill. The XRD patterns showed that the intensity decreases as the grinding time increases. Most of the amorphous phase obtained by 24 h grinding of boehmites was estimated to be hydrated alumina on the basis of  $^{27}\text{Al}$  MAS-NMR spectra, which presented appearance of an  $\text{Al}_{\text{tot}}$  line. The amorphous alumina can be expected to be more reactive and adsorb water molecules, which leads to an increase in the total weight loss. Finally, the formation of amorphized particles led to a lowering of the temperature of dehydration and  $\alpha$ -transformation. In conclusion, after 24 h of grinding, the boehmites changed to an amorphous hydrated alumina, part of which transformed to alumina by an additional mechanochemical dehydration. It was proved that the mechanochemical dehydration of diasporite did not occur. It is considered that such a structural similarity between diasporite and  $\alpha\text{-Al}_2\text{O}_3$  caused a topotactic transformation at a temperature as low as  $510^\circ\text{C}$ .

S. Andonova *et al.* (2006) studied the effect of mechanical–chemical activation (MCA) of Co–Mo/ $\gamma$ -Al<sub>2</sub>O<sub>3</sub> and Ni–Mo/ $\gamma$ -Al<sub>2</sub>O<sub>3</sub> catalysts for thiophene hydrodesulfurization (HDS). The MCA of 7 h has been done in a planet-ball mill. The results show that the rate of thiophene decomposition using the mechano-chemically-activated catalysts is about twice higher than the activity of the non-treated catalysts. The applied MCA caused a partial amorphization of the active components, deposited on the support, a decrease in the average particle size, separation and partial migration of the supported phase. Moreover, the activation led to redistribution of the Mo<sup>6+</sup> ions on the surface of the catalysts, whereupon the share of the Mo<sup>6+</sup> ions, involved in the formation of the superficial Ni(Co)–Mo–O phase, is increased.

D. Andreeva *et al.* (2007) studied influence of the preparation method on nanosized gold catalysts supported on ceria and ceria-alumina for WGS reaction. For the synthesis of the mixed ceria-alumina support two methods were applied—a new method of mechanochemical activation and ceria washcoating on alumina. Gold catalysts on ceria-alumina, prepared by mechanochemical activation show a high and stable WGS activity. The results confirm about the active Au<sup>δ+</sup> V<sub>o</sub> Ce<sup>3+</sup> complex and the existence of an optimum ratio between Ce<sup>3+</sup>, oxygen vacancies and positively charged nanosized gold particles. Under the influence of reactants in the course of redox reaction the active complex is being changed because of the electron transfer between gold and ceria through oxygen vacancies. The addition of alumina as a structural promoter prevents the agglomeration of both gold and ceria nanoparticles.

F. Karimzadeh *et al.* (2008) studied the synthesis and characterization of Zn/Al<sub>2</sub>O<sub>3</sub> nanocomposite by mechanical alloying. Aluminum and zinc oxide powder mixture was milled in a planetary ball mill. The zinc oxide was found to be reduced by Al through a rapid self-sustaining combustion reaction process. As a result, a zinc matrix composite reinforced by Al<sub>2</sub>O<sub>3</sub> particulate was formed. The microhardness value of produced nanocomposite powder after 5 h milling was 10–15 times higher than the microhardness of pure zinc. After milling for longer times, almost all the initial amorphous Al<sub>2</sub>O<sub>3</sub> are agglomerated to form large powder particles. In final stage of milling, Zn achieved a crystallite size of about 20 nm estimated with XRD.

M. Tavoosi *et al.* (2008) studied the fabrication of Al–Zn/ $\alpha$ -Al<sub>2</sub>O<sub>3</sub> nanocomposite by mechanical alloying. Aluminum and zinc oxide powders mixture milled by a planetary ball mill in order to produce Al–13.8 wt.% Zn/5 vol.%  $\alpha$ -Al<sub>2</sub>O<sub>3</sub> nanocomposite. The crystallite size of Al matrix in nanocomposite is about 40 nm. The results showed that milling of 60 h led to displacement reaction of the zinc oxide and aluminum to produce Zn and Al<sub>2</sub>O<sub>3</sub> phases. The milled powder had a microstructure consisting of nanosized Al<sub>2</sub>O<sub>3</sub> particles, which were very small and have low crystallinity structure (amorphous structure) and constructed of stacked, in an Al–Zn solid solution. During annealing the perfect crystalline structure of Al<sub>2</sub>O<sub>3</sub> was formed. Microhardness of this nanocomposite was found to be about 190 HV. This increase in microhardness can be due to the formation Al–Zn solid solution, reduction of crystallite size and formation of Al<sub>2</sub>O<sub>3</sub> particle in matrix.

### **3.6 Comments on previous studies**

From the previous studies, it was found that the commonly used support for palladium is  $\alpha$ -Al<sub>2</sub>O<sub>3</sub>. The selectivity of ethylene over palladium catalysts during selective hydrogenation of acetylene can be increased by promotion with a second metal to Pd catalyst, modification of alumina support for palladium catalyst, using different supports and pretreatment catalyst with O<sub>2</sub> and/or O<sub>2</sub>-containing compounds. Mechanical treatment has shown beneficial effect on catalytic performance in other catalytic reactions. Moreover, formation of Ni–Zn–Al mixed oxides showed high resistant to deactivation by coking. Therefore, it is interesting to study the effect of grinding of alumina and alumina mixed oxides on the properties of supported Pd catalysts in selective hydrogenation of acetylene. Mechanical treatment of supports or catalysts can provide beneficial effect due to their good properties such as high surface area, low average particle size, and suitable phase.

## CHAPTER IV

### EXPERIMENTAL

#### 4.1 Chemicals

The chemicals used in this experiment are specified as follows:

1. Aluminium oxide (99.7%) available from Sumitomo, Japan.
2. Palladium (II) nitrate hydrate from Aldrich.
3. Nickel oxide (99.8%) available from Aldrich.
4. Zinc oxide (99.0%+) available from Ajax Finechem Pty Ltd.

#### 4.2 Catalyst Preparation

##### 4.2.1 Preparation of $\text{Al}_2\text{O}_3$ by grinding method

About 100 gram of powder was ground in an attrition mill for 14 hours, using alumina balls as grinding media and 300 ml of water as solvent. Alumina balls were filled to a half volume of the milling pot. The mixture was collected every 4 hours and dried at  $105^\circ\text{C}$  overnight in an oven to remove the water.

##### 4.2.2 Palladium loading

0.3 wt% Pd over grinding  $\alpha\text{-Al}_2\text{O}_3$  supports were prepared by the incipient impregnation technique detailed as follow:

1. grinding  $\alpha\text{-Al}_2\text{O}_3$  supports were impregnated with a solution of palladium by the incipient wetness technique. Using the water capacity measurement obtained previously for grinding  $\alpha\text{-Al}_2\text{O}_3$  particles, a sufficient amount of the palladium salt was added to obtain a 0.3% weight of palladium.

2. The impregnated support was left to stand for 6 hours to assure adequate distribution of metal complex. The support was subsequently dried at 110°C in air overnight.

3. The dried impregnated support was calcined under 60 mL/min nitrogen with the heating rate of 10°C/min until the temperature reached 500°C. A 100 mL/min of flowing air was then switched into the reactor to replace nitrogen and the temperature was held at 500°C for 2 hours.

4. The calcined sample was finally cooled down and stored in a glass bottle for later use.

### **4.3 Catalyst Characterization**

#### 4.3.1 X-ray diffraction (XRD)

XRD was performed to determine the bulk phase of catalysts by SIEMENS D 5000 X-ray diffractometer using  $\text{CuK}_\alpha$  radiation with Ni filter in the  $2\theta$  range of 20-80 degrees resolution 0.04°. The crystallite size was calculated from Scherrer's equation.

#### 4.3.2 $\text{N}_2$ Physisorption

Surface area measurements were carried out by low temperature nitrogen adsorption in a Micromeritic ChemiSorb 2750 system. Calculations were performed on the basis of the BET isotherm. 0.2 grams of sample was loaded into u-shape cell made from Pyrex and heated in helium to 200°C for 1 hour in order to eliminate trace amount of water adsorbed on surface, then cooled down to room temperature. The analysis gas consist of 30%  $\text{N}_2$  in helium was introduced to Pyrex cell. Sample adsorbed nitrogen at low temperature by dipped cell into liquid nitrogen dewar until it's surface was saturated with nitrogen and desorped nitrogen at room temperature at room temperature by moved away the dewar. The nitrogen that was desorbed from sample was measure by TCD detector.

#### 4.3.3 CO-Pulse Chemisorption

Metal active sites and metal dispersion were determined by pulsing carbon monoxide over the reduced catalyst. The amounts of CO chemisorbed on the catalysts were measured using a Micromeritic Chemisorb 2750 automated system attached with ChemiSoft TPx software at room temperature. The number of metal active sites was measured in the basis assumption that only one CO molecule adsorbed on one metal active site (Vannice *et al.*, 1981; Anderson *et al.*, 1995; Ali *et al.*, 1998 and Mahata *et al.*, 2000).

Approximately 0.1 grams of catalyst was filled in a Pyrex tube, incorporated in a temperature-controlled oven and connected to a thermal conductivity detector (TCD). He was introduced into the reactor at the flow rate of 30 ml/min in order to remove remaining air. Prior to chemisorption, the samples were reduced in a H<sub>2</sub> flow rate at 50 ml/min with heated at an increasing rate of 10°C/min from room temperature to 500°C and held at this temperature for 2 hours after that cooled down to ambient temperature in a He flow, then CO was pulsed into the catalyst bed at room temperature. Carbon monoxide that was not adsorbed was measured using thermal conductivity detector. Pulsing was continued until no further carbon monoxide adsorption was observed.

#### 4.3.4 NH<sub>3</sub>-Temperature Programmed Desorption (TPD)

Temperature programmed desorption (TPD) study of NH<sub>3</sub> was performed in a Micromeritic ChemiSorb 2750 automated system attached with ChemiSoft TPx software. The amount of NH<sub>3</sub> adsorbed on the surface was determined by temperature programmed desorption. The thermal conductivity detector was used to measure the amount of NH<sub>3</sub>

Approximately 0.1 grams of sample was placed in a quartz tube in a temperature-controlled oven. Helium gas with flow rate at 15 ml/min was released to flow through sample. The sample was heated from room temperature to 200°C with a heating rate of 10°C/min and held for 1 hour. Then, the sample was cooled down to 40°C. In the next step, 15 vol% ammonium gas with flow rate at 20 ml/min flowed through sample instead of helium, and hold for 30 minutes. Adsorption of 15 vol% ammonium on the catalyst



surface occurred in this step. Consequently, helium gas at the same flowed through our sample instead of ammonium and also holds for another hour. In the final step which was the desorption step; sample was heated from 40°C to 650°C with a heating rate of 10°C/min. The signal from this step was recorded every second and reported on a microcomputer.

#### 4.3.5 X-ray photoelectron spectroscopy (XPS)

The XPS analysis was performed originally using an AMICUS spectrometer equipped with a Mg K<sub>α</sub> X-ray radiation. For a typical analysis, the source was operated at voltage of 20 kV and current of 10 mA. The pressure in the analysis chamber was less than 10<sup>-5</sup> Pa. The AMICUS system is computer controlled using the AMICUS “VISION 2” software.

#### 4.3.6 Transmission Electron Microscopy (TEM)

The palladium oxide particle size and distribution of palladium on alumina supported will be observed using JEOL-JEM 200CX transmission electron microscope operated at 100kV.

#### 4.3.7 Laser Diffraction Particle Size Analysis

The particle size distributions of the milled powders were performed by means of a laser diffraction granulometer (Malvern Mastersizer). The proportion of each particle class in the sample was expressed as number percentage. The average size, *d*<sub>50</sub>, corresponding to a cumulative frequency of 50%, was also determined.

#### 4.3.8 Electron Spin Resonance (ESR)

ESR was performed to determine the defect of surface catalysts by JEOL model JES-RE2X at the Scientific and Technological Research Equipment Center, Chulalongkorn University (STREC)

#### 4.3.9 Thermal Gravimetric Analysis (TGA)

Thermal gravimetric analysis (TGA) and differential thermal analysis (DTA) were performed using an SDT Analyzer Model Q600 from TA Instruments, USA. The TGA/DTA analysis of the spent catalysts were carried out from room temperature to 1000°C at a heating rate of 5°C/min in oxygen.

#### 4.4 Reaction study in selective acetylene hydrogenation

Selective acetylene hydrogenation was performed in a Pyrex tube reactor. Feed gas was composed of 1.5% C<sub>2</sub>H<sub>2</sub>, 1.7% H<sub>2</sub> and balanced C<sub>2</sub>H<sub>4</sub>. The composition of product and feed stream were analyzed by a Shimadzu GC 8A equipped with TCD and FID detectors (molecular sieve-5A and carbosieve S-II columns, respectively). The operating conditions for each instrument are summarized in Table 4.1.

**Table 4.1** Operating conditions of gas chromatograph

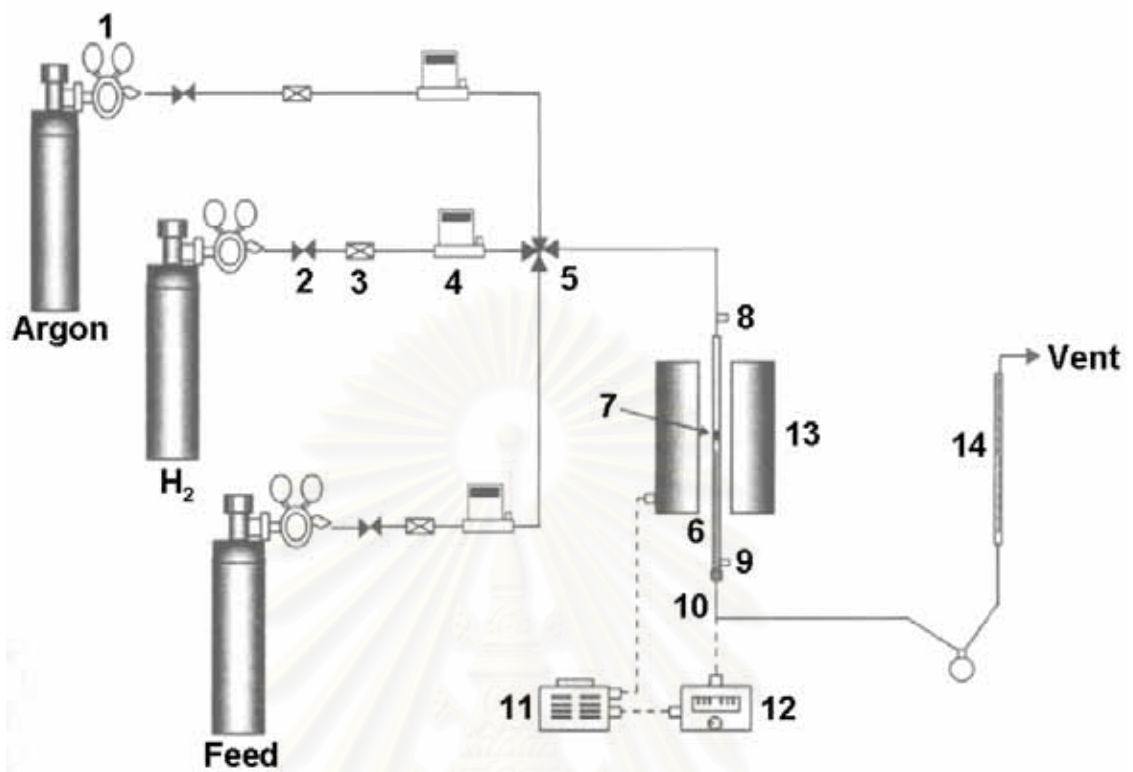
Gas Chromatograph	SHIMADZU FID GC 9A	SHIMADZU TCD GC 8A
Detector	FID	TCD
Packed column	Carbosieve column S-II	Molecular sieve 5A
Carrier gas	Ultra high purity N <sub>2</sub>	Ultra high purity Ar
Carrier gas flow rate (ml/min)	30	30
Injector temperature (°C)	185	80
Detector temperature (°C)	185	80
Initial column temperature	100	50
Initial holding time (min)	50	-
Programmed rate (°C/min)	10	-
Final column temperature (°C)	160	50
Final holding time (min)	160	-
Current (mA)	-	70
Analyzed gas	CH <sub>4</sub> , C <sub>2</sub> H <sub>2</sub> , C <sub>2</sub> H <sub>4</sub> , C <sub>2</sub> H <sub>6</sub>	H <sub>2</sub>

Approximately 0.15 grams of catalyst was packed in a Pyrex tubular down flow reactor. The catalyst bed length was about 0.3 cm. The reactor was placed into the furnace and argon was introduced into the reactor in order to remove remaining air. Prior to reaction, the catalyst was reduced with 100 ml/min hydrogen flow at a temperature of 150°C and held at that temperature for 2 hours. Afterwards, argon was switched in to replace hydrogen for cooling down to the reaction temperature, 40°C and to remove the remaining hydrogen.

The reactant was introduced at elevated temperature from 40°C to 120°C (40 60 80 100 and 120°C), 1 atm and flowed 40 ml/min, sampling was undertaken when the steady state of the system was reached, which was approximately within 2 h. Effluent gases were sampled to analyze the concentration of CH<sub>4</sub>, C<sub>2</sub>H<sub>2</sub>, C<sub>2</sub>H<sub>4</sub> and C<sub>2</sub>H<sub>6</sub> using GC-9A equipped with a carbosieve S-II column, whereas H<sub>2</sub> concentration was analyzed by GC-8A equipped with a molecular sieve 5A column. System of acetylene hydrogenation is shown in Figure 4.1.



สถาบันวิทยบริการ  
จุฬาลงกรณ์มหาวิทยาลัย



- |                         |                                  |
|-------------------------|----------------------------------|
| 1. pressure regular     | 8. sampling point (feed)         |
| 2. on-off valve         | 9. sampling point (product)      |
| 3. filter               | 10. thermocouple                 |
| 4. mass flow controller | 11. variable voltage transformer |
| 5. 4-ways fitting       | 12. Temperature controller       |
| 6. reactor              | 13. electric furnace             |
| 7. catalyst bed         | 14. bubble flow meter            |

**Figure 4.1** A schematic of acetylene hydrogenation system

สถาบันวิทยบริการ  
จุฬาลงกรณ์มหาวิทยาลัย

## CHAPTER V

### RESULTS AND DISCUSSION

The main topic of this study involves an attempt to investigate the characteristics and catalytic properties of the Pd catalysts supported on milled  $\text{Al}_2\text{O}_3$  and NiO-, ZnO- and Zn- modified  $\text{Al}_2\text{O}_3$  with various molar ratio of Ni/Al and Zn/Al (0.1 and 0.5) prepared by milling method in selective acetylene hydrogenation in excess ethylene. In this chapter, the experimental results and discussion are described. The results in this chapter are divided into three major parts. The first part describes the effect of milled  $\text{Al}_2\text{O}_3$  on the properties of Pd/ $\text{Al}_2\text{O}_3$  catalysts. The second part describes the effect of mixed oxides (ZnO- $\text{Al}_2\text{O}_3$  and NiO- $\text{Al}_2\text{O}_3$ ) on the properties of Pd/ $\text{Al}_2\text{O}_3$  catalysts. The other part describes the effect of alumina grinding and mixed oxides (ZnO- $\text{Al}_2\text{O}_3$  and NiO- $\text{Al}_2\text{O}_3$ ) grinding on the properties of Pd/ $\text{Al}_2\text{O}_3$  catalysts.

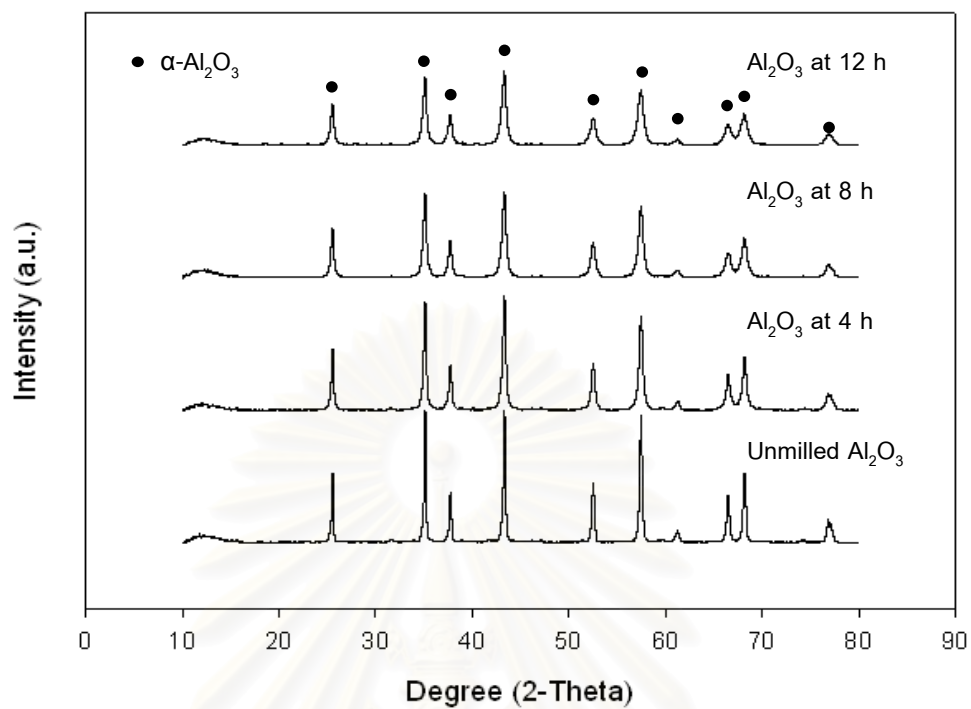
#### 5.1 Milled $\text{Al}_2\text{O}_3$ Supported Pd Catalyst

For nomenclature of the samples, the samples of unmilled  $\text{Al}_2\text{O}_3$ , milled  $\text{Al}_2\text{O}_3$  at various time 4, 8, 12 h with an attrition ball mill were named as ,  $\text{Al}_2\text{O}_3$  at 4 h,  $\text{Al}_2\text{O}_3$  at 8 h, and  $\text{Al}_2\text{O}_3$  at 12 h, respectively. Pd catalysts supported on the corresponding unmilled  $\text{Al}_2\text{O}_3$  and milled  $\text{Al}_2\text{O}_3$  were called as Pd/unmilled  $\text{Al}_2\text{O}_3$ , Pd/  $\text{Al}_2\text{O}_3$  at 4 h, Pd/ $\text{Al}_2\text{O}_3$  at 8 h and Pd/ $\text{Al}_2\text{O}_3$  at 12 h, respectively.

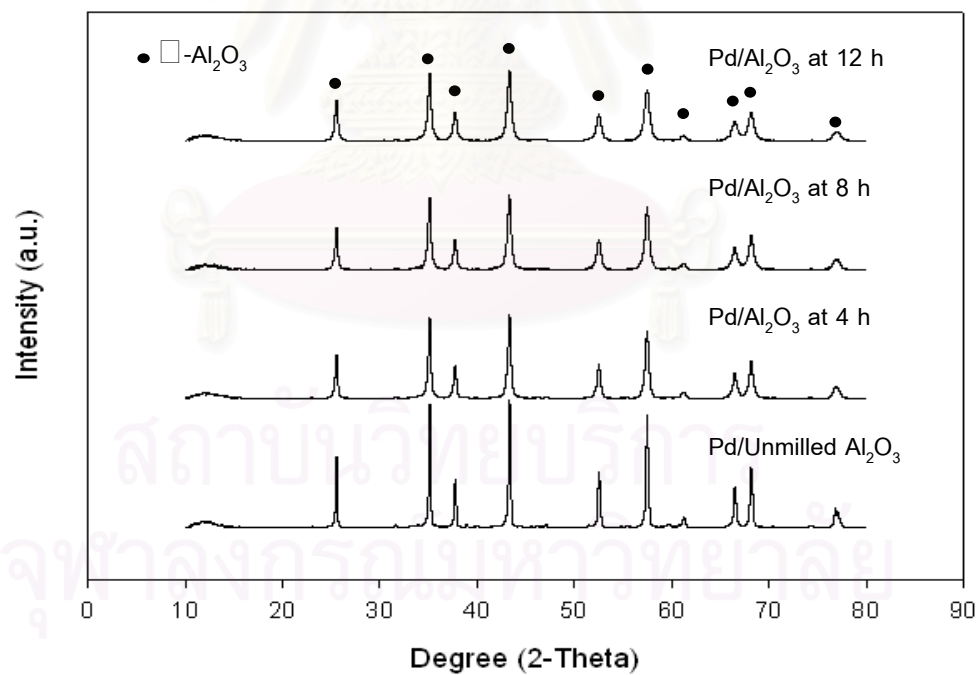
##### 5.1.1 Characterization of the Catalysts

###### 5.1.1.1 X-ray Diffraction (XRD)

Material structures and chemical phase composition were characterized by X-ray diffraction technique because of its qualitative and nondestructive analysis. The phase identification is carried out on the basis of data from X-ray diffraction. The XRD patterns of  $\text{Al}_2\text{O}_3$  milled at various time with an attrition ball mill are shown in Figure 5.1.



(A)



(B)

**Figure 5.1** The XRD patterns of (A)  $\alpha$ - $\text{Al}_2\text{O}_3$  supports milled at various time and (B) Pd/ $\alpha$ - $\text{Al}_2\text{O}_3$  catalysts.

The Al<sub>2</sub>O<sub>3</sub> supports milled at various time with an attrition ball mill exhibited similar XRD characteristic peaks. The characteristic peaks of  $\alpha$ -Al<sub>2</sub>O<sub>3</sub> structure were appeared at 25.52°, 35.10°, 37.74°, 43.32°, 52.52°, 57.46°, 61.22°, 66.50°, 68.18°, and 77.86° 2 $\theta$  (Mekasuwandumrong *et al.*,2006). For Pd/ $\alpha$ -Al<sub>2</sub>O<sub>3</sub> catalysts, only the characteristic peaks of  $\alpha$ -Al<sub>2</sub>O<sub>3</sub> were detected and the characteristic peaks associated with PdO were not found. This was probably due to low amount of Pd present or the Pd was highly dispersed on the Al<sub>2</sub>O<sub>3</sub>. As evident from XRD analysis, diffraction lines of both Al<sub>2</sub>O<sub>3</sub> supports and Pd/ $\alpha$ -Al<sub>2</sub>O<sub>3</sub> catalysts gradually decreased and the width of the intensity broadened with increasing milling time indicating the decreasing amount of crystal areas and increasing lattice deformations due to the enormous stresses acting on the particles during milling process (Stenger *et al.*,2005).

#### 5.1.1.2 Average Crystallite Size

The average crystallite sizes of  $\alpha$ -Al<sub>2</sub>O<sub>3</sub> phase were calculated from the Scherrer equation using the XRD major peak at 2 $\theta$ =43.32°. The crystallite size of the  $\alpha$ -Al<sub>2</sub>O<sub>3</sub> supports milled at various time and Pd/ $\alpha$ -Al<sub>2</sub>O<sub>3</sub> catalysts are shown in Table 5.1

**Table 5.1** The average crystallite sizes of  $\alpha$ -Al<sub>2</sub>O<sub>3</sub> supports milled at various time and Pd/ $\alpha$ -Al<sub>2</sub>O<sub>3</sub> catalysts.

Sample	Crystallite size(nm)	
	Support	Catalyst
Pd/unmilled Al <sub>2</sub> O <sub>3</sub>	146	n.d.
Pd/Al <sub>2</sub> O <sub>3</sub> at 4 h	32	34
Pd/Al <sub>2</sub> O <sub>3</sub> at 8 h	21	24
Pd/Al <sub>2</sub> O <sub>3</sub> at 12 h	18	22

n.d. : not determined

As the milling time increased, crystallite size of  $\alpha$ -Al<sub>2</sub>O<sub>3</sub> decreased. The results were in accordance to those reported by Bodaghi *et al.* that there was a decrease in the crystallite size of  $\alpha$ -Al<sub>2</sub>O<sub>3</sub> powder during the mechanical activation (Bodaghi *et al.*,2009). According to Scherrer equation, crystallite size of milling supports was reduced from about 0.15  $\mu$ m to nanometer size in the range of 18-32 nm. For the catalysts, the average crystallite sizes were presented in term of  $\alpha$ -Al<sub>2</sub>O<sub>3</sub>. The average crystallite size of the Pd/unmilled Al<sub>2</sub>O<sub>3</sub> catalyst was not determined due to its relatively large crystallite size over the calculation range. In case of Pd/milled Al<sub>2</sub>O<sub>3</sub> catalysts, the average crystallite sizes were ranged from 22-34 nm. It was obvious that the average crystallite sizes of Pd/Al<sub>2</sub>O<sub>3</sub> catalysts were bigger than those of  $\alpha$ -Al<sub>2</sub>O<sub>3</sub> supports due to heat treatment during calcinations process at 500°C.

#### 5.1.1.3 BET Surface Areas

The most common procedure for determining surface area of a solid is based on adsorption and condensation of nitrogen at liquid nitrogen temperature using static vacuum procedure. This method is also called BET (Brunauer Emmett Teller) method. The BET surface areas of the  $\alpha$ -Al<sub>2</sub>O<sub>3</sub> supports and Pd/ $\alpha$ -Al<sub>2</sub>O<sub>3</sub> catalysts are shown in Table 5.2.

**Table 5.2** BET surface areas of  $\alpha$ -Al<sub>2</sub>O<sub>3</sub> supports milled at various time and Pd/ $\alpha$ -Al<sub>2</sub>O<sub>3</sub> catalysts.

Sample	BET Surface Support	areas (m <sup>2</sup> /g) Catalyst
Pd/unmilled Al <sub>2</sub> O <sub>3</sub>	0.9	1.0
Pd/Al <sub>2</sub> O <sub>3</sub> at 4 h	4.8	6.2
Pd/Al <sub>2</sub> O <sub>3</sub> at 8 h	11.7	11.2
Pd/Al <sub>2</sub> O <sub>3</sub> at 12 h	15.7	16.0

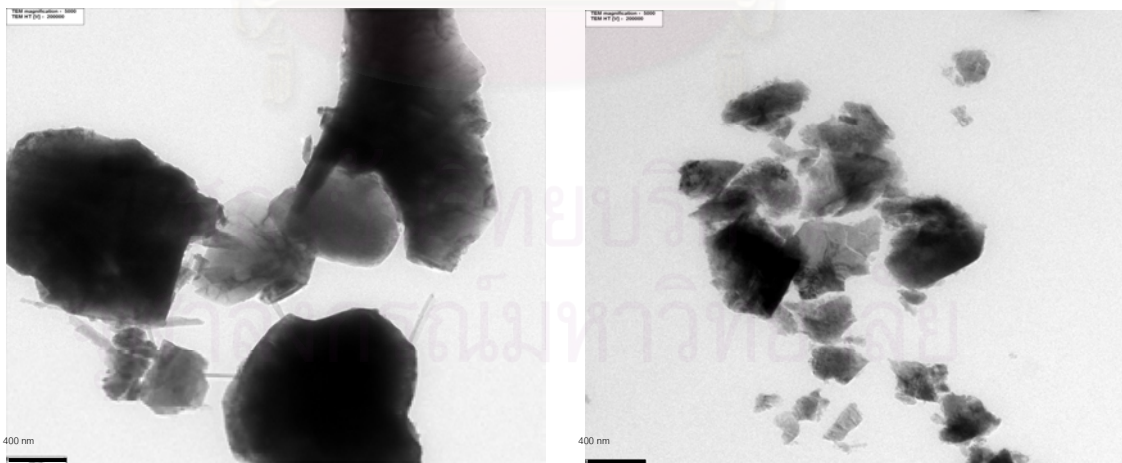


The surface areas of the  $\alpha$ -Al<sub>2</sub>O<sub>3</sub> supports milled at various time were ranged from 0.9-15.7 m<sup>2</sup>/g while Pd/ $\alpha$ -Al<sub>2</sub>O<sub>3</sub> catalysts were ranged from 1.0-16.0 m<sup>2</sup>/g. Corresponding to the experiment, milling  $\alpha$ -Al<sub>2</sub>O<sub>3</sub> supports at various time significantly affect the surface areas of the resulting samples. Furthermore it has been reported that the specific surface area decreased with increasing milling time (Karagedov *et al.*,1999). After Pd loading by the impregnation method, the surface areas of Pd/ $\alpha$ -Al<sub>2</sub>O<sub>3</sub> catalysts were quite similar to the  $\alpha$ -Al<sub>2</sub>O<sub>3</sub> supports. Such results indicate most of the Pd were deposited on the external surface of  $\alpha$ -Al<sub>2</sub>O<sub>3</sub> supports.

#### 5.1.1.4 Transmission Electron Microscopy (TEM)

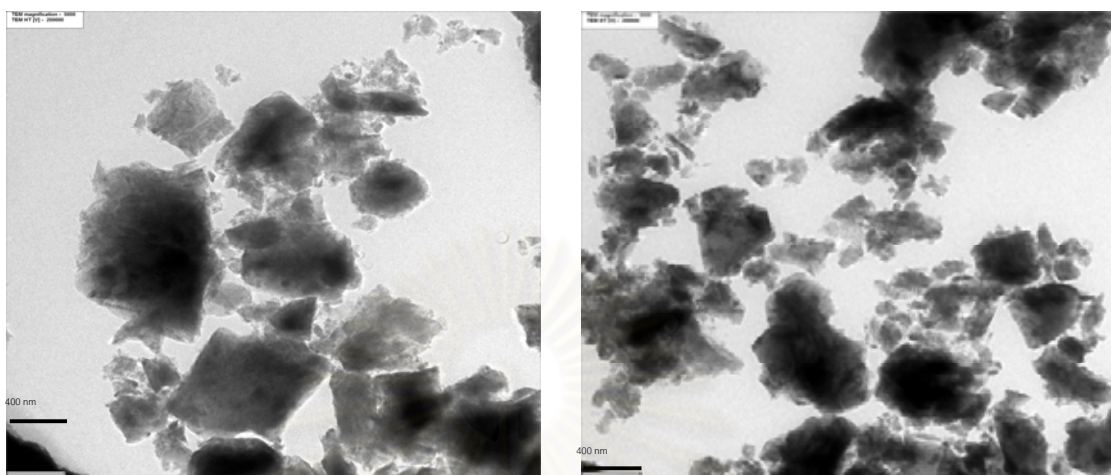
TEM is a useful tool for measuring particle size and particle size distribution of supported metals. TEM micrographs of  $\alpha$ -Al<sub>2</sub>O<sub>3</sub> supports milled at various time are shown in Figure 5.2.

It can be seen that the  $\alpha$ -Al<sub>2</sub>O<sub>3</sub> supports milled at various time consisted of agglomerated particles with primarily irregular shape structure. Based on TEM analysis, crystallite size of  $\alpha$ -Al<sub>2</sub>O<sub>3</sub> supports decreased as the milling time increased. Moreover, the particle size distribution of the milled Al<sub>2</sub>O<sub>3</sub> was more uniform.



(A) unmilled Al<sub>2</sub>O<sub>3</sub>

(B) Al<sub>2</sub>O<sub>3</sub> at 4 h



(C) Al<sub>2</sub>O<sub>3</sub> at 8 h

(D) Al<sub>2</sub>O<sub>3</sub> at 12 h

**Figure 5.2** TEM micrographs of  $\alpha$ -Al<sub>2</sub>O<sub>3</sub> supports milled at various time.

#### 5.1.1.5 Metal Active Sites

The metal active sites, the Pd dispersion, and the average Pd metal particle size from CO chemisorption experiments are summarized in Table 5.3. The technique is based on the assumption that only one CO molecule adsorbed on one metal active site (Anderson *et al.*,1985). It is also known that CO did not chemisorb on Al<sub>2</sub>O<sub>3</sub> support (Soma-Noto *et al.*,1974, Cormack *et al.*,1975, and Heinrichs *et al.*,1997). The details for calculation of the metal active sites, the Pd dispersion, and the average Pd metal particle size are given in Appendix C.

Without milling of the Al<sub>2</sub>O<sub>3</sub> supports, Pd/ $\alpha$ -Al<sub>2</sub>O<sub>3</sub> possessed the amounts of Pd active sites  $13.1 \times 10^{17}$  sites/g cat. The Pd active sites significantly increased when the catalysts were supported on milled Al<sub>2</sub>O<sub>3</sub> corresponding to the increasing in Pd metal dispersion and decreasing in the average Pd metal particle sizes. The average Pd metal particle sizes for the catalysts were ranged from 3-13 nm.

**Table 5.3** Results from CO chemisorption of Pd supported on  $\alpha$ -Al<sub>2</sub>O<sub>3</sub> milled at various time.

Sample	CO chemisorption $\times 10^{17}$ (molecule CO/g cat.)	Pd dispersion (%)	d <sub>P</sub> Pd <sup>0</sup> (nm)
Pd/unmilled Al <sub>2</sub> O <sub>3</sub>	13.1	8.7	13
Pd/Al <sub>2</sub> O <sub>3</sub> at 4 h	14.4	10.6	11
Pd/Al <sub>2</sub> O <sub>3</sub> at 8 h	23.0	16.5	7
Pd/Al <sub>2</sub> O <sub>3</sub> at 12 h	46.9	32.3	3

#### 5.1.1.6 NH<sub>3</sub> Temperature Programmed Desorption (NH<sub>3</sub>-TPD)

NH<sub>3</sub> temperature program desorption was a commonly used technique for determining surface acid sites. The strength of an acid site could be related to the corresponding desorption temperature, while the total amount of ammonia desorption after saturation coverage permits quantification of the number of acid sites at the surface (Kung *et al.*,1985). The temperature-programmed desorption profiles for the  $\alpha$ -Al<sub>2</sub>O<sub>3</sub> supports milled at various time are shown in Figure 5.3.

The desorption peak areas of all the supports showed relatively lower acidity than other 'transition' alumina (Chinayon *et al.*,2008). For unmilled Al<sub>2</sub>O<sub>3</sub>, only one distinctive peak at ca. 120°C was observed and the profile became nearly flat. However, three desorption peaks corresponding to different acid sites could be observed at ca. 120, 320 and 520°C for milled samples. The low-temperature and high-temperature peak represented the ammonia desorbed from the weaker acid sites, whereas the medium-temperature peak represented the ammonia desorbed from the stronger acid sites. From experimental, it was found that the all desorption peak area of the Al<sub>2</sub>O<sub>3</sub> samples prepared by milling method were higher as the milling time was longer indicating milling process enhances the catalyst acidity and acid strength. The results are in good agreement with

those reported by other researchers. For examples, Onoda (Onoda *et al.*, 2008) reported that the acid sites of  $\text{Cu}_2\text{P}_4\text{O}_{12}$  milled for several minutes increased by mechanical treatment.

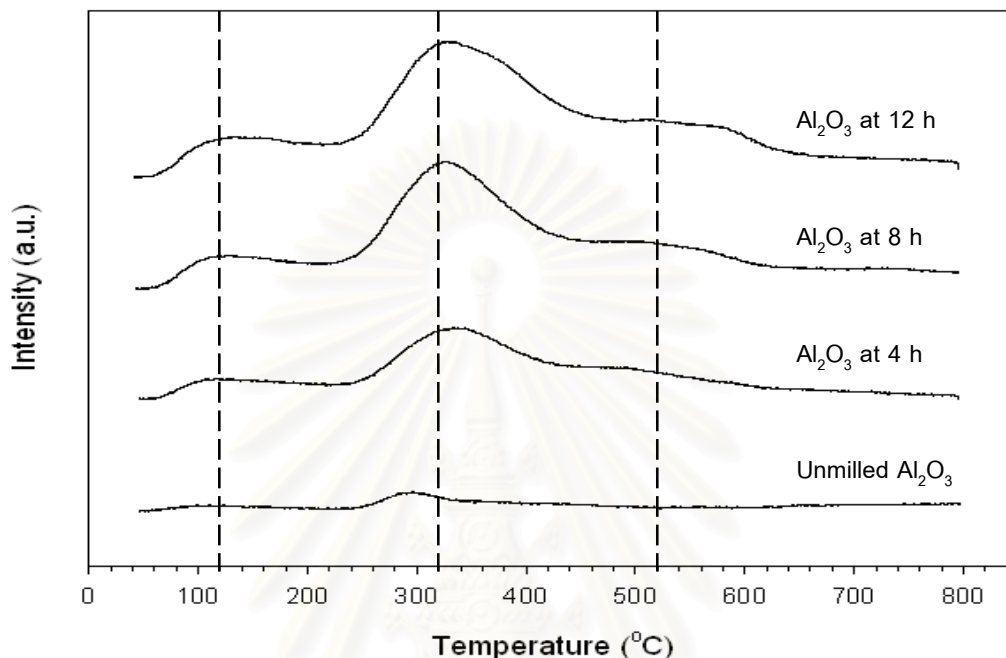


**Figure 5.3**  $\text{NH}_3$  temperature programmed desorption of  $\alpha\text{-Al}_2\text{O}_3$  milled at various time.

#### 5.1.1.7 Laser Diffraction

The particle size distributions of milled powders were performed by means of a laser diffraction. This method could not exactly measure size distributions below 50 nm. The particle size distribution of  $\text{Al}_2\text{O}_3$  milled at various time with an attrition ball mill are presented in Figure 5.4.

Initially, the sample had a wide size distribution centred on 1.55  $\mu\text{m}$ . During the first 8 h of milling, the size distributions shifted towards the left. This led to a rapid decrease of the mean size during this period. Then, the evolution of the distributions was lower, and so was the mean size decrease. Finally, the mean size leveled off around 62 nm, and all the particles had a size lower than 120 nm. These results are in agreement with that of Zapata-Massot and Bolay. They have shown that during milling, the

evolution of the distributions of carbon nanotubes is lower, and the mean size decreased (Zapata-Massot and Bolay., 2008).

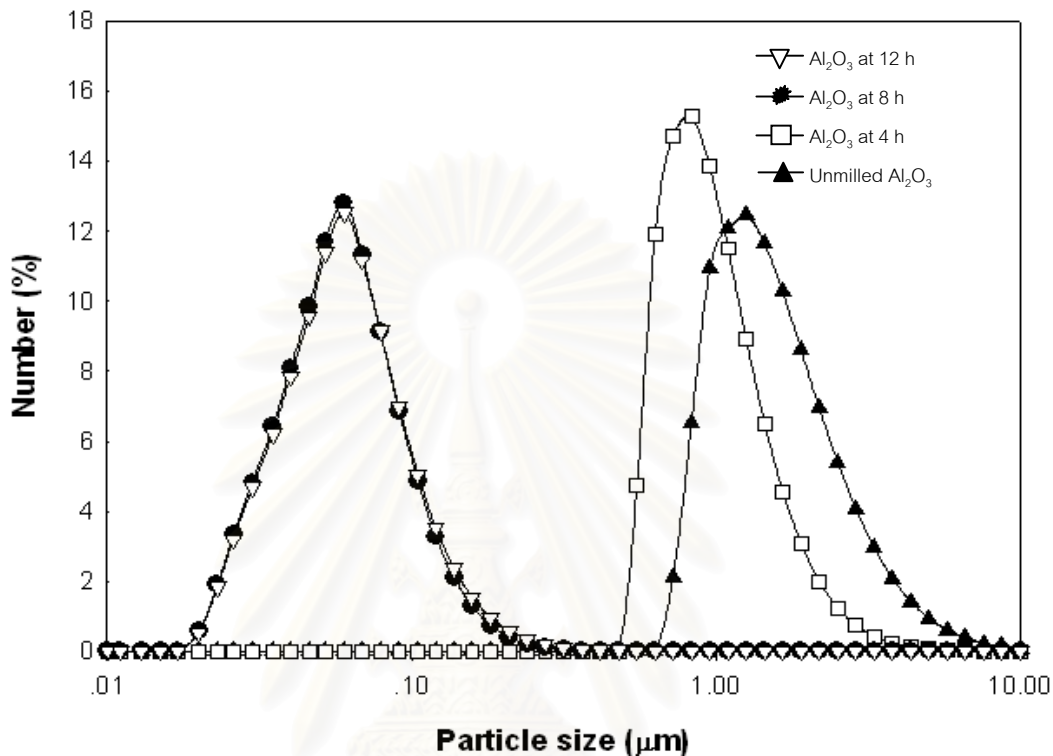


**Figure 5.4** The particle size distribution of Al<sub>2</sub>O<sub>3</sub> milled at various time.

#### 5.1.1.9 X-ray Photoelectron Spectroscopy (XPS)

Surface compositions of the catalysts and interaction between metal and supports were analyzed using a Kratos Amicus X-ray photoelectron spectroscopy. A survey scan was performed in order to determine the elements on the catalyst surface. The elemental scan was carried out for C 1s, O 1s, Al 2p and Pd 3d. Binding energies of each element was calibrated internally with carbon C 1s identified at 285.0 eV. (J. Guillot *et al.*, 2001). Photoemission peak areas are determined by using a linear routine. Deconvolution of complex spectra are done by fitting with Gaussian (70%)–Lorentzian (30%) shapes using a VISION 2 software equipped with the XPS system. The deconvoluted XPS photoelectron spectra for the Pd 3d core level region of all the catalysts are shown in Figure 5.5.

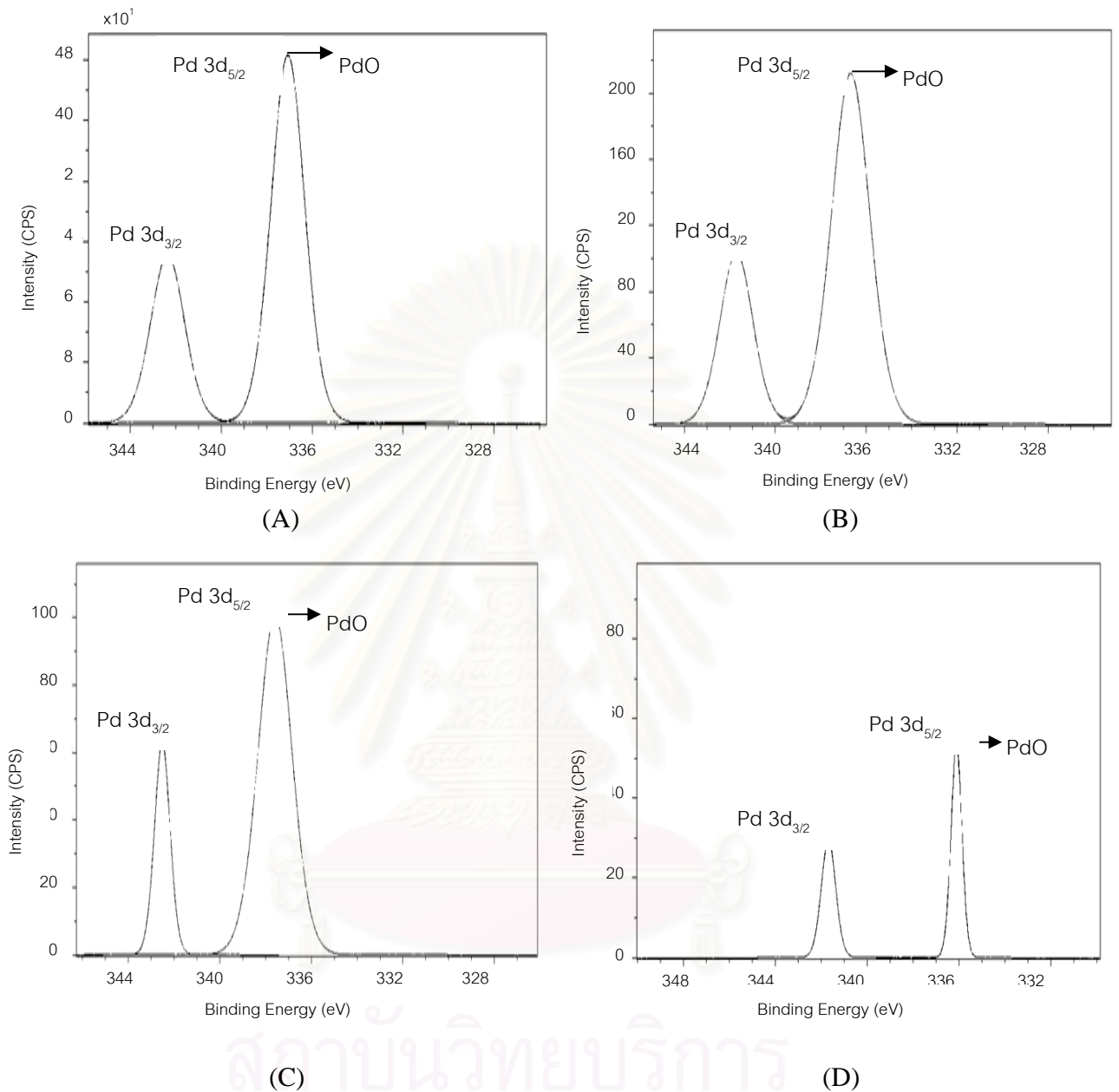


**Figure 5.5** XPS results for the Pd 3d core level region of (A) unmilled  $\text{Al}_2\text{O}_3$  (B)  $\text{Al}_2\text{O}_3$  at 4 h (C)  $\text{Al}_2\text{O}_3$  at 8 h and (D)  $\text{Al}_2\text{O}_3$  at 12 h

From the figure, the Pd doublet was clearly evident. PdO species was observed at the binding energies in the range of 336.1–337.6 eV which was consistent to the values reported by P. Legare (P. Legare *et al.*, 1989). The binding energy and atomic concentration are also given in Table 5.4. The Pd/Al ratios were found to be range from

0.001-0.021 which was very low. It is suggested that large amount of palladium existed on the outside of the support surface and not in the pores. The atomic concentration ratios for Pd/Al decreased with the increase of milling time. The results were consistent with the CO chemisorption results that larger Pd particle sizes were obtained on unmilled Al<sub>2</sub>O<sub>3</sub>. Furthermore, the binding energies of Pd 3d of all catalysts were not significantly different. These results indicate that there was no interaction between Pd and Al<sub>2</sub>O<sub>3</sub> supports.

**Table 5.4** Atomic concentrations of catalysts from XPS

Sample	Binding energy (eV)			Atomic conc. %		Atomic ratio
	Pd 3d	Al 2p	O 1s	Pd 3d	Al 2p	
Pd/unmilled Al <sub>2</sub> O <sub>3</sub>	337.1	74.0	531.2	0.58	27.68	0.021
Pd/Al <sub>2</sub> O <sub>3</sub> at 4 h	336.7	74.2	531.3	0.20	26.97	0.007
Pd/Al <sub>2</sub> O <sub>3</sub> at 8 h	337.6	75.1	532.2	0.09	21.25	0.004
Pd/Al <sub>2</sub> O <sub>3</sub> at 12 h	336.1	n.d.	n.d.	0.02	26.98	0.001

#### 5.1.1.8 Electron spin resonance spectroscopy (ESR)

Electron spin resonance technique is a selective and sensitive technique for studying chemical species that have one or more unpaired electrons, such as organic and inorganic free radicals or inorganic complexes possessing a transition metal ion. The ESR results are shown in Figure 5.6.

Within 12 h of milling, two different groups of paramagnetic centres can be observed and identified as two different spectral responses of Fe<sup>3+</sup> ions. The two groups of Fe<sup>3+</sup> species are: (i) Fe<sup>3+</sup> points defects, representing the typical crystalline parts of the Al<sub>2</sub>O<sub>3</sub> matrix (signals at g'=5.2 and g'=2) and (ii) Fe<sup>3+</sup> ions in amorphous parts, represented by the characteristic signal at g'=4.3 (Scholz *et al.*, 2001).

It was found that the signals of  $\text{Fe}^{3+}$  ions in the crystalline parts of  $\text{Al}_2\text{O}_3$  (signals at  $g'=5.2$  and  $g'=2$ ) decreased in intensity with increasing milling time. After milling of even 4 h, a small signal at  $g'=4.3$  representing  $\text{Fe}^{3+}$  ions in amorphous parts was appeared. This signal enlarged with increasing milling time. According to the results, it is suggested that  $\text{Fe}^{3+}$  metal incorporated in the supports can act as sensitive reaction centres offering local structural changes of supports.

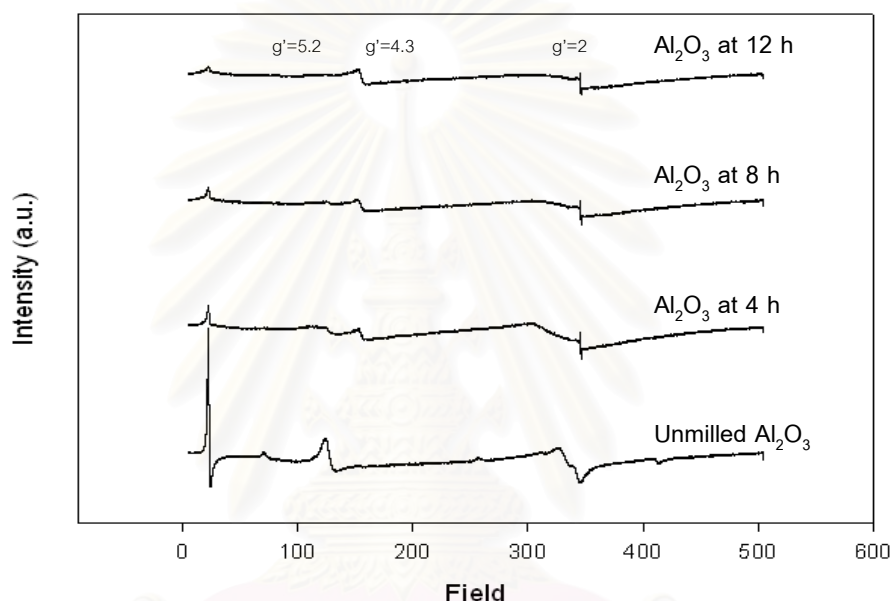


**Figure 5.6** ESR spectra of  $\text{Al}_2\text{O}_3$  milled at various time.

### 5.1.2 Catalytic Performance of the Catalysts

The performance of a catalyst for the selective hydrogenation of acetylene is evaluated in terms of acetylene conversion and selectivity towards ethylene. Acetylene conversion is defined as moles of acetylene converted with respect to acetylene in the feed. Selectivity is the ratio of the amount of acetylene converted to ethylene and total amount of acetylene converted. Ideally, there should be one acetylene molecule converted to ethylene for every hydrogen molecule consumed, or 100% selectivity, since all of the acetylene is converted into ethylene. In actual practice, some hydrogen will always be consumed in the side reaction of ethylene conversion to ethane. The selectivity in term of ethylene gain could also be measured by looking at the hydrogen consumed in



the converter and the amount of acetylene converted. The performances of the catalysts in this study, were therefore reported in terms of acetylene conversion and ethylene gain observed from hydrogen and acetylene concentrations.

Typically, the normal operating temperature in an acetylene converter lies in the range 65-85°C (Derrien *et al.*,1986 and Molnár *et al.*,2001). During start-up, the reaction can proceed at as low as 45°C. After a short period during which the catalyst has stabilized, the reactor temperature would reach the normal operating range and remain constant throughout its life-time. In a brief initial period (0-2 min on stream), the reaction is rapid forming both ethylene and ethane. In the second phase (2-60 min on stream), the rates of acetylene consumption, and ethylene and ethane production are all constant. During this period, hydrogenation of acetylene is the primary reaction. The selectivity is usually high, and is the characteristic of changes occurring in the catalyst. The third phase begins when acetylene hydrogenation is nearly complete and in this region approximates to the industrial situation. As previously described, the reaction during 2-60 min on stream is in the constant rate period, consequently, the performance of the catalyst as a function of reaction temperature is evaluated from the data taken in this period.

The catalytic properties of Pd/milled Al<sub>2</sub>O<sub>3</sub> catalysts were evaluated in the selective hydrogenation of acetylene using a fixed bed flow reactor with a GHSV of 16901 h<sup>-1</sup>. For study of temperature dependence of the catalysts on acetylene conversion and selectivity toward ethylene, the temperature range between 40-120°C and feed gas composed of 1.5% C<sub>2</sub>H<sub>2</sub>, 1.7% H<sub>2</sub>, and balanced C<sub>2</sub>H<sub>4</sub> (TIG Co., Ltd.) were used

As shown in Figure 5.7., activity of all the catalysts directly increased with rising temperature as the kinetic energy of the system increased with increasing temperature. All the Pd/milled Al<sub>2</sub>O<sub>3</sub> catalysts exhibited higher activity than that of the Pd/unmilled Al<sub>2</sub>O<sub>3</sub> catalyst and Pd/Al<sub>2</sub>O<sub>3</sub> at 12 h showed the highest activity.

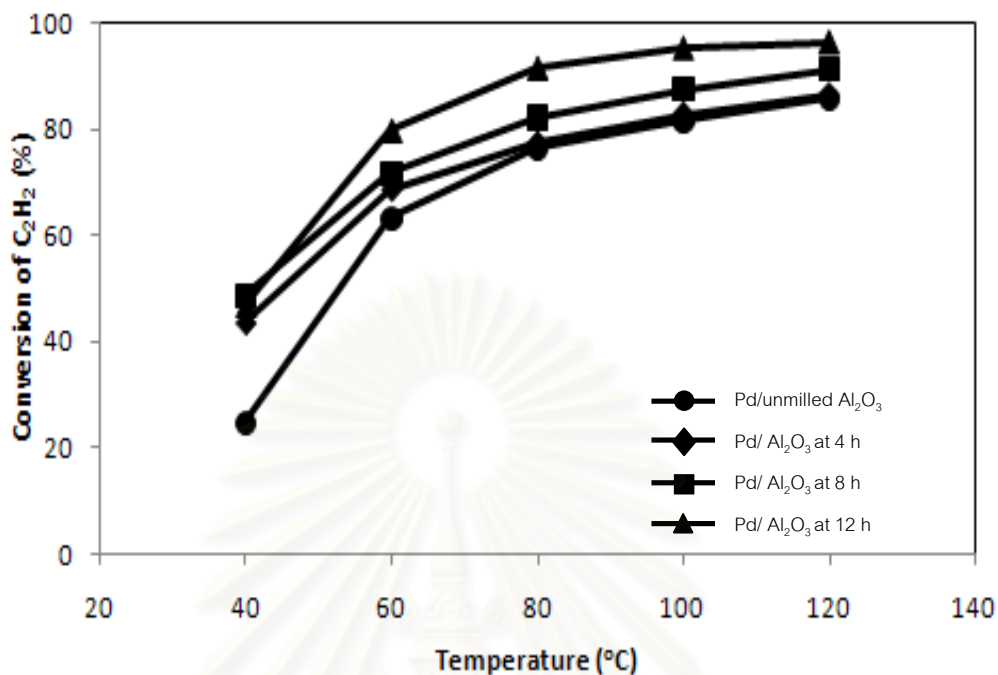


**Figure 5.7** Temperature dependence of the catalytic performance (% conversion of C<sub>2</sub>H<sub>2</sub>) of Pd/milled Al<sub>2</sub>O<sub>3</sub> catalysts with various time.

The selectivity of ethylene (Figure 5.8) observed over all the samples was slightly declined when the temperature was increased due to the fact that the ethylene is produced as an intermediate in acetylene hydrogenation reaction (Ngamsom *et al.*,2004). All the Pd/milled Al<sub>2</sub>O<sub>3</sub> catalysts exhibited higher selectivity than that of the Pd/unmilled Al<sub>2</sub>O<sub>3</sub> catalyst except the Pd/ Al<sub>2</sub>O<sub>3</sub> that showed the lowest selectivity while Pd/Al<sub>2</sub>O<sub>3</sub> at 12 h showed the highest activity. Overall, it was clearly seen from Figure 5.9 that the catalysts prepared from milled supports showed better catalytic properties than the catalysts prepared from unmilled supports. Ethylene selectivity was found to improve in the order: Pd/Al<sub>2</sub>O<sub>3</sub> at 12 h > Pd/Al<sub>2</sub>O<sub>3</sub> at 8 h > Pd/unmilled Al<sub>2</sub>O<sub>3</sub> > Pd/Al<sub>2</sub>O<sub>3</sub> at 4 h.

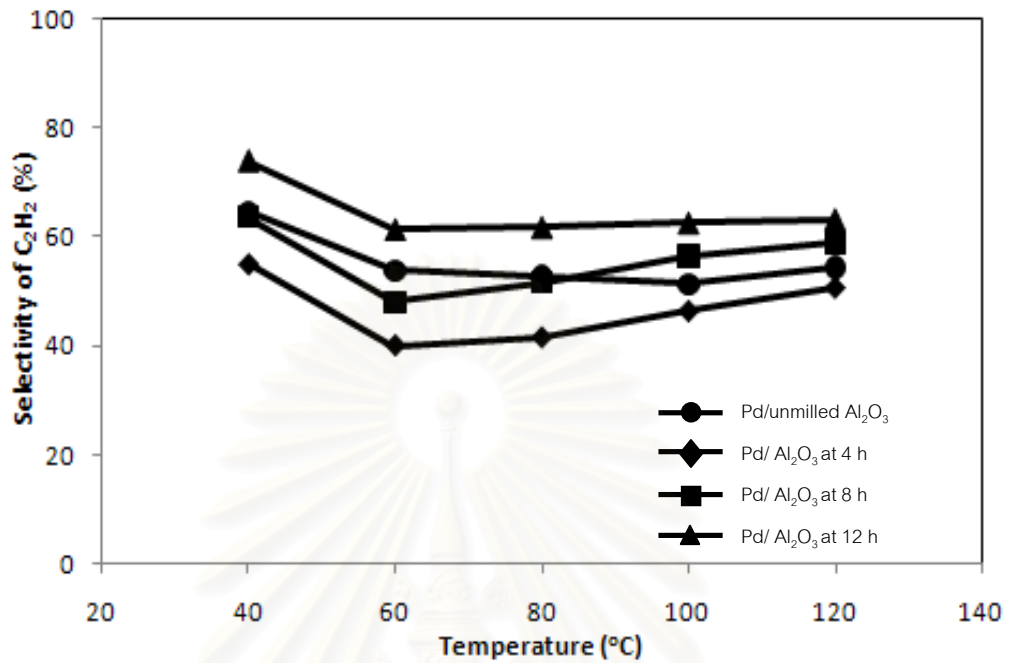


**Figure 5.8** Temperature dependence of the catalytic performance (% selectivity of C<sub>2</sub>H<sub>4</sub>) of Pd/milled Al<sub>2</sub>O<sub>3</sub> catalysts with various time.

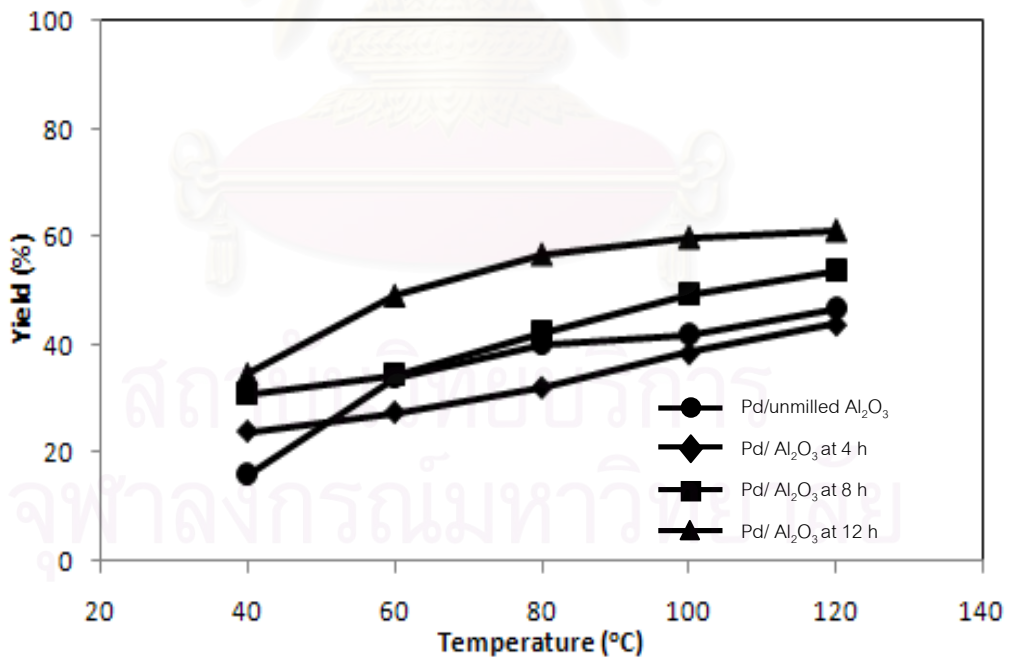


**Figure 5.9** Temperature dependence of the catalytic performance (% yield of C<sub>2</sub>H<sub>4</sub>) of Pd/milled Al<sub>2</sub>O<sub>3</sub> catalysts with various time.

### 5.1.3 Characterization of the Spent Catalysts

After reaction, some amounts of carbonaceous may deposit on the catalyst surface and cover the active metal resulting in loss of activity and selectivity. The amounts of coke deposited on the samples in selective hydrogenation of acetylene were measured by thermal gravimetric analysis and the results are shown in Figure 5.10 and 5.11.

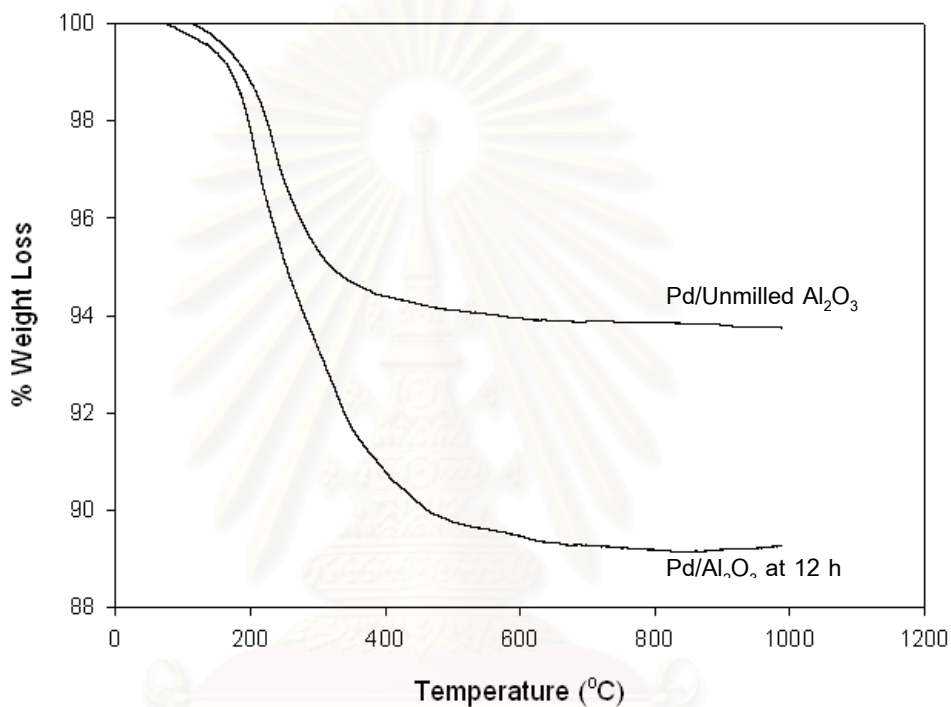


**Fig. 5.10** TGA profiles of Pd/unmilled Al<sub>2</sub>O<sub>3</sub> and Pd/milled Al<sub>2</sub>O<sub>3</sub> catalysts after reaction.

From Figure 5.10, the weight loss observed in the TGA profiles was due to oxidation of the carbonaceous deposited on the surface of used catalysts (Soares *et al.*, 1997). As shown by the exothermic peaks in Figure 5.11, the type of coke species occurred during reaction was probably “soft coke” since it could be removed from the used catalysts by oxidation at a relative lower temperature (~350°C) as suggested by Xiangjing *et al.* (Xiangjing *et al.*, 2006). Based on the TGA results, the amount of coke deposits on the catalyst prepared from milled supports were higher than one prepared from unmilled support. The results were in good agreement with acidity of the Al<sub>2</sub>O<sub>3</sub> supports measured from NH<sub>3</sub> TPD technique.

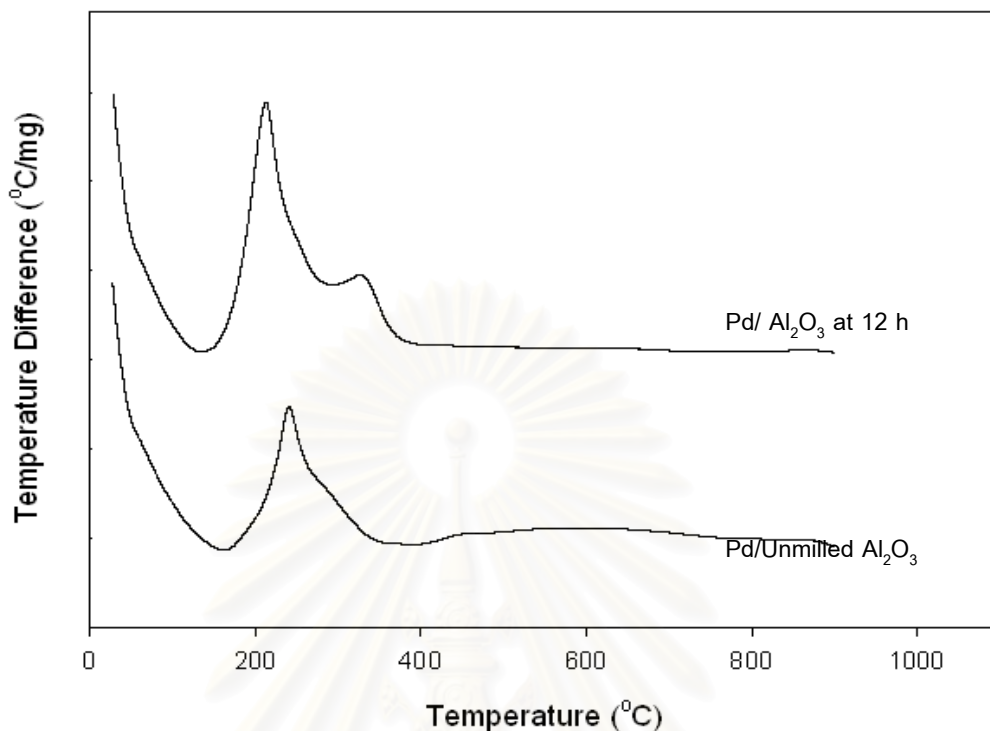


**Fig. 5.11** DTA profiles of Pd/unmilled Al<sub>2</sub>O<sub>3</sub> and Pd/milled Al<sub>2</sub>O<sub>3</sub> catalysts after reaction.

## 5.2 Milled Mixed Oxides Supported Pd Catalyst

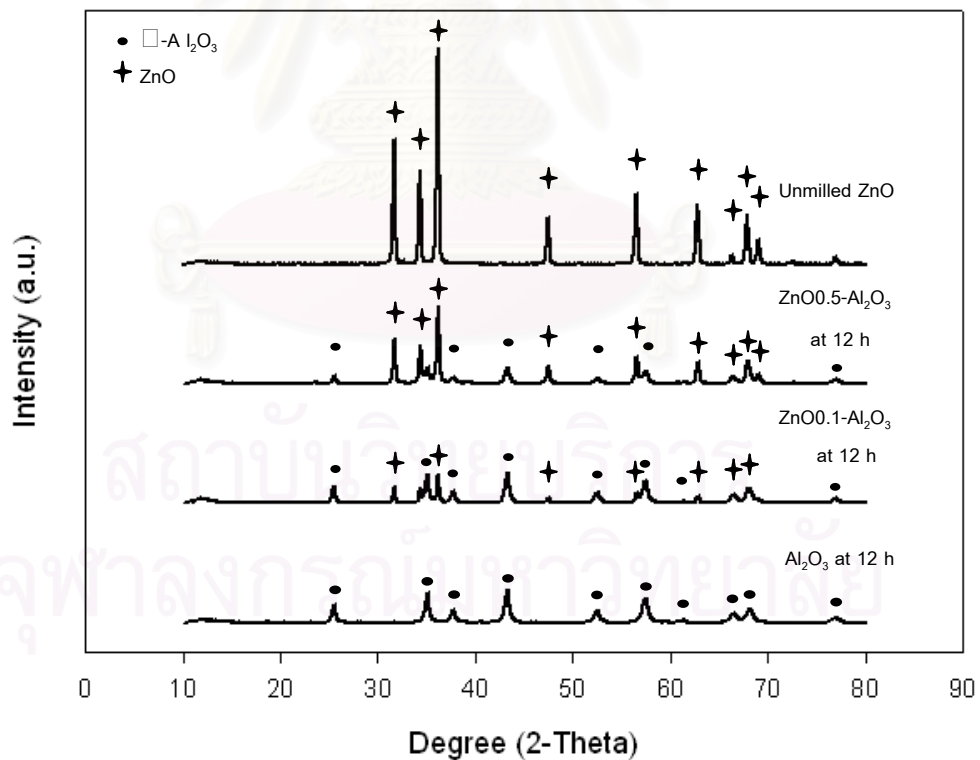
For nomenclature of the samples, the samples of mixed ZnO-Al<sub>2</sub>O<sub>3</sub> with various molar ratios of Zn to Al 0.1 and 0.5 milled by an attrition ball mill at 12 h were named as ZnO0.1-Al<sub>2</sub>O<sub>3</sub>SG and ZnO0.5-Al<sub>2</sub>O<sub>3</sub>, respectively. The mixed NiO-Al<sub>2</sub>O<sub>3</sub> samples prepared by same method were named as NiO0.1-Al<sub>2</sub>O<sub>3</sub> and NiO0.5-Al<sub>2</sub>O<sub>3</sub>, respectively. Pd catalysts supported on the corresponding mixed oxides were called as Pd/ZnO0.1-Al<sub>2</sub>O<sub>3</sub>, Pd/ZnO0.5-Al<sub>2</sub>O<sub>3</sub>, Pd/NiO0.1-Al<sub>2</sub>O<sub>3</sub>, Pd/NiO0.5-Al<sub>2</sub>O<sub>3</sub>, respectively.

### 5.2.1 Characterization of the Catalysts

#### 5.2.1.1 X-ray Diffraction (XRD)

The XRD patterns of the Al<sub>2</sub>O<sub>3</sub> and milled mixed oxides supports with various molar ratios of Zn to Al and Ni to Al milled for 12 h by an attrition ball mill are shown in Figure 5.12.

For the  $\text{Al}_2\text{O}_3$  supports, the characteristic peaks of  $\alpha\text{-Al}_2\text{O}_3$  structure were observed at  $25.52^\circ$ ,  $35.10^\circ$ ,  $37.74^\circ$ ,  $43.32^\circ$ ,  $52.52^\circ$ ,  $57.46^\circ$ ,  $61.22^\circ$ ,  $66.50^\circ$ ,  $68.18^\circ$ , and  $77.86^\circ$   $2\theta$  (Mekasuwandumrong *et al.*,2006). For milled mixed oxides supports, both  $\alpha\text{-Al}_2\text{O}_3$  and ZnO, and both  $\alpha\text{-Al}_2\text{O}_3$  and NiO characteristic peaks were detected in the samples ZnO- $\text{Al}_2\text{O}_3$  and NiO- $\text{Al}_2\text{O}_3$ , respectively. In the case of ZnO- $\text{Al}_2\text{O}_3$  supports, the diffraction lines of ZnO were apparent at  $31.7^\circ$ ,  $34.4^\circ$ ,  $36.2^\circ$ ,  $47.5^\circ$ ,  $56.6^\circ$ ,  $62.8^\circ$ ,  $66.4^\circ$ ,  $67.9^\circ$  and  $69.1^\circ$   $2\theta$  (Ghule *et al.*,2006). On the other hand, the XRD peaks of NiO were presented at  $37.2^\circ$  and  $62.8^\circ$   $2\theta$  for NiO- $\text{Al}_2\text{O}_3$  supports (Yuehua *et al.*,2007). As evident from XRD analysis, characteristic peaks of ZnO and NiO of the sample with molar ratios of Zn to Al and Ni to Al was 0.5 were more distinct than those with molar ratios of Zn to Al and Ni to Al was 0.1, respectively. From the experiments, it was found that Zn to Al and Ni to Al ratio directly affected the diffraction lines of and the width of the intensity of supports.



(A)

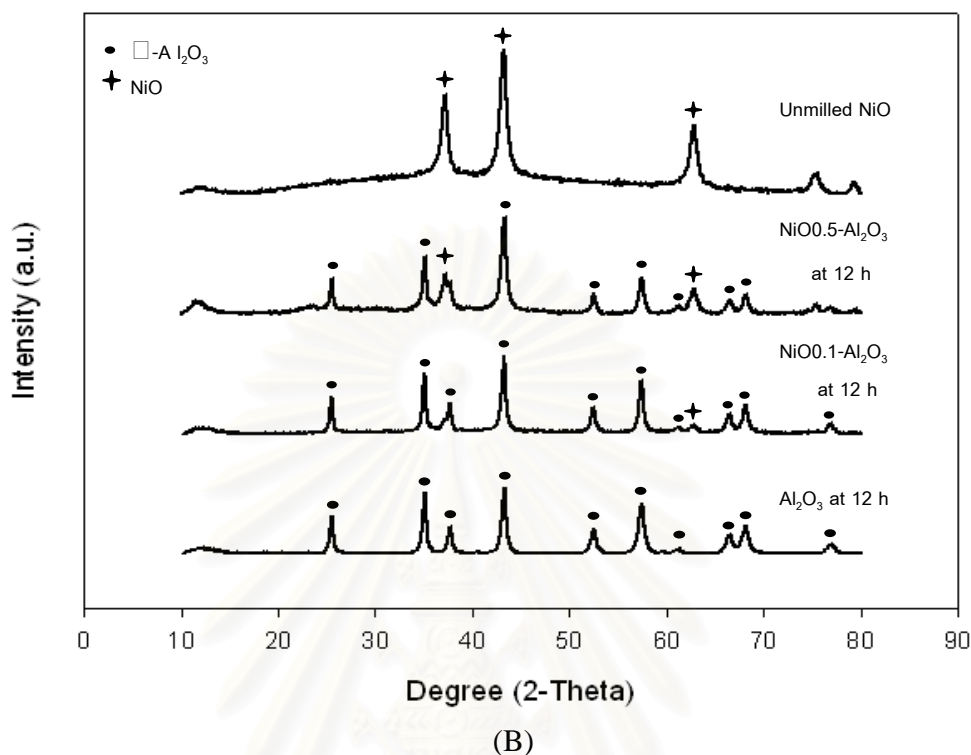


**Figure 5.12** The XRD patterns of milled mixed oxides supports (A) ZnO-Al<sub>2</sub>O<sub>3</sub> and (B) NiO-Al<sub>2</sub>O<sub>3</sub> milled at 12 h with various molar ratios of Zn to Al and Ni to Al.

#### 5.2.1.2 Average Crystallite Size

The crystallite size of the Zn-modified Al<sub>2</sub>O<sub>3</sub> supports with various molar ratios of Zn to Al prepared by sol-gel and solvothermal methods are shown in Table 5.5

The average crystallite sizes of the unmilled Al<sub>2</sub>O<sub>3</sub> and Al<sub>2</sub>O<sub>3</sub> at 12 h were 146 and 18 nm, respectively. In the case of ZnO-Al<sub>2</sub>O<sub>3</sub> supports, the crystallite sizes of ZnO0.5-Al<sub>2</sub>O<sub>3</sub> were smaller than the ZnO0.1-Al<sub>2</sub>O<sub>3</sub> support. While NiO-Al<sub>2</sub>O<sub>3</sub> supports, the crystallite sizes of  $\alpha$ -Al<sub>2</sub>O<sub>3</sub> of NiO0.5-Al<sub>2</sub>O<sub>3</sub> were smaller than NiO0.1-Al<sub>2</sub>O<sub>3</sub> support.

**Table 5.5** The average crystallite sizes of Al<sub>2</sub>O<sub>3</sub>, ZnO-Al<sub>2</sub>O<sub>3</sub> and NiO-Al<sub>2</sub>O<sub>3</sub> supports with various molar ratios of Zn to Al and Ni to Al milled at 12 h.

Sample	Crystallite size (nm)
unmilled Al <sub>2</sub> O <sub>3</sub>	146 <sup>Al</sup>
Al <sub>2</sub> O <sub>3</sub> at 12 h	18 <sup>Al</sup>
unmilled ZnO	54.3 <sup>ZO</sup>
ZnO0.1-Al <sub>2</sub> O <sub>3</sub>	21 <sup>Al</sup> , 53 <sup>ZO</sup>
ZnO0.5-Al <sub>2</sub> O <sub>3</sub>	18 <sup>Al</sup> , 50 <sup>ZO</sup>
unmilled NiO	9.8 <sup>NO</sup>
NiO0.1- Al <sub>2</sub> O <sub>3</sub>	20 <sup>Al</sup>
NiO0.5-Al <sub>2</sub> O <sub>3</sub>	15 <sup>Al</sup>

Al :  $\alpha$ -Al<sub>2</sub>O<sub>3</sub>

ZO : ZnO

NO : NiO

### 5.2.1.3 BET Surface Areas

The BET surface areas of the Al<sub>2</sub>O<sub>3</sub>, ZnO-Al<sub>2</sub>O<sub>3</sub> and NiO-Al<sub>2</sub>O<sub>3</sub> supports with various molar ratios of Zn to Al and Ni to Al milled at 12 h are shown in Table 5.6.

The surface areas of the unground Al<sub>2</sub>O<sub>3</sub> and Al<sub>2</sub>O<sub>3</sub> at 12 h were 0.9 and 15.7 m<sup>2</sup>/g, respectively while milled mixed oxides supports were ranged from 11.7-31.8 m<sup>2</sup>/g. Corresponding to the experiment, the modification of ZnO on Al<sub>2</sub>O<sub>3</sub> and NiO on Al<sub>2</sub>O<sub>3</sub> affect significantly the surface areas of the resulting samples. Moreover, the surface areas were quite high probably due to high dispersion of these particles during milling.



**Table 5.6** BET surface areas of Al<sub>2</sub>O<sub>3</sub>, ZnO-Al<sub>2</sub>O<sub>3</sub> and NiO-Al<sub>2</sub>O<sub>3</sub> supports with various molar ratios of Zn to Al and Ni to Al milled at 12 h.

Sample	BET Surface areas (m <sup>2</sup> /g)
unmilled Al <sub>2</sub> O <sub>3</sub>	0.9
Al <sub>2</sub> O <sub>3</sub> at 12 h	15.7
unmilled ZnO	2.8
ZnO0.1-Al <sub>2</sub> O <sub>3</sub>	17.6
ZnO0.5-Al <sub>2</sub> O <sub>3</sub>	11.7
unmilled NiO	53.8
NiO0.1- Al <sub>2</sub> O <sub>3</sub>	16.1
NiO0.5-Al <sub>2</sub> O <sub>3</sub>	31.8

#### 5.2.1.5 Metal Active Sites

The metal active sites, the Pd dispersion, and the average Pd metal particle size from CO chemisorption experiment are summarized in Table 5.7.

Without ZnO addition on the Al<sub>2</sub>O<sub>3</sub> supports, Pd/unmilled Al<sub>2</sub>O<sub>3</sub> and Pd/Al<sub>2</sub>O<sub>3</sub> at 12 h possessed the amounts of Pd active sites  $13.1 \times 10^{17}$  and  $46.9 \times 10^{17}$  sites/g cat., respectively. The Pd active sites significantly decreased when the catalysts were supported on ZnO-Al<sub>2</sub>O<sub>3</sub> corresponding to the decreasing in Pd metal dispersion and increasing in the average Pd metal particle sizes. For Pd/NiO-Al<sub>2</sub>O<sub>3</sub> samples, the amount of active sites was significantly high and Pd dispersion was not determined due to its relatively large amount over the calculation range due probably to the reduction of the NiO supports to Ni active metal. The average Pd metal particle sizes for the Pd/ZnO-Al<sub>2</sub>O<sub>3</sub> catalysts were 5 nm.

**Table 5.7** Results from CO chemisorption of Pd supported on Al<sub>2</sub>O<sub>3</sub>, ZnO-Al<sub>2</sub>O<sub>3</sub> and NiO-Al<sub>2</sub>O<sub>3</sub> catalysts with various molar ratios of Zn to Al and Ni to Al milled at 12 h.

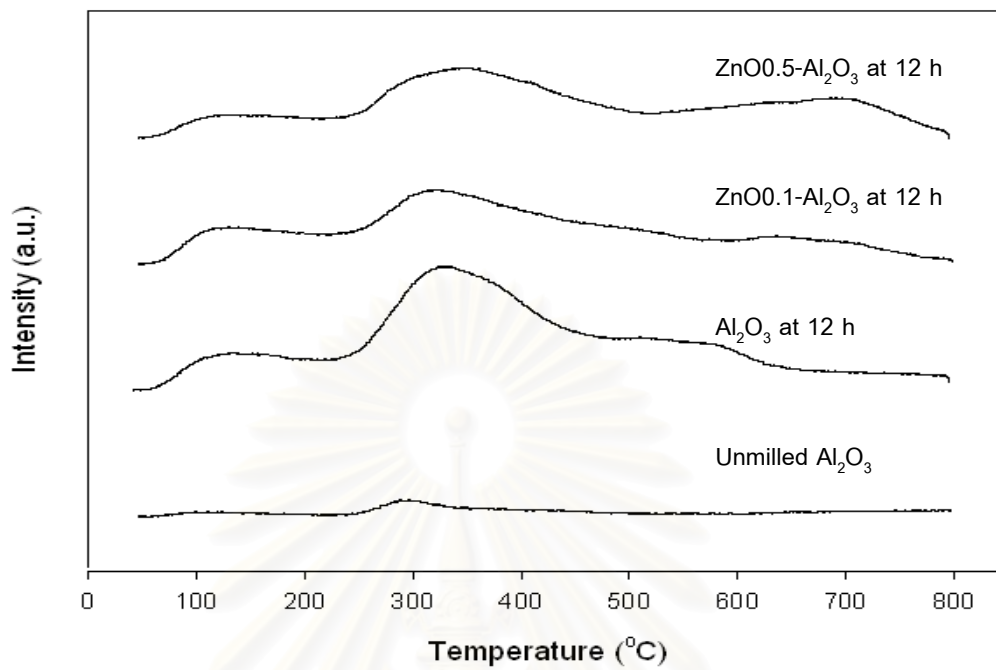
Sample	CO chemisorption ×10 <sup>17</sup> (molecule CO/g cat.)	Pd dispersion (%)	d <sub>p</sub> Pd <sup>0</sup> (nm)
Pd/unmilled Al <sub>2</sub> O <sub>3</sub>	13.1	8.7	13
Pd/Al <sub>2</sub> O <sub>3</sub> at 12 h	46.9	32.3	3
Pd/ZnO0.1-Al <sub>2</sub> O <sub>3</sub>	28.1	20.6	5
Pd/ZnO0.5-Al <sub>2</sub> O <sub>3</sub>	32.4	21.9	5
Pd/NiO0.1-Al <sub>2</sub> O <sub>3</sub>	160.4	n.d.	n.d.
Pd/NiO0.5-Al <sub>2</sub> O <sub>3</sub>	397.2	n.d.	n.d.

n.d. : not determined

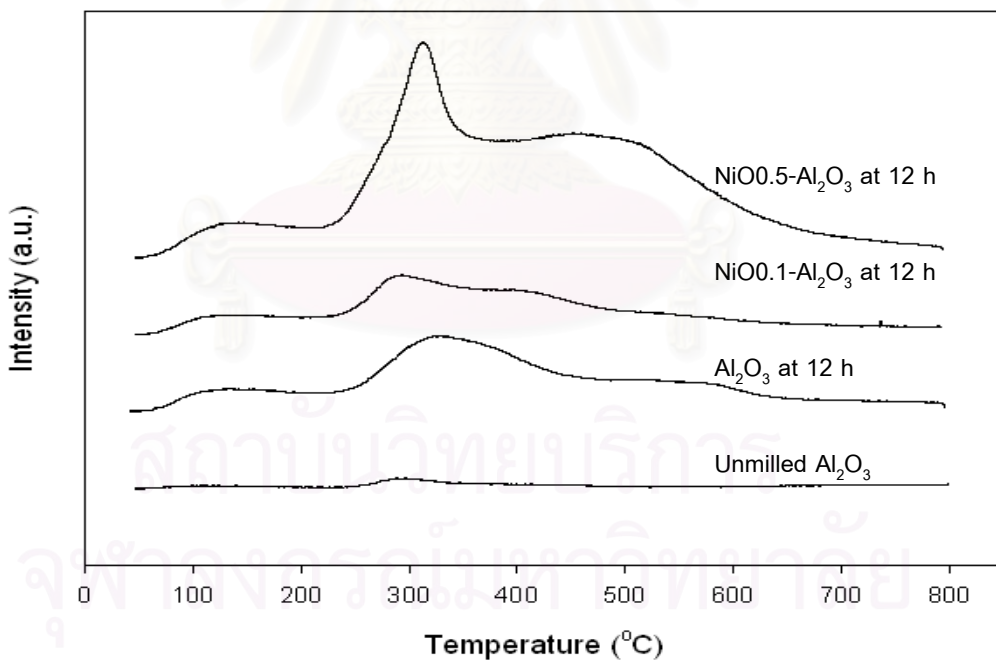
#### 5.2.1.6 NH<sub>3</sub> Temperature Programmed Desorption (NH<sub>3</sub>-TPD)

The temperature-programmed desorption profiles for the Al<sub>2</sub>O<sub>3</sub>, ZnO-Al<sub>2</sub>O<sub>3</sub> and NiO-Al<sub>2</sub>O<sub>3</sub> supports with various molar ratios of Zn to Al and Ni to Al milled at 12 h are shown in Figure 5.13.

From experimental, it was found that the desorption peak areas of the milled ZnO-Al<sub>2</sub>O<sub>3</sub> samples were lower than pure Al<sub>2</sub>O<sub>3</sub> milled at the same time. These results were in good agreement with those reported by Deborah *et al.* They suggested that a decrease of surface acidity can be attributed to an increasing of zinc oxide (Deborah *et al.*,2008). As shown in Figure 5.10B, two large desorption peak at ca. 320°C and 480°C were observed for the NiO-Al<sub>2</sub>O<sub>3</sub> with Ni/Al ratio = 0.5 due probably to the presence of NiO.



(A)



(B)

**Figure 5.13**  $\text{NH}_3$  temperature programmed desorption of (A)  $\text{ZnO-Al}_2\text{O}_3$  and (B)  $\text{NiO-Al}_2\text{O}_3$  supports with various molar ratios of Zn to Al and Ni to Al milled at 12 h.

### 5.2.2 Catalytic Performance of the Catalysts

The catalytic properties of Pd/Zn-modified  $\text{Al}_2\text{O}_3$  catalysts were evaluated in the selective hydrogenation of acetylene using a fixed bed flow reactor with a GHSV of  $16901 \text{ h}^{-1}$ . For study of temperature dependence of the catalysts on acetylene conversion and selectivity toward ethylene, the temperature range between  $40\text{--}100^\circ\text{C}$  and feed gas composed of 1.5%  $\text{C}_2\text{H}_2$ , 1.7%  $\text{H}_2$ , and balanced  $\text{C}_2\text{H}_4$  (TIG Co., Ltd.) were used

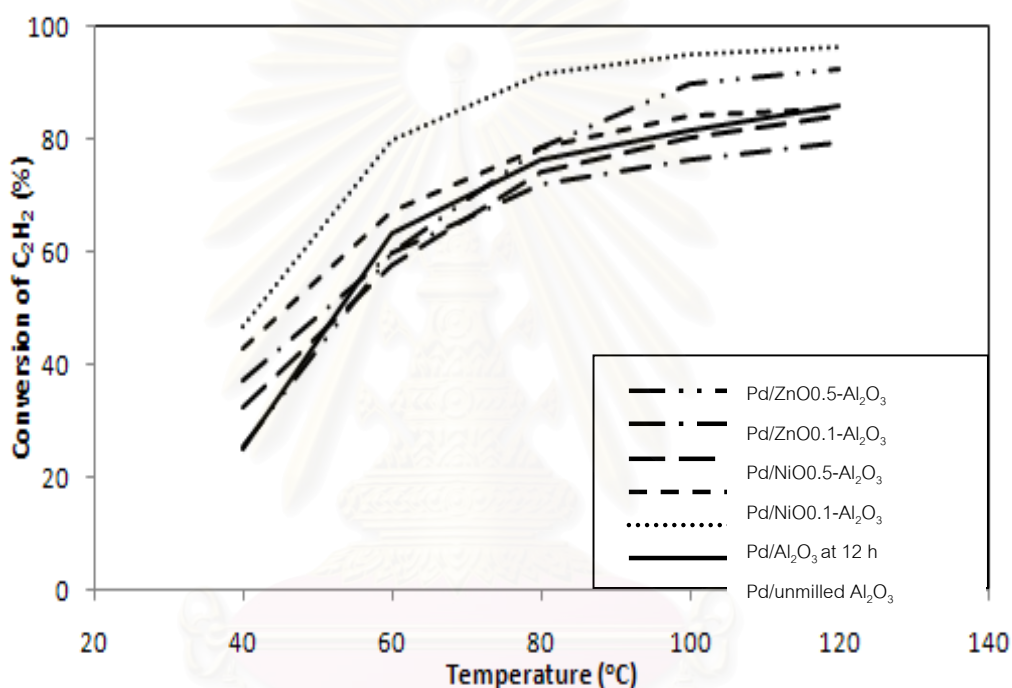


**Figure 5.14** Temperature dependence of the catalytic performance (% conversion of  $\text{C}_2\text{H}_2$ ) of Pd/milled mixed oxide catalysts with various molar ratios of Zn to Al and Ni to Al.

As shown in Figure 5.14., activity of all the catalysts directly increased with rising temperature as the kinetic energy of the system increased with increasing temperature. In case of the catalysts prepared from milled mixed oxides with molar ratio of Zn to Al and Ni to Al was 0.5, the catalysts exhibited higher activity than that of the catalyst prepared from unmilled alumina while Pd/ $\text{Al}_2\text{O}_3$  at 12 h showed the highest activity. Opposite to the catalysts prepared from milled mixed oxides with molar ratio of Zn to Al and Ni to Al

was 0.1, the catalysts showed lower activity than that of the catalyst prepared from unmilled alumina.

The selectivity of ethylene (Figure 5.15) observed over all the samples was slightly declined when the temperature was increased due to the fact that the ethylene is produced as an intermediate in acetylene hydrogenation reaction (Ngamsom *et al.*,2002). For the catalysts prepared from milled mixed oxides with molar ratio of Zn to Al was 0.5 (ZnO0.5-Al<sub>2</sub>O<sub>3</sub>) and Al<sub>2</sub>O<sub>3</sub> at 12 h showed higher selectivity of ethylene than catalyst prepared from unmilled alumina with Pd/Al<sub>2</sub>O<sub>3</sub> at 12 h catalyst exhibited the highest selectivity of ethylene. In contrast, the catalysts prepared from milled mixed oxides with molar ratio of Zn to Al and Ni to Al was 0.1, the catalysts presented lower selectivity of ethylene than that of the catalyst from unmilled alumina. From Figure 5.16, Ethylene yield was found to improve in the order: Pd/Al<sub>2</sub>O<sub>3</sub> at 12 h > Pd/Zn0.5-Al<sub>2</sub>O<sub>3</sub> > Pd/unmilled Al<sub>2</sub>O<sub>3</sub> > Pd/Ni0.1-Al<sub>2</sub>O<sub>3</sub> > Pd/Ni0.5-Al<sub>2</sub>O<sub>3</sub> > Pd/Zn0.1-Al<sub>2</sub>O<sub>3</sub>.

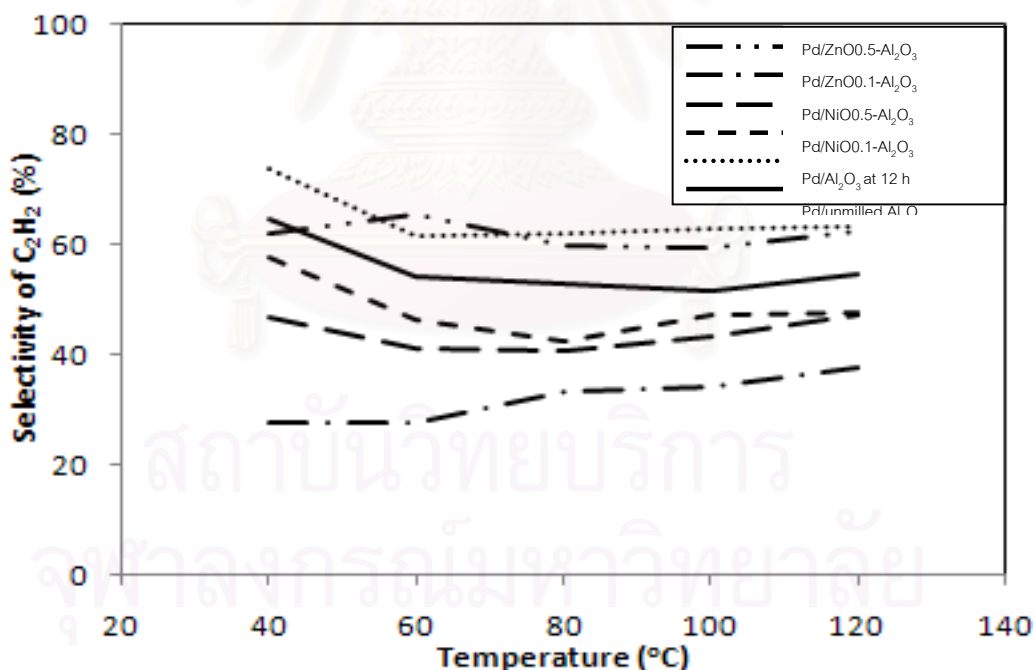


**Figure 5.15** Temperature dependence of the catalytic performance (% selectivity of C<sub>2</sub>H<sub>4</sub>) of Pd/milled mixed oxide catalysts with various molar ratios of Zn to Al and Ni to Al.

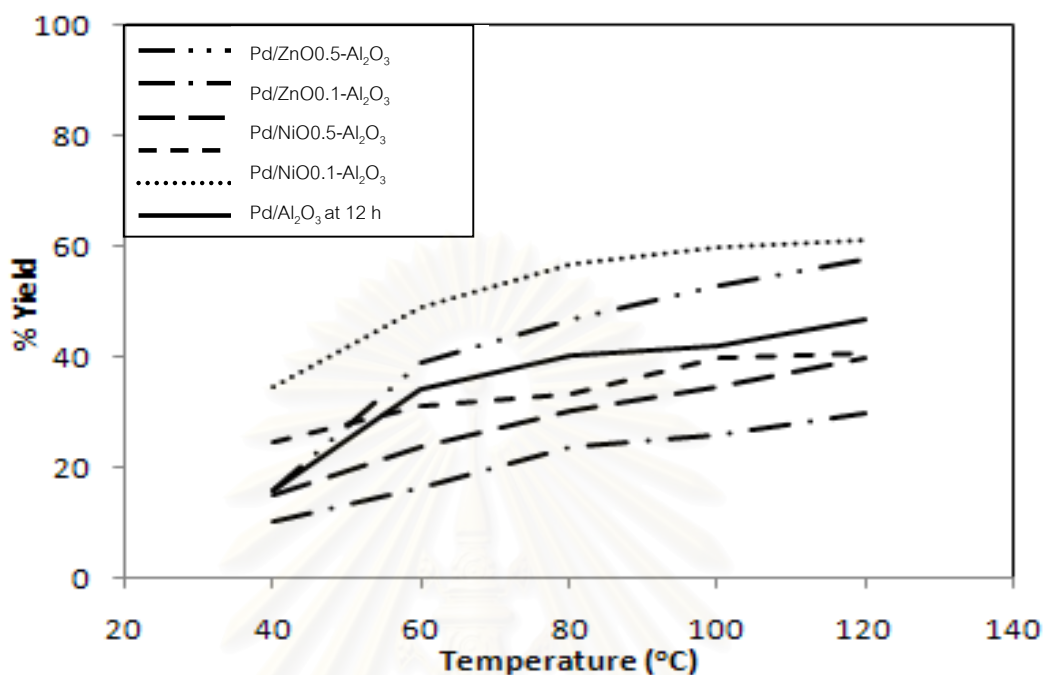


**Figure 5.16** Temperature dependence of the catalytic performance (% yield of C<sub>2</sub>H<sub>4</sub>) of Pd/milled mixed oxide catalysts with various molar ratios of Zn to Al and Ni to Al.

### 5.3 Effect of Alumina Grinding and Mixed Oxides (ZnO-Al<sub>2</sub>O<sub>3</sub> and NiO-Al<sub>2</sub>O<sub>3</sub>) Grinding on the Properties of Pd/Al<sub>2</sub>O<sub>3</sub> Catalysts

From the experimental results in section 5.1 and 5.2, it was found that the Pd catalyst supported on Al<sub>2</sub>O<sub>3</sub> milled for 12 h and the Pd catalyst supported on ZnO0.5-Al<sub>2</sub>O<sub>3</sub> milled for 12 h prepared by an attrition ball mill exhibited higher performances than the Pd catalysts supported on unmilled Al<sub>2</sub>O<sub>3</sub>. However, all the catalysts prepared from milled mixed oxides presented lower acetylene conversion and ethylene selectivity than that of catalyst prepared from alumina milled for 12 h.

Based on the XRD analysis and TEM micrographs, the average crystallite size of the milled samples decreased as the grinding time increased. From CO chemisorption and BET surface area results, the catalysts prepared from milled Al<sub>2</sub>O<sub>3</sub> had higher surface area than the catalysts prepared from unmilled Al<sub>2</sub>O<sub>3</sub>. In addition, the catalysts prepared

from milled  $\text{Al}_2\text{O}_3$  possessed higher amount of Pd active sites and higher Pd dispersion than the catalysts prepared unmilled  $\text{Al}_2\text{O}_3$  due probably to more distribution of the supports as noticed from TEM measurements. Moreover, the Pd catalysts supported on the milled  $\text{Al}_2\text{O}_3$  supports exhibited lower average Pd metal particle size than those prepared from unmilled  $\text{Al}_2\text{O}_3$ . These results could also be the reason for activity enhancement for those prepared from milled  $\text{Al}_2\text{O}_3$ . The results were in good agreement with those reported by Sarkany *et al.* They suggested that small particles of a medium dispersed catalyst exhibited slightly higher activity as suggested (Sarkany *et al.*,1986).

According to the  $\text{NH}_3$ -TPD results, it was found that acidity of the milled  $\text{Al}_2\text{O}_3$  supports was higher than that prepared from unmilled  $\text{Al}_2\text{O}_3$ . The results were in good agreement with the amount of coke deposits on the catalysts measured from TGA. Moreover, milling of  $\text{Al}_2\text{O}_3$  supports increased surface acidity of  $\text{Al}_2\text{O}_3$  so that the catalysts exhibited higher amount of carbonaceous deposits resulted in blockage of Pd sites responsible for direct ethane formation, ethylene selectivity was thus increased as a consequence. It has been reported that the carbonaceous layer was supposed to affect selectivity though a ligand effect, which caused a diminution of the adsorption strength of unsaturated molecules and favored the selectivity towards ethylene (Duca *et al.*,1996 and Duca *et al.*,1998).

From several previous investigations, it has been generally accepted that four main types of surface site were involved in Pd/ $\text{Al}_2\text{O}_3$  catalyst in the selective acetylene hydrogenation. Three types of active sites locating on the Pd surface were responsible for selective hydrogenation of acetylene to ethylene, direct ethane formation from acetylene, and oligomer formation from acetylene. Another site located on the  $\text{Al}_2\text{O}_3$  support surface involved the hydrogenation of ethylene to ethane (Lobo and Trimm,1973, Somorjai *et al.*, 1979, Moses *et al.*,1984, and, Lamb *et al.*,2004). It was proposed that spillover hydrogen from carbonaceous layer was tentatively identified as the source of hydrogen for ethylene hydrogenation. The parallelism between polymer formation and ethylene hydrogenation suggested that the surface polymer served as a hydrogen pool and facilitated diffusion of hydrogen from palladium surface to the support (Lobo and Trimm,1973, Somorjai *et al.*,

1979, Moses *et al.*,1984, and, Lamb *et al.*,2004). This explanation can be simply understood by the conceptual model in Figure 5.17.

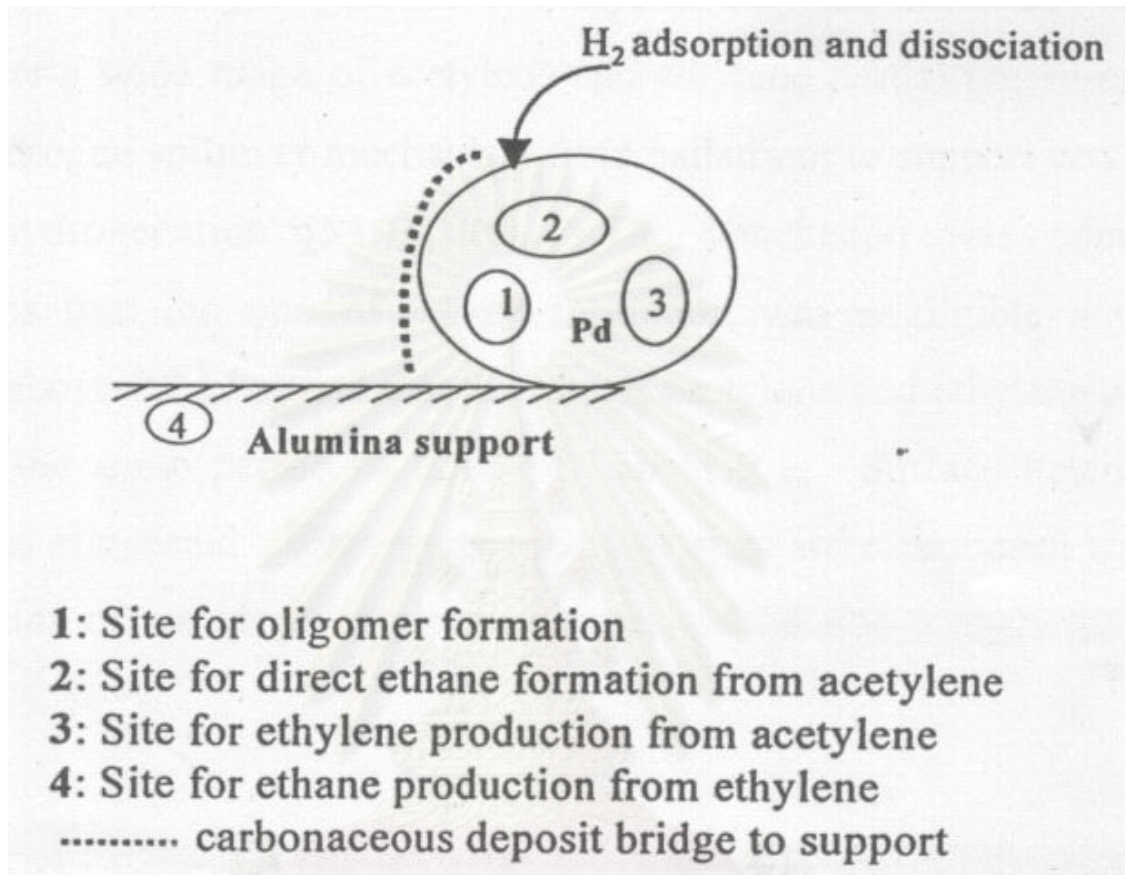
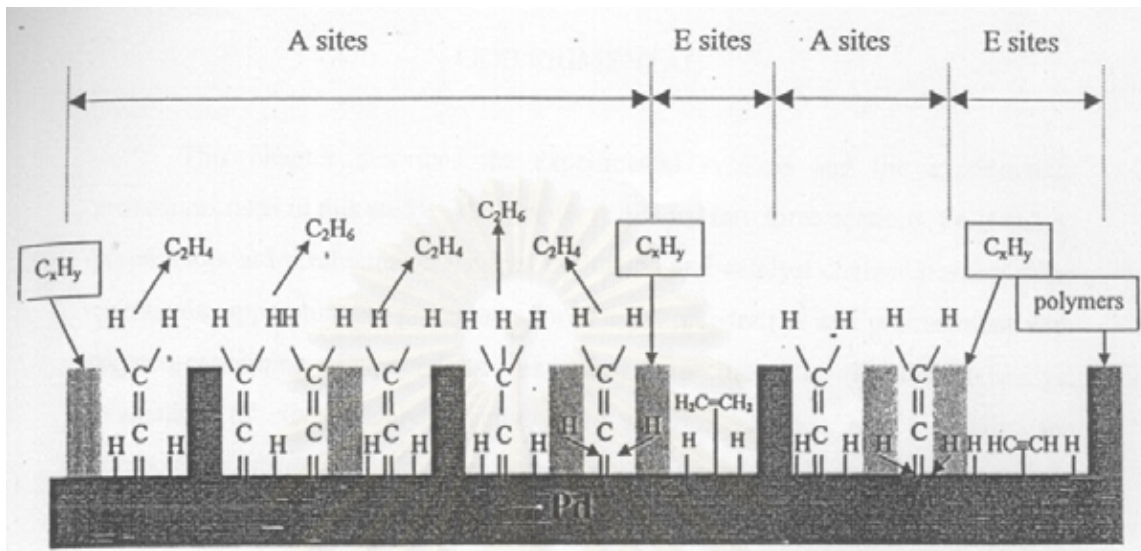


**Figure 5.17** Conceptual model demonstrating four main types of surface on alumina-supported palladium catalyst.

However, a disparity in the selective mechanism has also been reported. Kinetic study on the hydrogenation of acetylene-ethylene mixtures over a Pd/ $\alpha$ -Al<sub>2</sub>O<sub>3</sub> catalyst over a wide range of acetylene and ethylene partial pressures has suggested hydrogen spillover mechanism from palladium from support was inactive for the ethylene hydrogenation (Borodzinski, 1999). The conclusion was confirmed by the observations that the rate of ethane formation was negligible at high acetylene pressures (above 0.2 kPa) and that the rate of acetylene and ethylene attained a steady state after the same period of time, i.e., about 9 h. Surface heterogeneity of the catalyst was suggested. Two



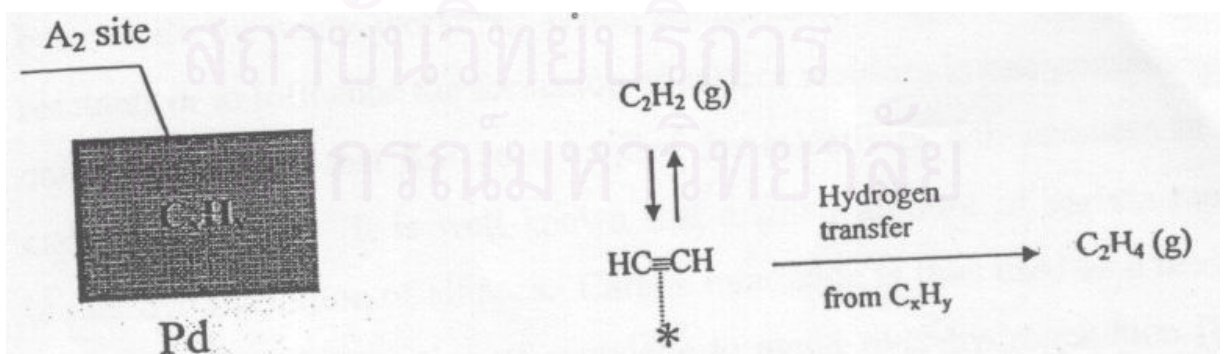
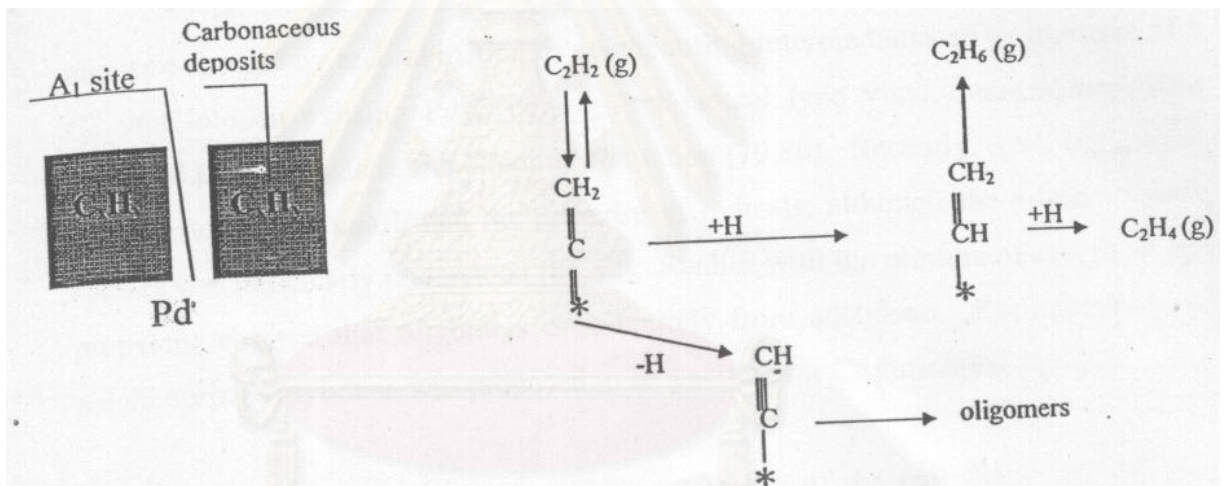
types of active sites were proposed to involve in the hydrogenation of acetylene-ethylene mixtures, denoted as A and E sites as illustrated in Figure 5.18.



**Figure 5.18** A simplified representation of active sites created on a palladium surface by carbonaceous deposits (C<sub>x</sub>H<sub>y</sub>)

A comprehensive mechanistic scheme assuming the existence of three types of active sites created on palladium surface by carbonaceous deposits has been proposed, and is illustrated in Figure 5.19 (Borodzinski, 1997). Certain sites representing small spaces of the palladium surface between carbonaceous deposits (A sites) are sterically inaccessible to ethylene. The hydrogenation of ethylene was believed to take place on large palladium spaces, where ethylene and acetylene competitively adsorb (E sites). However, as ethylene was not supposed to adsorb on A sites, the two substrates that competitively adsorb on A sites should be acetylene and hydrogen. Two types of active sites were then suggested; A<sub>1</sub> and A<sub>2</sub> sites. A<sub>1</sub> sites on palladium are where hydrogenation proceeds according to a mechanism involving the competitive adsorption of acetylene and hydrogen. A<sub>2</sub> sites exist on the carbonaceous deposits where only hydrogenation of acetylene to ethylene proceeds involving the non-competitive adsorption of acetylene. In this latter case, acetylene is hydrogenated by hydrogen transferred to acetylene from the carbonaceous deposits. Accordingly, it was suggested that hydrogenation of acetylene on A sites primarily proceeds to ethylene. A key

intermediate in hydrogenation of acetylene on A sites is believed to be vinylidene species, whereas  $\pi$ -bonded ethylene adsorbed on E sites is a key intermediate in ethylene hydrogenation. The larger steric hindrance to the adsorbed ethylene compared to that for adsorbed acetylene is a result of the difference in position of the molecules in the adsorbed state:  $\pi$ -adsorbed ethylene is flat lying, whereas acetylene adsorbed as vinylidene is either perpendicular or tilted with respect to the surface. A simplified representation of active sites created on a palladium surface by carbonaceous deposits ( $C_xH_y$ ) is shown in Figure 5.19. This proposed model, does not consider the effect of transport hindrance on consecutive reactions and the effect of the accumulation of deposits on the local effective diffusivity (Lee, 1994). Additionally, the above mentioned model cannot explain the reactivity of freshly reduced supported palladium catalysts.



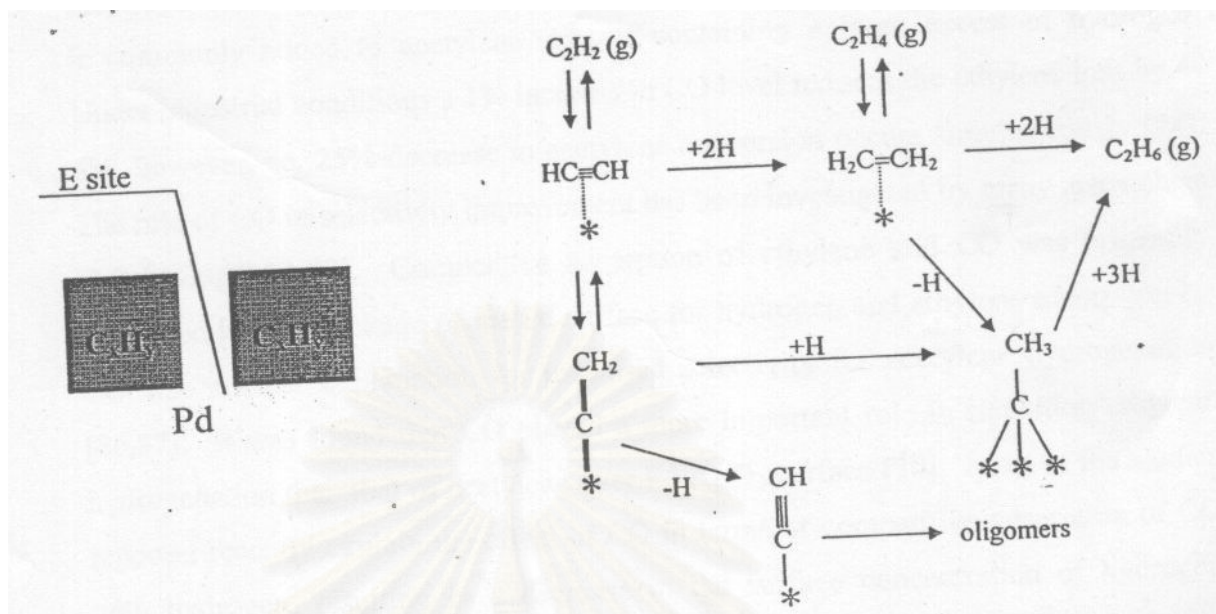


**Figure 5.19** Three types of active sites created on the palladium surface by carbonaceous deposits ( $C_xH_y$ ) and schemes of the reactions occurring on the sites.

It has been reported that the increase in ethylene hydrogenation (decrease in ethylene selectivity) was related to the amount of carbonaceous deposited on the catalyst surface. In other words, the carbonaceous deposit diminished the average ensemble sites of the active metal available for the reaction. It is also well known that acidity on  $Al_2O_3$  surface promoted formation of carbonaceous deposited on catalyst surface. This study has shown that milling of  $Al_2O_3$  supports by an attrition ball mill can increase amount of Pd active sites and Pd dispersion of  $Al_2O_3$  so that the catalysts exhibited higher activity. Furthermore, milling of  $Al_2O_3$  supports increased surface acidity of  $Al_2O_3$  so that higher amount of carbonaceous layer deposited, thus selectivity of ethylene was improved.

## CHAPTER VI

### CONCLUSIONS AND RECOMMENDATIONS

In this chapter, section 6.1 provides the conclusions obtained from the experimental results of Pd catalysts supported on milled  $\text{Al}_2\text{O}_3$  and milled mixed oxides ( $\text{ZnO-Al}_2\text{O}_3$ ,  $\text{NiO-Al}_2\text{O}_3$ ) with various molar ratios of Zn/Al and Ni/Al (0.1 and 0.5) prepared by an attrition ball mill in selective acetylene hydrogenation in excess ethylene. Additionally, recommendations for future study are given in section 6.2.

#### 6.1 Conclusions

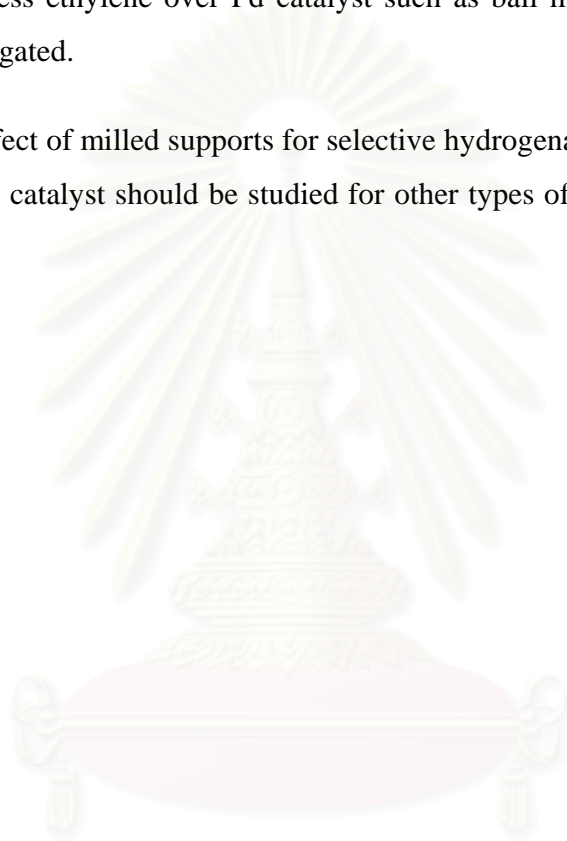
1. The Pd catalyst supported on the  $\text{Al}_2\text{O}_3$  milled for 12 h and the Pd catalyst supported on  $\text{ZnO}0.5\text{-Al}_2\text{O}_3$  milled for 12 h exhibited higher performances in selective hydrogenation of acetylene in excess ethylene than that of the unmilled  $\text{Al}_2\text{O}_3$ . However, all the catalysts prepared from milled mixed oxides presented lower acetylene conversion and ethylene selectivity than that of catalyst prepared from alumina milled for 12 h.

2. Differences in the catalyst activity as well as ethylene selectivity of the various Pd/ $\text{Al}_2\text{O}_3$  catalysts may be due to the differences in (1) amount of metal active site, (2) surface area of supports, and (3) acidity of the supports.

3. Regardless of the preparation method used, milling of  $\alpha\text{-Al}_2\text{O}_3$  could increase surface acidity of the  $\text{Al}_2\text{O}_3$  so that carbonaceous deposits was formed during selective acetylene hydrogenation.

## 6.2 Recommendations

1. The effect of carbonaceous layer on the catalyst performance should be studied using more sophisticated techniques.
2. The other types of miller for milling  $\text{Al}_2\text{O}_3$  for selective hydrogenation of acetylene in excess ethylene over Pd catalyst such as ball mill and planetary ball mill should be investigated.
3. The effect of milled supports for selective hydrogenation of acetylene in excess ethylene over Pd catalyst should be studied for other types of support such as silica and titania.



สถาบันวิทยบริการ  
จุฬาลงกรณ์มหาวิทยาลัย

## REFERENCE

- Ali, S. H., and Goodwin, J. G., Jr. SSITKA. Investigation of Palladium Precursor and Support Effects on CO Hydrogenation over Supported Pd Catalysts. J. Catal. 176 (1998): 3-13.
- Anderson, A. B., and Onwood, D. P. Why carbon monoxide is stable lying down on a negatively charge Ru(001) surface but on Pt(111). Surf. Sci. Lett. 154 (1985): 261-267.
- Andonova, S., Vladov, Ch., Kunev, B., Mitov, I., Tyuliev, G., Fierro, J. L. G., Damyanova, S., and Petrov, L. Study of the effect of mechanical–chemical activation of Co–Mo/ $\gamma$ -Al<sub>2</sub>O<sub>3</sub> and Ni–Mo/ $\gamma$ -Al<sub>2</sub>O<sub>3</sub> catalysts for hydrodesulfurization. Appl. Catal. A. 298 (2006): 94-102.
- Andreeva, D., Ivanov, I., Ilieva, L., Sobczak, J. W., Avdeev, G., and Tabakova, T. Nanosized gold catalysts supported on ceria and ceria-alumina for WGS reaction: Influence of the preparation method. Appl. Catal. A. 333 (2007): 153-160.
- Angkana Kanyanucharat. Determination of the thermal stability of CoAl<sub>2</sub>O<sub>4</sub>, ZnAl<sub>2</sub>O<sub>4</sub> and NiAl<sub>2</sub>O<sub>4</sub> single nanocrystals. Master's thesis, Department of Chemical Engineering, Faculty of Engineering, Chulalongkorn University, 2001.
- Bodaghi, M., Zolfonoon, H., Tahriri, M., and Karimi, M. Synthesis and characterization of nanocrystalline  $\alpha$ -Al<sub>2</sub>O<sub>3</sub> using Al and Fe<sub>2</sub>O<sub>3</sub> (hematite) through mechanical alloying. Stud. Surf. Sci. 11 (2009): 496-500.
- Boitiaux, J. P., Cosyns, J., And Vasudevan, S. Hydrogenation of highly unsaturated hydrocarbons over highly dispersed palladium catalyst: Part I: behaviour of small metal particles. Appl. Catal. 6 (1983): 41-51.
- Bos, A. N. R., and Westerterp, K. R. Mechanism and kinetics of the selective hydrogenation of ethylene and ethane. Chem. Eng. Process. 32 (1993): 1-7.
- Chen, M. H., Chu, W., Dai, X. Y., and Zhang, X. W. New Palladium catalysts prepared by glow discharge plasma for the selective hydrogenation of acetylene. Catal Today 89 (2004): 201-204.

- Chinayon, S., Mekasuwandumrong, O., Praserthdam, P., and Panpranot, J., Selective Hydrogenation of Acetylene over Pd Catalysts Supported on Nanocrystalline  $\gamma$ - $\text{Al}_2\text{O}_3$  and Zn-Modified  $\gamma$ - $\text{Al}_2\text{O}_3$ . Catal. Com. (2008), In Press.
- Chu, W., Chen, M., Qin, W., and Dai, X. Support effect of palladium catalysts for acetylene hydrogenation to ethylene. Proceeding of the 13<sup>th</sup> International Congress on Catalysis, Paris, July (2004)
- Cormack, D., Pritchard, J., and Moss, R. L. CO chemisorption on silica-supported palladium-silver alloys. J. Catal. 37 (1975): 548-552.
- Derrien, M. L. Selective Hydrogenation applied to the refining of petrochemical raw material produced by steam cracking. Stud. Surf. Sci. Catal. 27 (1986): 613-666.
- Dynys, F. W., and Halloran, J. W. Alpha alumina Formation in Alum-Derived Gamma Alumina. J. American Ceramic Society 65 (1982): 442-448.
- Edelstein, A., and Cammarata, R. C. Synthesis, Properties and Applications, Nanomaterials. Institute of physics Publishing, Bristol and Philadelphia, 1996.
- Ertl, G., Knozinger, H., and Weitkamp, J. Preparation of Solid Catalysts. Wiley-VCH. (1997).
- Guczi, L., Schay Z., Stefler, G., Liotta, L. F., Deganello, G., and Venezia, A. M. Pumice-supported Cu-Pd catalyst: influence of copper on the activity and selectivity of palladium in hydrogenation of phenylacetylene and but-1-ene. J. Catal. 182 (1999): 456-462.
- Guimon, C., Auroux, A., Romero, E., and Monzon, A. Acetylene hydrogenation over Ni-Si-Al mixed oxides prepared by sol-gel technique. Appl. Catal. A. 251 (2003): 199-214.
- Heinrichs, B., Delhez, P., Schoebrecht, J. -P., and Pirard, J. -P. Palladium-silver sol-gel catalysts for selective hydrogenation of 1,2-dichloroethane into ethylene. J. Catal. 172 (1997): 322-335.
- Huang, Y. J., Shun, C. F., Daniel, L. G., Mohundro, E. L., and Hartgerick, J. E. Regeneration of acetylene converter catalysts by hydrogen stripping. US Patent 5,332,705 (to Exxon Chemical Patents Inc.), 1994.

- Hub, S., Hilaire, L., and Touroude, R. Hydrogenation of But-1-yne and But-1-ene on Palladium Catalysts: Particle Size Effect. Appl. Catal. 36 (1998): 307-322.
- Inoue, M., Kondo, Y., and Inui, T. Ethylene Glycol Derivation of Boehmite. Inorganic Chemistry Industry. 27 (1988): 215-221.
- Inoue, M., Kominami, H., and Inui, T. Thermal Transformation of  $\gamma$ -alumina Formed by Thermal Decomposition of Aluminum Alkoxide in organic Media. J. American Ceramic Society. 75 (1992): 2597-2598.
- Kang, J. H., Shin, E. W., Kim, W. J., Park, J. D., and Moon, S. H. Selective hydrogenation of acetylene on Pd/SiO<sub>2</sub> catalysts promoted with Ti, Nb and Ce oxides. Catal. Today. 63 (2000): 183-188.
- Kang, J. H., Shin, E. W., Kim, W. J., Park, J. D., and Moon, S. H. Selective Hydrogenation of Acetylene on TiO<sub>2</sub>-Added Pd Catalysts. J. Catal. 208 (2002): 310-320.
- Karagedov, G. R., and Lyakhov, N. Z. Preparation and Sintering of Nanosized  $\alpha$ -Al<sub>2</sub>O<sub>3</sub> Powder. NanoStructured Materials. 11 (1999): 559-572
- Karimzadeh, F., Enayati, M. H., and Tavoosi, M. Synthesis and characterization of Zn/Al<sub>2</sub>O<sub>3</sub> nanocomposite by mechanical alloying. Materials Science and Eng. A. 486 (2008): 45-48.
- Kim, W. J., Kang, J. H., Ahn, I. Y., and Moon, S. H. Deactivation behavior of a TiO<sub>2</sub> added Pd catalyst in acetylene hydrogenation. J. Catal. 226 (2004): 226-229.
- Kim, W. J., Shin, E. W., Kang, J. H., and Moon, S. H. Performance of Si-modified Pd catalyst in acetylene hydrogenation: catalyst deactivation behavior. Appl. Catal. A. 251: 305-313.
- Kouzu, M., Uchida, K., Kuriki, Y., and Ikazaki, F. Micro-crystalline molybdenum sulfide prepared by mechanical milling as an unsupported model catalyst for the hydrodesulfurization of diesel fuel. Appl. Catal. A. 276 (2004): 241-249.
- Legendre, F., Poissonnet, S., and Bonnaillie P. Synthesis of nanostructured SnO<sub>2</sub> materials by reactive ball-milling. J. Alloys and Compounds 434-435 (2007): 400-404.
- Levin, I., and Brandon, D. Metastable Alumina Polymorph: Crystal Structures and Transition Sequences. J. American Ceramic Society. 81 (1998): 61.



- Mahata, N., and Vishwanathan, V. Influence of Palladium Precursors on Structural Properties and Phenol Hydrogenation Characteristics of Supported Palladium Catalysts J. Catal. 196 (2000): 262-270.
- Mekasuwandumrong, O., Silveston, P. L., Praserthdam, P., Inoue, M., Pavarajarn, V., and Tanaklungsank, W. Synthesis of thermally stable micro spherical  $\gamma$ -alumina via solvothermal synthesis. Mater. Chem. Phys. 100 (2006): 445.
- Mirosław, Z. Synthesis of nanosized and microporous zinc aluminate spinel by microwave assisted hydrothermal method (microwave-hydrothermal synthesis of  $ZnAl_2O_4$ ) Sol. State. Sci. 8 (2006): 14-18.
- Molnár, Á., Sárkány, A., and Varga, M. Hydrogenation of carbon-carbon multiple bonds: chemo-, region- and stereo-selectivity. J. Mol. Catal. 173 (2001): 185-221.
- Ngamson, B., Bogdanchikova, N., Borja, M. A., and Praserthdam, P. Characterisations of Pd-Ag/ $Al_2O_3$  catalysts for selective acetylene hydrogenation : effect of pretreatment with NO and  $N_2O$ . Catal. Commun. 5 (2004): 243-248.
- Nitikon Wongwaranon. Effect of Ni-modified  $Al_2O_3$  on the properties of Pd/ $Al_2O_3$  catalyst in selective acetylene hydrogenation. Master's thesis, Department of Chemical Engineering, Faculty of Engineering, Chulalongkorn University, 2006.
- Onoda, H., Okumoto, K., and Tanaka I. Mechanochemical reforming of powder and acidic properties of copper *cyclo*-tetrates. Materials Chemistry and Physics 107 (2008): 339-343
- Park, Y. H., and Price G. L. Promotion effects of potassium on palladium/alumina selective hydrogenation catalyst. Ind. Eng. Chem. Res. 31 (1992): 469-474.
- Peacock, A. J. Handbook Polyethylene : Structures, properties, and applications, Marcel Decker, New York, 2000.
- Petre, A. L., Perdigón-Melón, J. A., Gervasini, A., and Auroux, A. Acid-base properties of alumina-supported  $M_2O_3$  (M=B, Ga, In) catalysts. Topics in Catal. 19 (2002): 271-281.

- Praserthdam, P., Ngamsom, B., Bogdanchikova, N., Phatanasri, S., and Pramotthana, M. Effect of the pretreatment with oxygen and/or oxygen-containing compounds on the catalytic performance of Pd-Ag/Al<sub>2</sub>O<sub>3</sub> for acetylene hydrogenation. Appl. Catal. A 230 (2002): 41-51.
- Sárkány, A., Horvath, A., and Beck, A. Hydrogenation of acetylene over low loaded Pd and Pd-Au/SiO<sub>2</sub> catalysts. Appl. Catal. A 229 (2002): 117-125.
- Sárkány, A., Zsoldos, Z., Gy Stefler, J., Hightower, W., and Gucci, L. Promoter effect of Pd in Hydrogenation of 1,3 Butadiene over Co-Pd Catalysts. J. Catal. 157 (1995): 179-189.
- Sárkány, A., Weiss, A.H., and Gucci, L. Structure sensitivity of acetylene-ethylene hydrogenation over Pd catalysts. J. Catal. 98 (1986): 550-553.
- Shin, E. W., Choi, C. H., Chang, K. S., Na, Y. H., and Moon, S. H. Properties of Si-modified Pd catalyst for selective hydrogenation of acetylene. Catal. Today 44 (1998): 137-143.
- Shin, E. W., Kang, J. H., Kim, W. J., Park, J. D., and Moon, S. H. Performance of Si-modified Pd catalyst in acetylene hydrogenation: the origin of the ethylene selectivity improvement. Appl. Catal. A 223 (2002): 161-172.
- Shinohara, K., Golman, B., Uchiyama, T., and Otani, M. Fine-grinding characteristics of hard materials by attrition mill. Powder Tech. 103 (1999): 292-296.
- Simpson, T. W., Wen, Q. Z., Yu, N., and Clarke, D. R. Kinetics of the Amorphous  $\rightarrow\gamma\rightarrow\alpha$  Transformation in Aluminum oxide: Effect of Crystallography Orientation. J. American Ceramic Society. 81 (1998): 1995.
- Soares, R. W., Menezes, V. J., Fonseca, M. V. A., and Dweck, J. Characterization of carbonaceous products by TG and DTA. J. Thermal Analysis. 49 (1997): 657-661.
- Soma-Noto, Y., and Sachtler, W. M. H. Infrared spectra of carbon monoxide adsorbed on supported palladium and palladium-silver alloys. J. Catal. 32 (1974): 315-324.
- Songphol Aungkapipattanachai. Effect of regeneration on the properties of palladium-silver catalysts in selective hydrogenation of acetylene. Master's thesis, Department of Chemical Engineering, Faculty of Engineering, Chulalongkorn University, 2005.

- Stenger, F., Mende, S., Schwedes, J., and Peukert, W. The influence of suspension properties on the grinding behavior of alumina particles in the submicron size range in stirred media mills. Powder Tech. 156 (2005): 103–110.
- Tsuchida, T., and Horigome, K. The effect of grinding on the thermal decomposition of alumina monohydrates,  $\alpha$ - and  $\beta$ - $\text{Al}_2\text{O}_3 \cdot \text{H}_2\text{O}$ . Thermochimica Acta 254 (1995): 359-370
- Tanitta Prasitwuttisak. Comparative study of alumina powder synthesis techniques to the physical and optical properties of colored alumina ceramics. Master's thesis, Department of Chemical Engineering, Faculty of Engineering, Chulalongkorn University, 2004.
- Tavoosi, M., Karimzadeh, F., and Enayati M. H. Fabrication of Al-Zn/ $\alpha$ - $\text{Al}_2\text{O}_3$  nanocomposite by mechanical alloying. Materials Letters 62 (2008): 282–285.
- Valenzuela, M. A., Bosch, P., Aguilar-rios, G., Montoya, A., and Schifter, I. Comparison Between Sol-Gel, Coprecipitation and Wet Mixing Synthesis of  $\text{ZnAl}_2\text{O}_4$ . J. Sol-Gel Sci. Techn. 8 (1997): 107-110.
- Valenzuela, M. A., Jacobs, J. P., and Bosch, P. The influence of the preparation method on the surface structure of  $\text{ZnAl}_2\text{O}_4$ . Appl. Catal. A. 148 (1997): 315-324.
- Vannice, M. A., Wang, S. Y., and Moon, S. H. The effect of SMSI (strong metal-support interaction) behavior on CO adsorption and hydrogenation on Pd catalyst: I. IR spectra of adsorbed CO prior to and during reaction conditions. J. Catal. 71 (1981): 152-166.
- Wei, X., and Chen, D. Synthesis and characterization of nanosized zinc aluminate spinel by sol-gel technique. Mater. Lett. 60 (2006): 823-827.
- Wongwaranon, N., Mekasuwandumrong, O., Praserttham, P., and Panpranot, P. Performance of Pd catalysts supported on nanocrystalline  $\alpha$ - $\text{Al}_2\text{O}_3$  and Ni-modified  $\alpha$ - $\text{Al}_2\text{O}_3$  in selective hydrogenation of acetylene. Catal, Today 131 (2008): 553–558.
- Wood, J., Alldrick, M. J., Winterbottom, J. M., Stitt, E. H., and Bailey S. Diffuse reflectance infrared Fourier transform spectroscopy (DRIFTS) study of ethyne hydrogenation on Pd/ $\text{Al}_2\text{O}_3$ . Catal, Today 128 (2007): 52–62

- Wrzyszczyk, J., Zawadzki, M., Trzczyński, J., Grabowska, H., and Miśta, W. Some catalytic properties of hydrothermally synthesized zinc aluminate spinel. Appl. Catal. A 210 (2001): 263-269.
- Xiangjing, Z., Yan, W., and Feng, X. Coke deposition and characterization on titanium silicalite-1 catalyst in cyclohexanone ammoxidation. Appl. Catal. A 307 (2006): 222-230.
- Yoldas, B. E. Method of producing ceramic-forming metal hydroxide and oxide powders. Appl. Chem. and Bio. 23 (1973): 803-809.
- Yoldas, B. E. Alumina gels that form porous transparent  $\text{Al}_2\text{O}_3$ . Mater. Sci. 10 (1975): 1856-1860.
- Zawadzki, M., Miśta, W., and Kępczyński L. Metal-support effects of platinum supported on zinc aluminate. Vacuum. 63 (2001): 291-296.
- Zawadzki, M., and Wrzyszczyk, J. Hydrothermal synthesis of nanoporous zinc aluminate with high surface area. Mater. Res. Bull. 35 (2000): 109-114.



สถาบันวิทยบริการ  
จุฬาลงกรณ์มหาวิทยาลัย



**APPENDICES**

สถาบันวิทยบริการ  
จุฬาลงกรณ์มหาวิทยาลัย

## APPENDIX A

### CALCULATION FOR CATALYST PREPARATION

#### Calculation of support composition (ZnO-Al<sub>2</sub>O<sub>3</sub>)

Preparation of ZnO-Al<sub>2</sub>O<sub>3</sub> with various molar ratios of Zn to Al (0.1 and 0.5).

Reagent:     - Aluminium oxide (Al<sub>2</sub>O<sub>3</sub>)  
                   Molecular weight     = 101.96 g/mol  
                   - Zinc oxide (ZnO)  
                   Molecular weight     = 81.37 g/mol

Calculation:

- For molar ratio of Zn/Al = 0.1 is shown as follow:

Aluminium oxide 100 g consisted of aluminium equal to:

$$\begin{aligned} \text{Aluminium} &= (26.98 \times 2 \times 100) / 101.96 = 52.9227 \text{ g} \\ &= 52.9227 / 26.98 = 1.9616 \text{ mol} \end{aligned}$$

For Zn/Al = 0.1, 1.9616 mole of aluminium

$$\begin{aligned} \text{Zinc required} &= 1.9616 \times 0.1 = 0.1962 \text{ mol} \\ &= 0.1962 \times 65.37 = 12.8256 \text{ g} \end{aligned}$$

Zinc 12.8256 g was prepared from ZnO and molecular weight of Zn is 65.37 mol

$$\begin{aligned} \text{ZnO required} &= \frac{\text{MW of ZnO} \times \text{zinc required}}{\text{MW of Zn}} \\ &= (81.37 / 65.37) \times 12.8256 = 15.9648 \text{ g} \end{aligned}$$

- For molar ratio of Zn/Al = 0.5 is shown as follow:

Aluminium oxide 70 g consisted of aluminium equal to:

$$\begin{aligned} \text{Aluminium} &= (26.98 \times 2 \times 70) / 101.96 = 37.0459 \text{ g} \\ &= 37.0459 / 26.98 = 1.3731 \text{ mol} \end{aligned}$$

For Zn/Al = 0.5, 1.3731 mole of aluminium

$$\begin{aligned} \text{Zinc required} &= 1.3731 \times 0.5 = 0.6865 \text{ mol} \\ &= 0.6865 \times 65.37 = 44.8765 \text{ g} \end{aligned}$$

Zinc 44.8765 g was prepared from ZnO and molecular weight of Zn is 65.37 mol

$$\begin{aligned}\text{ZnO required} &= \frac{\text{MW of ZnO} \times \text{zinc required}}{\text{MW of Zn}} \\ &= (81.37/65.37) \times 44.8765 = 55.8605 \text{ g}\end{aligned}$$

### Calculation of support composition (NiO-Al<sub>2</sub>O<sub>3</sub>)

Preparation of NiO-Al<sub>2</sub>O<sub>3</sub> with various molar ratios of Ni to Al (0.1 and 0.5).

Reagent: - Aluminium oxide (Al<sub>2</sub>O<sub>3</sub>)  
 Molecular weight = 101.96 g/mol  
 - Nickel oxide (NiO)  
 Molecular weight = 74.69 g/mol

Calculation:

- For molar ratio of Ni/Al = 0.1 is shown as follow:

Aluminium oxide 100 g consisted of aluminium equal to:

$$\begin{aligned}\text{Aluminium} &= (26.98 \times 2 \times 100) / 101.96 = 52.9227 \text{ g} \\ &= 52.9227 / 26.98 = 1.9616 \text{ mol}\end{aligned}$$

For Ni/Al = 0.1, 1.9616 mole of aluminium

$$\begin{aligned}\text{Nickel required} &= 1.9616 \times 0.1 = 0.1962 \text{ mol} \\ &= 0.1962 \times 58.69 = 11.5124 \text{ g}\end{aligned}$$

Nickel 11.5124 g was prepared from NiO and molecular weight of Ni is 58.69 mol

$$\begin{aligned}\text{NiO required} &= \frac{\text{MW of NiO} \times \text{nickel required}}{\text{MW of Ni}} \\ &= (74.69/58.69) \times 11.5124 = 14.6509 \text{ g}\end{aligned}$$

- For molar ratio of Ni/Al = 0.5 is shown as follow:

Aluminium oxide 70 g consisted of aluminium equal to:

$$\begin{aligned}\text{Aluminium} &= (26.98 \times 2 \times 70) / 101.96 = 37.0459 \text{ g} \\ &= 37.0459 / 26.98 = 1.3731 \text{ mol}\end{aligned}$$

For Ni/Al = 0.1, 1.9616 mole of aluminium

$$\begin{aligned}\text{Nickel required} &= 1.3731 \times 0.5 = 0.6865 \text{ mol} \\ &= 0.6865 \times 58.69 = 40.2933 \text{ g}\end{aligned}$$

Nickel 40.2933 g was prepared from NiO and molecular weight of Ni is 58.69 mol

$$\begin{aligned}\text{NiO required} &= \frac{\text{MW of NiO} \times \text{nickel required}}{\text{MW of Ni}} \\ &= (74.69 / 58.69) \times 40.2933 = 51.2780 \text{ g}\end{aligned}$$

### Calculation of support composition (Zn-Al<sub>2</sub>O<sub>3</sub>)

Preparation of Zn-Al<sub>2</sub>O<sub>3</sub> with various molar ratios of Zn to Al (0.1 and 0.5).

Reagent: - Aluminium oxide (Al<sub>2</sub>O<sub>3</sub>)  
Molecular weight = 101.96 g/mol  
- Zinc (Zn)  
Molecular weight = 65.37 g/mol

Calculation:

- For molar ratio of Zn/Al = 0.1 is shown as follow:

Aluminium oxide 100 g consisted of aluminium equal to:

$$\begin{aligned}\text{Aluminium} &= (26.98 \times 2 \times 100) / 101.96 = 52.9227 \text{ g} \\ &= 52.9227 / 26.98 = 1.9616 \text{ mol}\end{aligned}$$

For Zn/Al = 0.1, 1.9616 mole of aluminium

$$\begin{aligned}\text{Zinc required} &= 1.9616 \times 0.1 = 0.1962 \text{ mol} \\ &= 0.1962 \times 65.37 = 12.8256 \text{ g}\end{aligned}$$



- For molar ratio of Zn/Al = 0.5 is shown as follow:

Aluminium oxide 70 g consisted of aluminium equal to:

$$\begin{aligned}\text{Aluminium} &= (26.98 \times 2 \times 70) / 101.96 = 37.0459 \text{ g} \\ &= 37.0459 / 26.98 = 1.3731 \text{ mol}\end{aligned}$$

For Zn/Al = 0.5, 1.3731 mole of aluminium

$$\begin{aligned}\text{Zinc required} &= 1.3731 \times 0.5 = 0.6865 \text{ mol} \\ &= 0.6865 \times 65.37 = 44.8765 \text{ g}\end{aligned}$$

### Calculation of palladium loading

Preparation of 0.3%wt Pd on supports by the incipient wetness impregnation method is shown as follows:

Reagent: - Palladium (II) nitrate hexahydrate ( $\text{Pd}(\text{NO}_3)_2 \cdot 6\text{H}_2\text{O}$ )  
 Molecular weight = 338.42  
 - Support: -  $\text{Al}_2\text{O}_3$   
                   -  $\text{ZnO-Al}_2\text{O}_3$   
                   -  $\text{NiO-Al}_2\text{O}_3$   
                   -  $\text{Zn-Al}_2\text{O}_3$

Based on 100 g of catalyst used, the composition of the catalyst will be as follows:

$$\begin{aligned}\text{Palladium} &= 0.3 \text{ g} \\ \text{Alumina} &= 100 - 0.3 = 99.7 \text{ g}\end{aligned}$$

For 1 g of  $\text{Al}_2\text{O}_3$  support

$$\text{Palladium required} = 1 \times (0.3 / 99.7) = 0.003 \text{ g}$$

Palladium 0.003 g was prepared from  $\text{Pd}(\text{NO}_3)_2 \cdot 6\text{H}_2\text{O}$  and molecular weight of Pd is 106.42

$$\begin{aligned}\text{Pd}(\text{NO}_3)_2 \cdot 6\text{H}_2\text{O} \text{ required} &= \frac{\text{MW of Pd}(\text{NO}_3)_2 \cdot 6\text{H}_2\text{O} \times \text{palladium required}}{\text{MW of Pd}} \\ &= (338.42 / 106.42) \times 0.003 = 0.0095 \text{ g}\end{aligned}$$

Since the pore volume of  $\text{Al}_2\text{O}_3$  support is 0.4 ml/g. Thus, the total volume of impregnation solution which must be used is 0.4 ml for alumina by the requirement of incipient wetness impregnation method, the de-ionized water is added until equal pore volume for dissolve Palladium (II) nitrate hexahydrate.



สถาบันวิทยบริการ  
จุฬาลงกรณ์มหาวิทยาลัย

## APPENDIX B

### CALCULATION OF THE CRYSTALLITE SIZE

#### Calculation of the crystallite size by Scherrer equation

The crystallite size was calculated from the half-height width of the diffraction peak of XRD pattern using the Debye-Scherrer equation.

From Scherrer equation:

$$D = \frac{K\lambda}{\beta \cos \theta} \quad (\text{B.1})$$

- where
- D = Crystallite size, Å
  - K = Crystallite-shape factor = 0.9
  - $\lambda$  = X-ray wavelength, 1.5418 Å for CuK $\alpha$
  - $\theta$  = Observed peak angle, degree
  - $\beta$  = X-ray diffraction broadening, radian

The X-ray diffraction broadening ( $\beta$ ) is the pure width of a powder diffraction free of all broadening due to the experimental equipment. Standard  $\alpha$ -alumina is used to observe the instrumental broadening since its crystallite size is larger than 2000 Å. The X-ray diffraction broadening ( $\beta$ ) can be obtained by using Warren's formula.

From Warren's formula:

$$\begin{aligned} \beta^2 &= B_M^2 - B_S^2 \\ \beta &= \sqrt{B_M^2 - B_S^2} \end{aligned} \quad (\text{B.2})$$

- Where
- $B_M$  = The measured peak width in radians at half peak height.
  - $B_S$  = The corresponding width of a standard material.

**Example:** Calculation of the crystallite size of unmilled  $\alpha$ -Al<sub>2</sub>O<sub>3</sub>

$$\begin{aligned}\text{The half-height width of peak} &= 0.24^\circ \text{ (from Figure B.1)} \\ &= (2\pi \times 0.24)/360 \\ &= 0.00422 \text{ radian}\end{aligned}$$

$$\text{The corresponding half-height width of peak of } \alpha\text{-alumina} = 0.0041 \text{ radian}$$

$$\begin{aligned}\text{The pure width} &= \sqrt{B_M^2 - B_S^2} \\ &= \sqrt{0.00422^2 - 0.0041^2} \\ &= 0.00102 \text{ radian}\end{aligned}$$

$$\beta = 0.00102 \text{ radian}$$

$$2\theta = 43.32^\circ$$

$$\theta = 21.66^\circ$$

$$\lambda = 1.5418 \text{ \AA}$$

$$\begin{aligned}\text{The crystallite size} &= \frac{0.9 \times 1.5418}{0.00102 \cos 21.66} = 1463.2 \text{ \AA} \\ &= 146.3 \text{ nm}\end{aligned}$$

สถาบันวิทยบริการ  
จุฬาลงกรณ์มหาวิทยาลัย

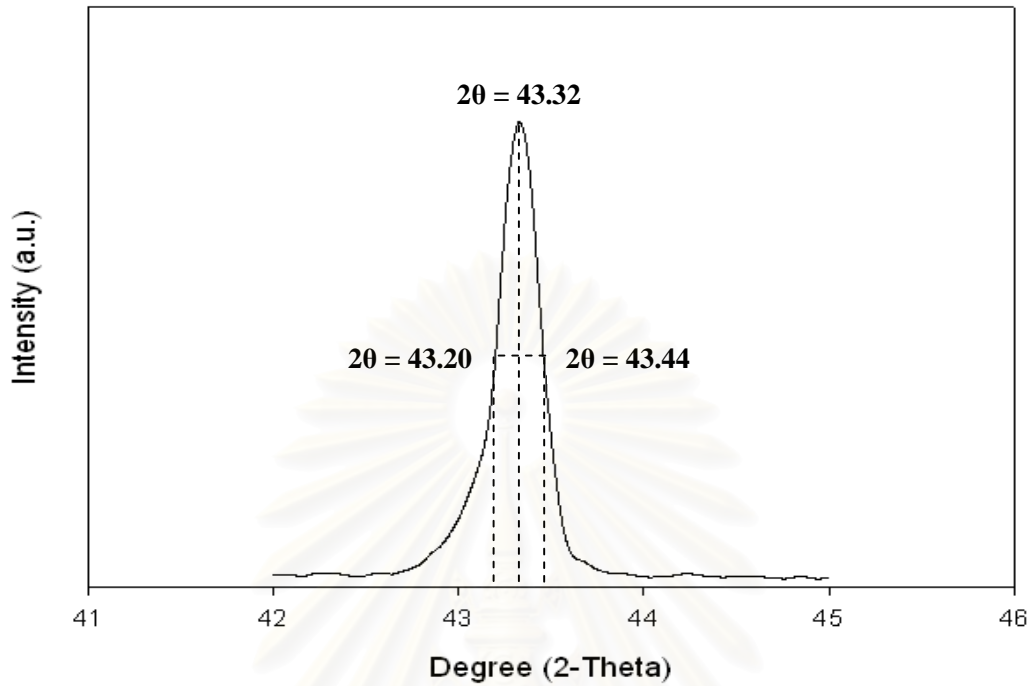


**Figure B.1** The measured peak of unground  $\alpha$ - $\text{Al}_2\text{O}_3$  to calculate the crystallite size.

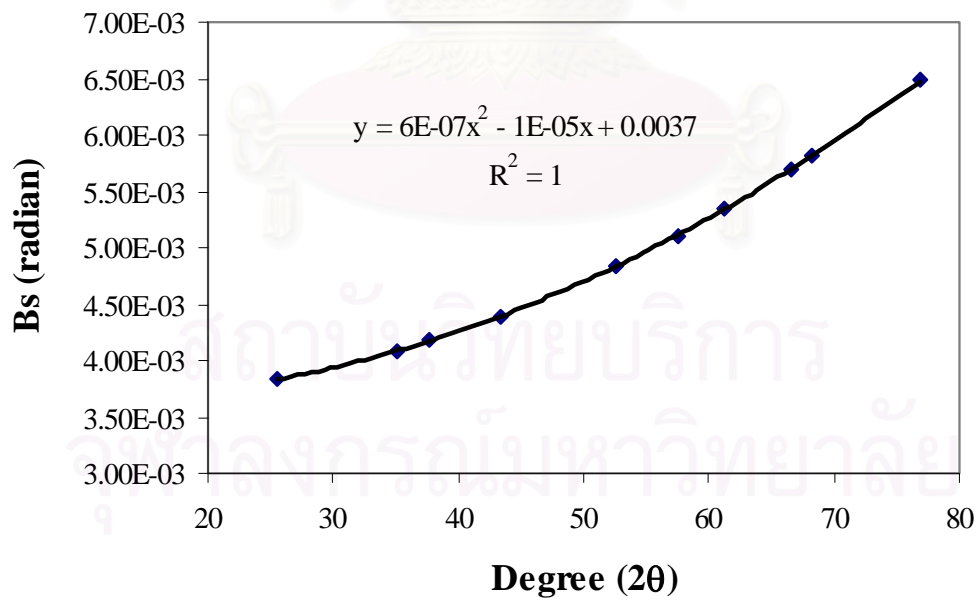


**Figure B.2** The plot indicating the value of line broadening due to the equipment. The data were obtained by using  $\alpha$ -alumina as standard

## APPENDIX C

### CALCULATION FOR METAL ACTIVE SITES AND DISPERSION

Calculation of the metal active sites and metal dispersion of the catalyst measured by CO adsorption is as follows:

Let the weight of catalyst used	= W	g
Integral area of CO peak after adsorption	= A	unit
Integral area of 100 $\mu$ l of standard CO peak	= B	unit
Amounts of CO adsorbed on catalyst	= B-A	unit
Volume of CO adsorbed on catalyst	= $100 \times [(B-A)/B]$	$\mu$ l
Volume of 1 mole of CO at 30°C	= $24.86 \times 10^6$	$\mu$ l
Mole of CO adsorbed on catalyst	= $[(B-A)/B] \times [100/24.86 \times 10^6]$	mole
Molecule of CO adsorbed on catalyst	= $[4.02 \times 10^{-6}] \times [6.02 \times 10^{23}] \times [(B-A)/B]$	molecules
Metal active sites	= $2.42 \times 10^{18} \times [(B-A)/B] \times [1/W]$	molecules of CO/g of catalyst
Molecules of Pd loaded	= $[\% \text{ wt of Pd}] \times [6.02 \times 10^{23}] / [\text{MW of Pd}]$	molecules/g of catalyst
Metal dispersion (%)	= $100 \times [\text{molecules of Pd from CO adsorption} / \text{molecules of Pd loaded}]$	

สถาบันวิทยบริการ  
จุฬาลงกรณ์มหาวิทยาลัย

## APPENDIX D

### CALIBRATION CURVES

This appendix showed the calibration curves for calculation of composition of reactant and products in selective acetylene hydrogenation reaction. The reactant is 1.5%  $C_2H_2$ , 1.7%  $H_2$ , and balanced  $C_2H_4$  (TIG Co., Ltd) and the desired product is ethylene. The other product is ethane.

The thermal conductivity detector, gas chromatography Shimadzu model 8A was used to analyze the concentration of  $H_2$  by using Molecular sieve 5A column.

The carbosieve S-II column is used with a gas chromatography equipped with a flame ionization detector, Shimadzu model 9A, to analyze the concentration of products including of methane, ethane, acetylene and ethylene.

Mole of reagent in y-axis and area reported by gas chromatography in x-axis are exhibited in the curves. The calibration curves of acetylene and hydrogen are illustrated in the following figures.

สถาบันวิทยบริการ  
จุฬาลงกรณ์มหาวิทยาลัย

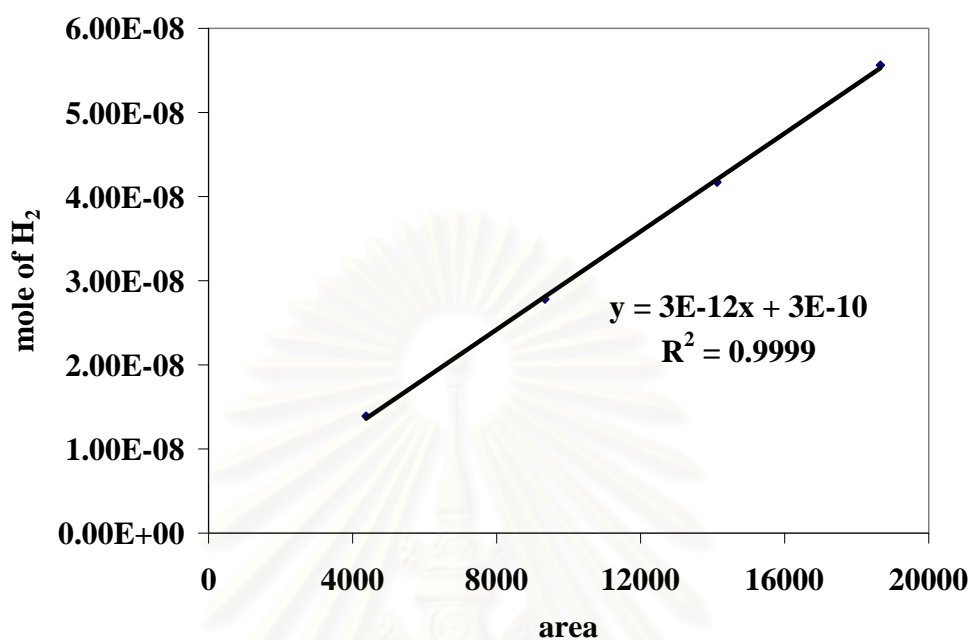


**Figure D.1** The calibration curve of hydrogen from TCD of GC-8A.

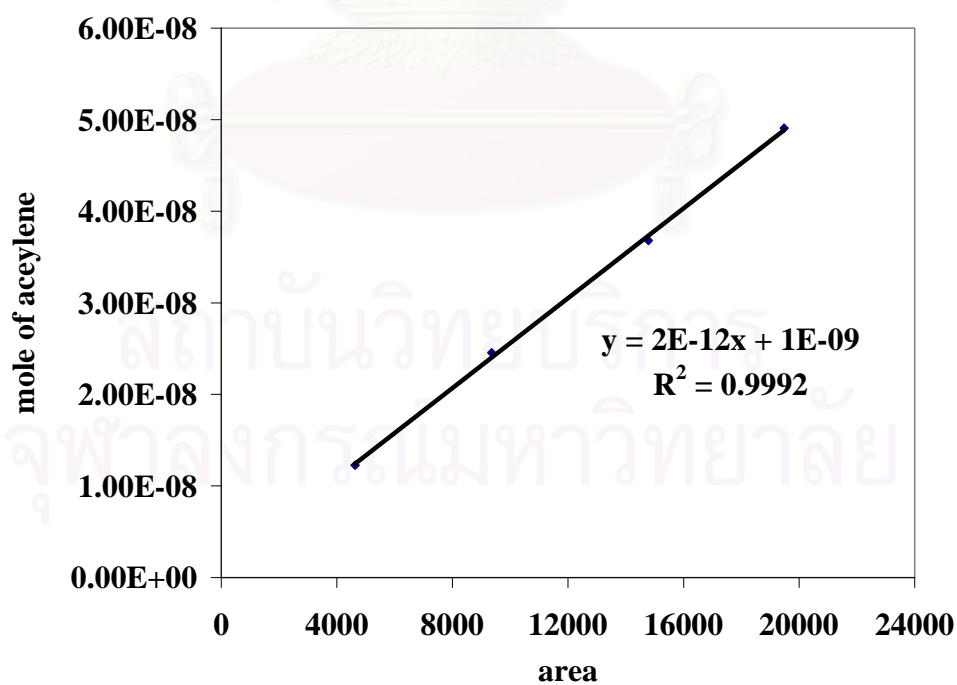


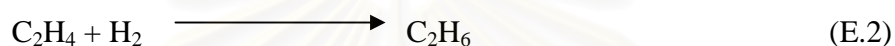
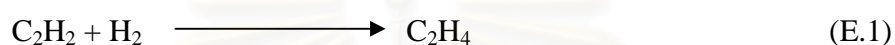
**Figure D.2** The calibration curve of acetylene from FID of GC-9A.



## APPENDIX E

### CALCULATION OF CONVERSION AND SELECTIVITY

The catalyst performance for the selective hydrogenation of acetylene was evaluated in terms of activity for acetylene conversion and selectivity base on the following equation.



Activity of the catalyst performed in term of acetylene conversion is defined as moles of acetylene converted with respect to acetylene in feed:

$$\text{C}_2\text{H}_2 \text{ conversion (\%)} = \frac{100 \times [\text{mole of C}_2\text{H}_2 \text{ in feed} - \text{mole of C}_2\text{H}_2 \text{ in product}]}{\text{mole of C}_2\text{H}_2 \text{ in feed}} \quad (\text{i})$$

where mole of  $\text{C}_2\text{H}_2$  can be measured employing the calibration curve of  $\text{C}_2\text{H}_2$  in Figure D.2, Appendix D., i.e.,

$$\text{mole of C}_2\text{H}_2 = (\text{area of C}_2\text{H}_2 \text{ peak from integrator plot on GC-9A}) \times 2.0 \times 10^{-12} \quad (\text{ii})$$

สถาบันวิทยบริการ  
จุฬาลงกรณ์มหาวิทยาลัย

Ethylene gain was calculated from moles of hydrogen and acetylene as explained in section 3.6:

$$\text{C}_2\text{H}_4 \text{ gain (\%)} = \frac{100 \times [\text{dC}_2\text{H}_2 - (\text{dH}_2 - \text{dC}_2\text{H}_2)]}{\text{mole of C}_2\text{H}_2 \text{ converted}} \quad (\text{iii})$$

where  $\text{dC}_2\text{H}_2$  = mole of acetylene in feed – mole of acetylene in product (iv)

$\text{dH}_2$  = mole of hydrogenation in feed – mole of hydrogen in product (v)

mole of  $\text{C}_2\text{H}_2$  is calculated by using (ii) whereas mole of  $\text{H}_2$  can be measured employing the calibration curve of  $\text{H}_2$  in Figure D.1, Appendix D., i.e.,

$$\text{mole of H}_2 = (\text{area of H}_2 \text{ peak from integrator plot on GC-8A}) \times 3.0 \times 10^{-12} \quad (\text{vi})$$



สถาบันวิทยบริการ  
จุฬาลงกรณ์มหาวิทยาลัย

## APPENDIX F

### LIST OF PUBLICATIONS

1. Kamolwan Chanmongkolthip, Joongjai Panpranot, and Sirithan Jiemsirilers, “Effect of  $\alpha$ -Al<sub>2</sub>O<sub>3</sub> grinding on the performance of Pd/ $\alpha$ -Al<sub>2</sub>O<sub>3</sub> catalysts in selective hydrogenation of acetylene”, Proceeding of the 2<sup>th</sup> SUT Graduate Conference, Nakornratchasima Thailand, January, 2009.



สถาบันวิทยบริการ  
จุฬาลงกรณ์มหาวิทยาลัย

## VITA

Miss Kamolwan Chanmongkolthip was born on 24<sup>th</sup> September 1984, in Bangkok, Thailand. She received her Bachelor degree of Science with Chemical Technology from Chulalongkorn University, Thailand in April 2007. Since June 1, 2007, she has been studying for her Master degree of Engineering from the department of Chemical Engineering, Chulalongkorn University.



สถาบันวิทยบริการ  
จุฬาลงกรณ์มหาวิทยาลัย